Experimental Characterization of a Novel Small-Scale Natural Circulation Loop Methanol Synthesis Reactor

Pratik Basarkar

Technische Universiteit Delft

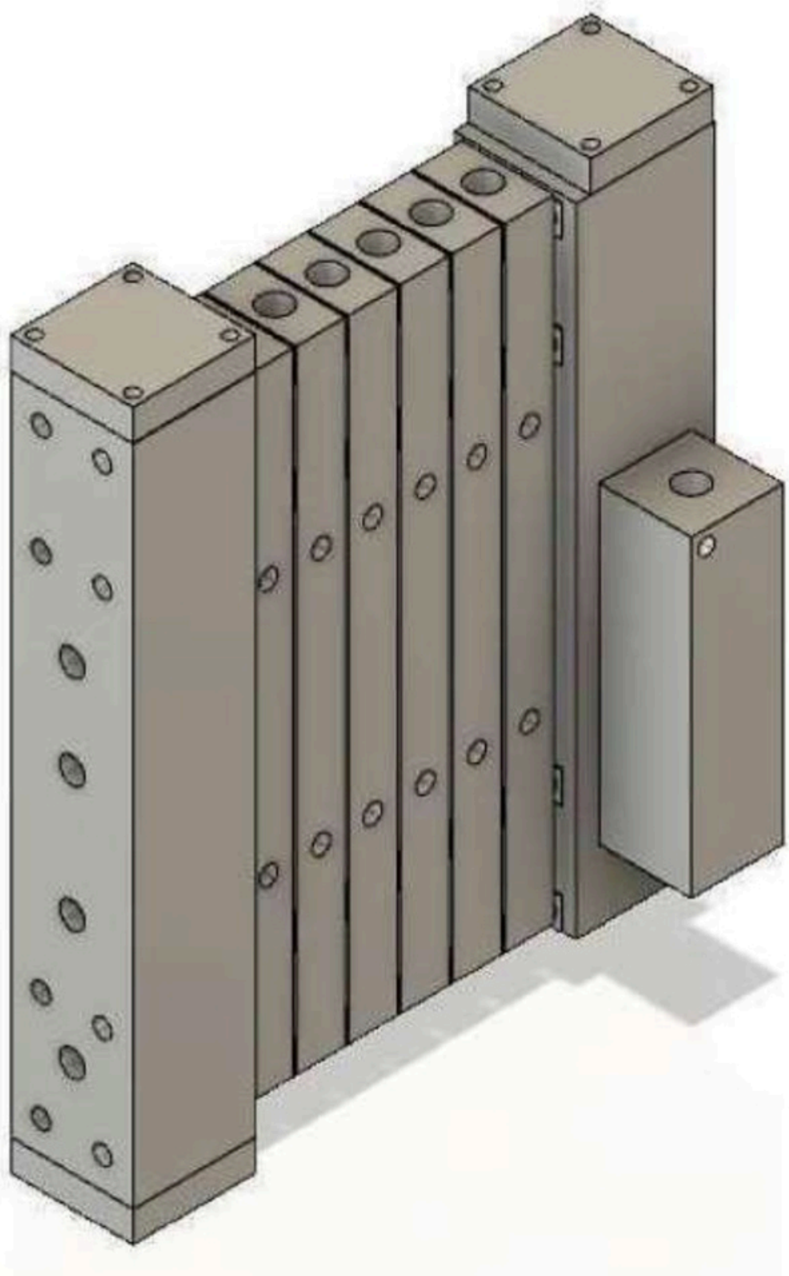

Delft University of Technology

Challenge the future

Experimental Characterization of a Novel Small-Scale Natural Circulation Loop Methanol Synthesis Reactor

by

Pratik Basarkar

in partial fulfillment of the requirements for the degree of

Master of Science
in Mechanical Engineering

at the Delft University Of Technology,
to be defended publicly on Thursday August 30, 2018 at 02:00 PM.

Student Number:	4616049	
Project Duration:	January, 2018-August, 2018	
Daily Supervisor:	ir. Jan van Kranendonk,	ZEF B.V., Delft, The Netherlands
Thesis committee:	Dr. ir. Wiebren de Jong	TU Delft, The Netherlands | Chair
	Dr. ir. Earl Goetheer	TU Delft, The Netherlands
	Dr. ir. Rob Stikkelman	TU Delft, The Netherlands

An electronic version of this thesis will be available on August 30, 2020.

Acknowledgements

This thesis is written in my voice, but it is actually a collaborative work between three people-Jan, Enrique and I. Even though it was I who did all the planning and experiments, the constant feedback I would get from the other two greatly helped me in doing my work. Special thanks to Wiebren for his guidance during the project and his valuable feedback for the first draft of this work. Credit also goes to Earl Goetheer and Wim Brilman, from TNO and UT Twente respectively, who helped shape this thesis to its present state. I am also grateful to Prof. Rob Stikkelman for agreeing to be in my thesis committee and for reviewing my thesis.

I would like to express my gratitude to Ulrich and Hessel for those laughs whenever I went to the office to take a break from experiments. Credit also goes to team ZEF 1 and 2 who built the entire subsystem from scratch. In particular, I would like to thank Diego and Rens, who helped me with and provided constructive criticisms of my design whenever I wanted some honest opinion. Special thanks to Jaap and Michel who helped me whenever I had some problems with my experimental setup.

I would like to specifically thank Zerui, Daniel and Sotiris who read my first draft and suggested possible areas for improvement.

In the end, I would like to thank my friends here at Delft for these two years of fun and specifically Renika, without whose constant ”support and guidance” I could have finished my thesis in half the time.

Pratik
Delft, August 2018

Abstract

The present-day industrialized nations reached high standards of living using cheap fossil fuel energy. The high CO_2 emissions as a result of burning these fuels over the years have started outpacing the natural carbon cycle, resulting in climate changes around the globe. We have reached a point in our history where merely reducing our carbon emissions would not solve the problem, rather carbon has to be captured from the atmosphere and either stored or converted to fuels. Converting the captured CO_2 into methanol has been gaining traction in recent years as it is not only an excellent fuel but also serves as the building block to manufacture other important chemicals like dimethyl ether (DME), paraffin, olefins, plastics and polymers.

This thesis focusses on the complete experimental characterization of a small-scale, energy efficient methanol synthesis reactor modelled on the concept developed by Wim Brilman of the University of Twente, with respect to feed flow rates, methanol production and overall efficiency. The problem of comparative energy inefficiency of the Brilman reactor was solved by carrying out the reactions in a novel, natural circulation loop (NCL) fixed packed bed reactor with internal heat recovery using $Cu/ZnO/Al_2O_3$ as the catalyst. A mixture of H_2 and CO_2 in the molar ratio of 3:1-the optimum ratio for methanol production was fed into the reactor. A sensitivity analysis was carried out with regards to the sampling time of the liquids at the outlet and the reaction temperature. Maximum methanol productivity of 6.8 mmole (millimoles) $CH_3OH/g_{cat}/h$ was obtained at 228 °C reactor wall temperature and 62 °C condenser wall temperature using 5 mm diameter pellets compared to 4.3 mmole $CH_3OH/g_{cat}/h$ obtained by Brilman at 210 °C reaction temperature and 85 °C condenser temperature. Also, a high carbon conversion of 99.2% and methanol selectivity of 99.0% was achieved. The energy demand (in MJ/kg_{CH_3OH}) was reduced from 75 in the Brilman reactor to 24 using the current design. From these results, it was established that methanol could be synthesized using a small, lab-scale reactor in an energy efficient manner.

It was further observed that reduced size of the catalyst did not contribute much to methanol yield due to the high-pressure drop. Finally, a brief analysis of the heat losses in the system led to the conclusion that an additional 14.6 W of heat would have enabled autothermal operation.

Contents

List of Tables **ix**

List of Figures **xi**

Abbreviations . . . xv
Nomenclature . . . xvii
Glossary . . . xix

1 Introduction **1**
1.1 Methanol as a sustainable fuel . . . 2
1.2 Role of the start-up company Zero Emission Fuels . . . 3
1.3 Research Questions . . . 4
1.4 Thesis Outline . . . 4

2 Literature Review **5**
2.1 History of methanol synthesis . . . 5
2.2 Low pressure methanol synthesis . . . 5
2.2.1 Sources of methanol . . . 5
2.2.2 Catalysts for methanol synthesis . . . 7
2.2.3 Kinetic Modeling . . . 9
2.2.4 Reactor types for methanol production . . . 12
2.2.5 Brilman Reactor . . . 16

3 Experiments **21**
3.1 Reactor Design and Fabrication . . . 21
3.2 Experimental System . . . 21
3.2.1 Process and Instrumentation Diagram . . . 22
3.2.2 Reactor . . . 22
3.2.3 Gas cylinders . . . 27
3.2.4 Electrical circuits and data logging . . . 27
3.2.5 Instruments used for analysis . . . 28
3.3 Reactor Operating Procedure . . . 28
3.4 Experimental Test Plan . . . 31

4 Results and Discussion **33**
4.1 Experiments using N_2 as the fluid . . . 33
4.2 Experiments using feed gas . . . 34
4.3 Fault Tree Analysis . . . 34
4.3.1 High fluid temperature in the condenser . . . 35
4.3.2 No reaction in the catalyst zone . . . 35
4.3.3 No liquid accumulation . . . 37
4.3.4 No gas flow in the reactor . . . 37
4.4 Experiments with 5 mm catalyst pellets . . . 40
4.4.1 Sampling time optimization . . . 41
4.4.2 Reaction temperature optimization . . . 42
4.5 Experiments with crushed catalyst particles . . . 47
4.6 Experiments with 5 mm pellets cut into two halves . . . 48
4.7 Comparison of experimental results with simulations in COCO and Fluent . . . 50
4.8 Heat Exchange Network . . . 51

5 Conclusions and Recommendations **55**
5.1 Conclusions . . . 55
5.2 Recommendations . . . 56

Bibliography 59

Appendices 65

A Parameters for estimating equilibrium conversion of methanol 67

B Reactor Dimensions 69
- B.1 Reaction Zone . . . 69
- B.2 Heat Integration Blocks . . . 70
- B.3 Condenser Block . . . 70

C Industrial methanol production 71

D Internal Fins 73

E Efficiency Calculations 75

F Heat Exchange Network Calculations 77
- F.1 Heat loss through bolts . . . 77
- F.2 Heat loss through PT 60. . . . 77
- F.3 Heat loss through the insulation. . . . 78
- F.4 Heat loss through air gap . . . 78
- F.5 Heat transferred to the condenser from COCO simulations . . . 80

G Effect of condenser temperature and channel diameter variation on methanol yield 81

H Corrosion in aluminium blocks 83

List of Tables

2.1 History of methanol synthesis [7, 11, 14, 15]. 5
2.2 Sources of syngas production. A stoicheometric ratio (SN) close to 2 is desired for maximum methanol production. [15]. 6
2.3 Composition of Cu methanol synthesis catalysts from different manufacturers [14]. . . . 7
2.4 Carbon source of methanol according to literature. As can be observed, there is little consensus among the authors regarding the source of methanol (table adopted from [15]). 9
2.5 Kinetic models for methanol synthesis (adapted from [14, 15]). 11
2.6 Adiabatic reactor technologies for methanol synthesis. 13
2.7 Isothermal reactors used for methanol synthesis. 15
2.8 Summary of liquid based reactors used for methanol synthesis. 16
2.9 Plants working on CO_2 to methanol conversion. 19
2.10 Parameters affecting the mass flux [93]. 19

3.1 Parameter values used to estimate heat integration for one block. 30
3.2 Sample calculation to estimate the mass flow rate. 31

4.1 Details of the experiments performed with N_2 as the fluid. Only the first test without the catalyst was simulated by Guttierez-Neri [104] in Fluent. 34
4.2 Temperatures at the top and bottom thermocouple of the heat integration blocks at the reaction temperature of 225 °C. Block 1 is closest to the reaction zone and Block 6 to the condensation zone. 39
4.3 Molar flow rate of the components at the outlet of the reactor for 5 mm pellets at 228 °C reaction temperature, presented as an example. 44
4.4 Estimation of carbon conversion and selectivity for 5 mm pellets at different temperatures. 44
4.5 Results of the experiment with 5 mm catalyst at 228 °C and 10 minutes of sampling time. 46
4.6 Comparison of the results of the current study with those of Brilman et al [16]. 46
4.7 Results of the experiments performed using 5 mm pellets cut into two halves at 14 minutes of sampling time. The methanol production and efficiency are lower compared to the results obtained using 5 mm pellets. 49
4.8 Simulation parameters for the COCO model for 5 mm pellets at 228 °reaction temperature. 51
4.9 Comparison of mass flow rate obtained from experiments and simulations. 51
4.10 Heat losses in the system. 52
4.11 Comparison of heat transferred to the condenser based on experimental and simulation results. 52

A.1 Parameters used for conversion of methanol in a single pass reactor. 68

B.1 Dimensions of various components of the reaction zone. 69
B.2 Dimensions of the various components of the heat integration block. 70
B.3 Dimensions of the various components of the condenser block. 70

C.1 Calculation of methanol production using the results of Chen et al. [21]. 71

E.1 Maximum theoretical efficiency calculation for different reaction temperatures using 5 mm pellets. 76
E.2 Maximum theoretical efficiency calculation for different reaction temperatures using 5 mm pellets cut into two halves. 76

F.1 Heat loss through bolts. 77

F.2 Heat loss through PT 60. 78
F.3 Heat loss through the insulation. 78
F.4 Heat loss through the air gap. 79
F.5 Flow rates and temperature values of some of the streams in the COCO model (Figure 4.21). 80
F.6 Mode of heat transfer in the condenser 80

List of Figures

1.1 World Total Final Consumption (TFC) by fuel in 2015 in Million Tonnes of Oil Equivalent (Mtoe) [10]. . . . 1
1.2 Methanol demand and production in millions of metric tons (MMT) per year. Since 2013, there has been a sharp growth in methanol demand and production driven mainly by the demand in China [12, 13]. . . . 2
1.3 Circular carbon loop of methanol [7, 11]. CO_2 released into the atmosphere by burning of fuels and also from point sources like industries can be captured and stored by the process of carbon capture and storage (CCS). The CO_2 can also be reacted with H_2 to produce methanol by the process of carbon capture and recycling (CCR). . . . 3
1.4 Schematic of the process by which ZEF plans to produce methanol. The focus of this thesis is on the experimental characterization of the methanol synthesis reactor. . . . 3

2.1 Variation of equilibrium conversion to methanol with temperature using syngas as the feed at 50 bar (Mole fraction H_2:CO_2:CO:Ar=0.82:0.03:0.04:0.11). . . . 7
2.2 Schematic of the reactions occuring at the catalyst surface. CO_2 and H_2 adsorb dissociatively (on different sites) on Cu. CO_2 is hydrogenated to bicarbonates, then to Cu formate, formaldehyde, methoxy species and finally to methanol. Hydrogenation of the formate is considered to be the rate determing step of the reaction, as formate species is the longest living intermediate [25]. . . . 8
2.3 Simplified flow diagram for methanol synthesis reactors. The feed gas is first compressed after which it exchanges heat with the unreacted recycled gas. The gas mixture is then heated to the reaction temperature and fed to the reactor. The products are then separated using membranes, solvents or in-situ condensation while the unreacted gas is recycled back [14]. . . . 12
2.4 Examples of adiabatic reactors used for methanol synthesis: (2.4a) Quench reactor and (2.4b) Kellogg, Brown and Root reactor. . . . 12
2.5 Examples of reactors used for methanol synthesis. . . . 14
2.6 Dew point temperature of the gas mixture as a function of the reaction pressure and temperature (H_2:CO_2=3:1). At a high temperature (523 K), a very high pressure is required to condense the gases at the reaction temperature. At lower pressures (50 bar) and temperatures (473 K), a decrease of temperature is required to initiate condensation. At these pressures, a temperature gradient can be achieved in the reactor to drive the flow. 17
2.7 Design of the reactor proposed by [16]. The feed gas enters through the inlet and flows through the inner tube before passing through the tube annulus which contains the catalyst. The catalyst bed is maintained at the reaction temperature using an oven. Methanol and water mixture are then condensed at the top using a cooling coil. The liquids formed are tapped out at regular intervals. . . . 18
2.8 Internal heat exchange (shown on the left) and external heat exchange design (shown on the right) with arrows showing the syngas flow direction. An internal heat exchange system would decrease the average temperature difference between the heating and the cooling zones, decreasing the mass flux. An external heat exchange system on the other hand increases the absolute temperature difference between the two zones, increasing the mass flux. The latter is used in this thesis. . . . 20

3.1 Process and instrumentation diagram of the methanol synthesis reactor setup. The gas cylinders (highlighted in green), the reactor (in red), the data logging circuit (in blue) and the instruments used for analysis (in yellow) can be clearly seen. . . . 22
3.2 Schematic of the Brilman reactor (3.2a) and the MBR (3.2b) as used in this thesis. . . . 23

3.3 Schematic of the complete reactor assembly. The six heat integration blocks are placed between the reaction zone on the right and the condensation zone on the left. Viton™ O-rings and PT 60 papers are placed between each block to provide effective sealing and reduce axial conduction of heat respectively. . . . 23
3.4 Reactor assembly as used in the experiment. Glass wool is used as the insulation material. The thermocouple connections can be clearly seen. The feed input is from the left and the methanol and water mixture is tapped from the bottom using the two open close valves. . . . 24
3.5 Isometric view of the reaction zone (left) and front and sectional view (on the right). The reaction zone consists of a cylindrical channel where the catalyst in inserted. All the dimensions are in mm. . . . 24
3.6 Catalyst pellets as sourced from the manufacturer (The red colour of some of the pellets is due to prior reduction with H_2). . . . 25
3.7 Schematic of the heat integration block with the isometric view on the left, the front view in the middle and the sectional view on the right. All the dimensions are in mm. . . . 26
3.8 Condenser block. . . . 26
3.9 Schematic of the electrical circuit for the reactor. . . . 27
3.10 Electrical circuit for the reactor made using a breadboard and then using a PCB. . . . 28
3.11 Reactor start-up procedure. . . . 28
3.12 Heat integration block. All dimensions are in mm. . . . 29
3.13 Heat integration in each block. . . . 30
3.14 Schematic of the procedure to calculate the mass flow rate. . . . 30

4.1 Schematics of the reactor during experiments with N_2 as the fluid. The reactor without catalyst (Figure 4.1a), with catalyst (Figure 4.1b), with catalyst and internal fins (Figure 4.1c) and with the flow completely blocked (Figure 4.1d) can be seen. . . . 33
4.2 Fluid temperature measurement in the condenser. The difference between the condenser surface and fluid temperature is a maximum of 5.5 °C using 1 bar N_2. . . . 35
4.3 Causes for no reaction taking place in the catalyst zone with their solutions. . . . 36
4.4 Causes for insufficient liquid accumulation in the bottom port of the condenser and their solutions. . . . 37
4.5 Causes for no gas flow in the reactor and their solutions. . . . 38
4.6 Modification at the outlet of the catalyst bed to measure the gas composition. Two open close valves were used to enable gas sampling. . . . 38
4.7 Pressure drop using (4.7a) six heat integration blocks and (4.7b) three heat integration blocks. Premature condensation in the case of six blocks was the cause of low liquid production and thus low pressure drop in time. . . . 39
4.8 Change in flow channel dimensions to solve the problem of flow blockage due to liquid condensation. . . . 40
4.9 Schematic of the Small Modified Brilman Reactor (SMBR) used for the experiments. The reactor now consists of the reaction zone, three heat integration blocks (with larger flow channels) and a condensation zone. . . . 40
4.10 Procedure followed for calculating the methanol production rate in mmole $CH_3OH/g_{cat}/h$. 41
4.11 Variation in methanol production with sampling time at 235 °C for 5 mm catalyst pellets. 41
4.12 Schematic of the reactor showing the inlet and outlet streams. . . . 42
4.13 Procedure to calculate the moles of gaseous components in the reactor. . . . 43
4.14 Flowchart for mass balance calculations. . . . 43
4.15 Variation in methanol production, energy efficiency and overall efficiency with time for 5 mm pellets. Methanol production, overall and energy efficiency of the system are found to increase with temperature (till 228 °C), and then start to decrease. 228 °C was identified as the optimum temperature to produce methanol in the SMBR using 5 mm pellets. . . . 45
4.16 Crushed catalyst pellets. . . . 47
4.17 Variation in CO formation with time for 5 mm and crushed catalyst pellets. Reduction in catalyst size did not lead to increased methanol production as the flow rate was restricted as a result of high pressure drop caused by the small particle size. . . . 47
4.18 5 mm catalyst pellets cut into two halves along the central axis. . . . 48

4.19 Variation in methanol production with sampling time. Maximum production is observed at 14 minutes of sampling compared to 10 minutes using 5 mm pellets, pointing towards flow limitations imposed by a higher pressure drop. 48
4.20 Variation of overall efficiency and methanol production with reaction temperature. . . . 49
4.21 Simulation model developed in COCO by Guttierez-Neri [104] incorporating the heat integration achieved by the aluminium blocks. 50
4.22 Steps to compare experimental and simulation results obtained from COCO. Red font indicates possible sources of error in the measurement. 50
4.23 Heat exchanging network depicting the pathway of heat loss in the reactor. Loss through the insulation is the highest suggesting that selection of proper insulation material should be a priority for future experimental designs. 52
4.24 Scenarios for estimating the performance of the reactor in case of no heat losses. Autothermal reactor operation is possible if an additional 14.6 W of heat is generated from the system. This can be achieved using higher heat integration or by producing more methanol. 53

A.1 Model developed in COCO for calculating equilibrium conversion to methanol in a single pass. 67

D.1 Internal fins. 73

G.1 Effect of changing condenser temperature on methanol mole fraction. Reducing the temperature ensures more liquid is condenser, leading to more methanol production. 81

H.1 Corrosion in the flow channels of the aluminium block. 83

List of Abbreviations

BASF	Badische Anilin und Soda Fabriek
CCS	Carbon Capture and Storage
CCR	Carbon Capture and Recycling
Co	Cobalt
CSV	Comma Separated Value
CMD	Collect-Mix-Distribute
DME	Dimethyl Ether
HHV	Higher Heating Value
ICI	Imperial Chemical Industries
LOGIC	Liquid Out Gas In Concept
LHHW	Langmuir-Hinshelwood-Hougen-Watson
LPG	Liquefied Petroleum Gas
MBR	Modified Brilman Reactor
MMT	Millions of metric tons
Mo	Molybdenum
Mn	Manganese
Mtoe	Million Tonnes of Oil Equivalent
NCL	Natural Circulation Loop
NOx	Nitrogen oxide
Pd	Palladium
Au	Gold
$\mathbf{ZrO_2}$	Zirconium dioxide
$\mathbf{SiO_2}$	Silicon dioxide
Rh	Rhodium
Ru	Ruthenium
RWGS	Reverse Water Gas Shift reaction
SSD	Solid State Drive
SMBR	Small Modified Brilman Reactor
SOx	Sulfur oxide
SN	Stoichiometric Ratio
TCD	Thermal Conductivity Detector
TFC	Total Final Consumption
WGS	Water Gas Shift reaction
ZEF	Zero Emission Fuels

Nomenclature

Sign	Name	Unit
A	Cross sectional area	m^2
$A1…6$	kinetic constants in literature expressions	-
C_p	Specific heat	J/kg-K
f	Fugacity	bar
f_i	Partial fugacity of component i	bar
h_T	Thiele modulus	-
k	Thermal conductivity	W/m-K
K	Adsorption equilibrium constant	bar^{-1}
K_p	Chemical equilibrium constant based on partial pressure	bar^{-2} or -
L	Length	m
$\dot{m}$	Mass flow rate	kg/s or kg/h
mmole	Millimoles	mmole
n	Moles	mole
p	Partial pressure	bar
r	Reaction rate per weight of the catalyst	mol s^{-1} kg^{-1}
T	Temperature	K
ΔT	Absolute temperature difference	K
$\Delta < T >$	Average temperature difference	K
$< T >$	Average temperature	K
$\log_{10} K_{\mathrm{pCO}}$	Equilibrium constant for CO hydrogenation	bar^{-2}
$\log_{10} K_{\mathrm{pRWGS}}$	Equilibrium constant for reverse water gas shift reaction	-
Δ H	Heat of the reaction	kJ/mole
ΔH^o_{298K}	Standard enthalpy of reaction at 298 K	kJ/mole

Subscripts

Index	Name
Ar	indicates component Argon
CO	indicates component Carbon monooxide
CO_2	indicates component Carbon dioxide
H_2	indicates component Hydrogen
H_2O	indicates component Water
CH_3OH	indicates component Methanol
Cu	indicates component Copper
Zn	indicates component Zinc
ZnO	indicates component Zinc oxide
Al_2O_3	indicates component Alumina
H_2S	indicates component Hydrogen sulphide
CH_4	indicates component Methane
$CO \rightarrow CH_3OH$	Conversion of CO to CH_3OH
$CO_2 \rightarrow CH_3OH$	Conversion of CO_2 to CH_3OH
CO_2 hydrogenation	indicates the CO_2 hydrogenation reaction
1..6	Denotes heat integration blocks 1 to 6
air gap	Air gap
Al	Aluminium
b	bottom
bolts	Bolts
c	Average heat transfer coefficient between the insulation surface and the ambient
cond	Conduction
condenser	Condenser
conv	Convection
first Al block, avg	Average temperature at the top and bottom of the first heat integration block
HEX	Heat integration
in	input
ins	Insulation
lat	Latent heat
liquid	indicates the Liquid stream of the reactor
out	indicates the sum of the molar flow rates of the Sample and Liquid stream
PT 60	PT 60 paper
rad	Radiation
reaction zone, avg	Average temperature at the top and bottom of the reaction zone
sample	indicates the Sample stream of the reactor
t	top
sens	Sensible heat

Superscripts

Index	Name
eq	Equilibrium

Greek Symbols

Symbol	Name	Unit
ϵ	Emissivity	-
η	Internal effectiveness factor	-
ρ	Density	kg/m^3
σ	Stefan-Boltzmann constant	W/m^2-K^4

Glossary

Aspen Plus®
Chemical process simulator and optimizer by Aspen Technology [1].

COCO
CAPE OPEN to CAPE OPEN- a free-of-charge CAPE-OPEN compliant steady-state simulation environment [2].

LPMEOH™
Liquid phase technology developed by Air Products for the production of methanol in a slurry reactor.

Viton™
A brand of fluoroelastomers, commonly used in O-rings.

Feed gas
The 3:1 molar mixture of H_2 and CO_2 that is fed into the reactor.

MATLAB
Multi-paradigm numerical computing environment and proprietary programming language developed by MathWorks [3].

Processing
An open source programming tool similar to Ardiuno environment. Used for data collection in comma separated value (CSV) format.

1

Introduction

The Kyoto Protocol in 1997 was the first instance where the nations agreed that global warming was indeed a pressing problem and ”anthropogenic CO_2 emissions were a major cause of it” [4]. While this protocol was based on differential agreements-where a few nations bear the most costs-the Paris Agreement of 2015 put the onus on all countries (which ratified it) to keep the temperature increase to 2 °C above pre-industrial levels, and if possible, to limit this to 1.5 °C [5]. As of 2016, 92% of the maximum CO_2 needed to restrict the increase to 1.5 °C is already in the atmosphere, which means we only have until 2020 before we miss the target [6].

Contrary to popular perception, the discovery of shale oil, methane hydrate, shale gas, tight oil and tar sands has meant that the world will not run out of fossil fuels for a long time. Rather, the use of these fuels will be constrained by the level of CO_2 emissions [7]. One of the ways to reduce emissions is to capture CO_2 from the air and store it underground in large spaces by a technique called Carbon Capture and Storage (CCS). While the technology is being currently used for enhanced oil recovery applications and also to store CO_2 underground in depleted oil and gas fields [8] such as the Sleipner facility in Norway, the safety aspect remains a question mark. Storage of high concentrations of CO_2 underground can lead to limnic eruptions (where CO_2 can erupt from deep water bodies and kill living beings), which is what happened at Lake Nyos in Cameroon [9].

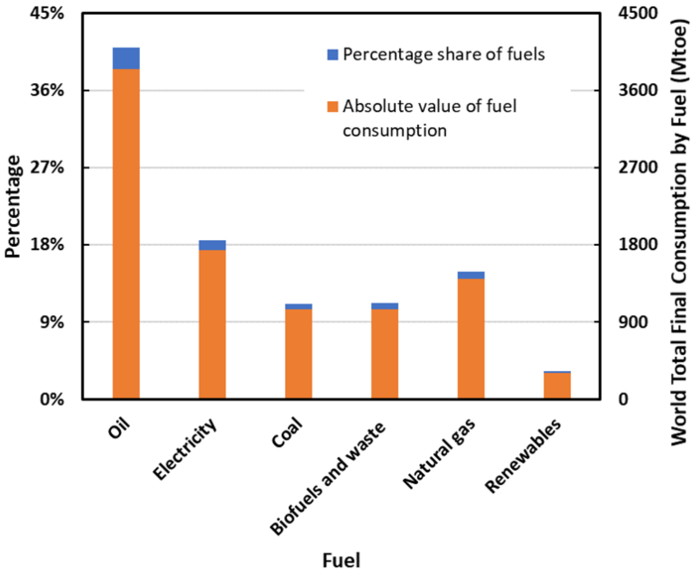

Figure 1.1: World Total Final Consumption (TFC) by fuel in 2015 in Million Tonnes of Oil Equivalent (Mtoe) [10].

Electricity comprises about 19% of our total energy demand (Figure 1.1). Therefore, even if renewable sources like wind and solar are used for electricity production, 81% of our energy needs still need to be met. Allowing for buses and cars to be run on batteries, heavy-duty, long-range transport, in general, will continue using liquid fuels as batteries are too heavy. One way to produce these fuels is to capture atmospheric CO_2 and react it with H_2 created using water electrolysis. Thus, Carbon Capture and Recycling (CCR) emerges as an attractive alternative to CCS, where the captured CO_2 is converted to liquid fuels [7, 11]. One such promising fuel and bulk chemical gaining attention in the international market is methanol which is evident from its increased demand and production in the recent years as shown in Figure 1.2.

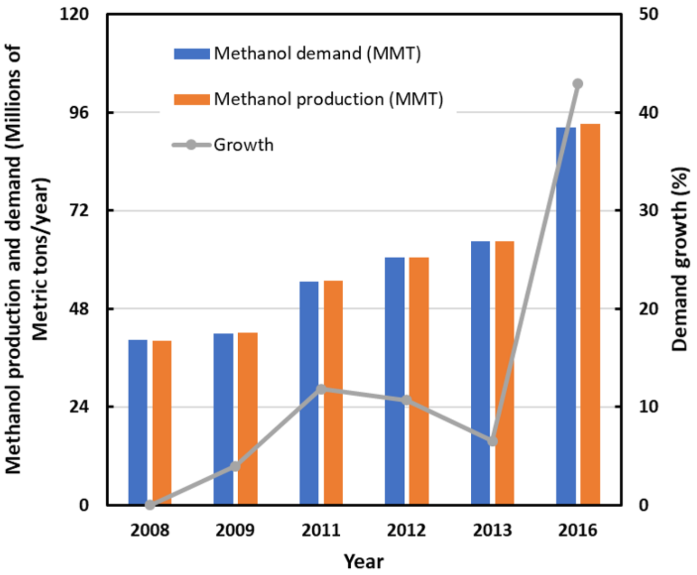

Figure 1.2: Methanol demand and production in millions of metric tons (MMT) per year. Since 2013, there has been a sharp growth in methanol demand and production driven mainly by the demand in China [12, 13].

1.1. Methanol as a sustainable fuel

Although H_2 is the simplest fuel which can be produced using renewable sources (by electrolysis of water), its storage and transportation issues mean that it is unattractive (based on cost-effectiveness) to be used as an energy carrier (or storage) medium with the current technological advancement. Methanol offers an attractive alternative to H_2 as it is a liquid at room temperature. Methanol production from sources like biomass, bio-methane, CO_2 etc. offers a way to achieve a closed carbon loop as shown in Figure 1.3 [7, 11].

Beside being a liquid at room temperature, methanol offers the following advantages [7, 11, 14, 15]:

1. It is biodegradable.
2. It has a high octane number and therefore, it can be blended with gasoline. It burns cleanly with no soot and low NO_x or SO_x emissions [16, 17].
3. It can be used in direct methanol fuel cells to charge portable electronic devices.
4. Dimethyl ether (DME) can be produced using methanol and the former is a good diesel substitute. Methanol and DME can also be used in gas turbine based power plants.
5. Methanol can be used to produce olefins, polymers and simple plastics [16, 18].

The fuel also has some disadvantages [19]:

1. It is less volatile than gasoline which would make pure methanol based engines difficult to start up in a cold environment.

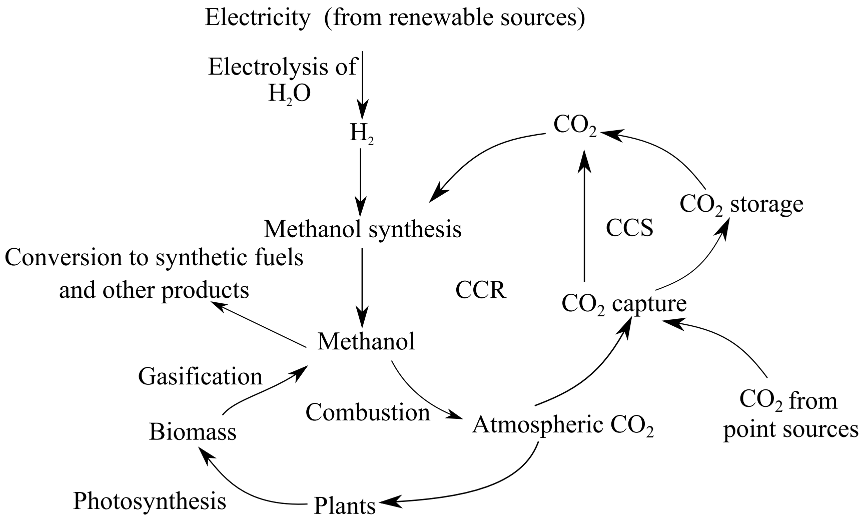
Electricity (from renewable sources)
Electrolysis of H_2O
H_2
CO_2
CO_2 storage
Methanol synthesis
CCS
Conversion to synthetic fuels and other products
CCR
CO_2 capture
Methanol
Gasification
CO_2 from point sources
Combustion
Atmospheric CO_2
Biomass
Photosynthesis
Plants

Figure 1.3: Circular carbon loop of methanol [7, 11]. CO_2 released into the atmosphere by burning of fuels and also from point sources like industries can be captured and stored by the process of carbon capture and storage (CCS). The CO_2 can also be reacted with H_2 to produce methanol by the process of carbon capture and recycling (CCR).

2. It is highly toxic as about 1-2 ml of methanol per kg of body weight is enough to cause death. It can lead to permanent blindness if ingested in small quantities of 10-20 ml.
3. It is corrosive to certain materials like aluminium, zinc and manganese. Therefore, if pure methanol is to be used in an engine, then other suitable materials need to be chosen or corrosion inhibitors need to be added.
4. Methanol has a greater fire risk than H_2 if released into the open atmosphere as the former is a liquid at room temperature. A fire caused by methanol is invisible, especially in bright sunlight. However, it can be easily extinguished using water whereas gasoline floats on water and continues to burn.

1.2. Role of the start-up company Zero Emission Fuels

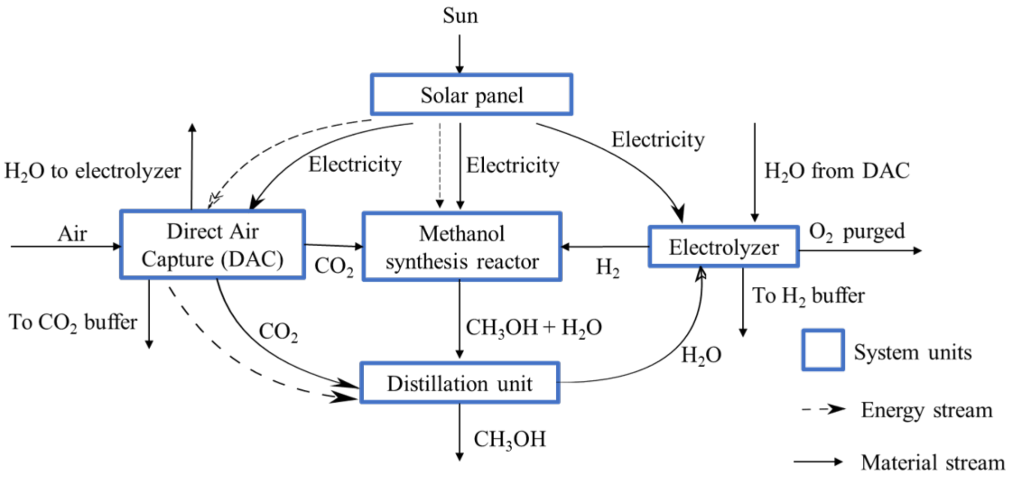
Sun
Solar panel
Electricity
Electricity
Electricity
H_2O to electrolyzer
H_2O from DAC
Air
Direct Air Capture (DAC)
CO_2
Methanol synthesis reactor
H_2
Electrolyzer
O_2 purged
To H_2 buffer
To CO_2 buffer
CO_2
$CH_3OH + H_2O$
H_2O
System units
Distillation unit
Energy stream
CH_3OH
Material stream

Figure 1.4: Schematic of the process by which ZEF plans to produce methanol. The focus of this thesis is on the experimental characterization of the methanol synthesis reactor.

Zero Emission Fuels (ZEF B.V.) is an ambitious start-up working on methanol production using renewable sources [20]. Their aim is to produce methanol using CO_2 and H_2O captured from the air, with the latter being used to make H_2 in an electrolyzer. The feed components, namely CO_2 and H_2 will be fed into a reactor which produces a mixture of methanol and water, with a downstream distillation unit being used to separate the two products. The entire plant will be fitted to the back of a solar panel and will be powered using solar energy (Figure 1.4).

1.3. Research Questions

This thesis focuses on the experimental characterization of a novel, small-scale, NCL methanol synthesis reactor and aims to answer the following research questions:

1. What is the maximum methanol productivity and overall system efficiency that can be obtained experimentally using the reactor given the process conditions?
    (a) How does this productivity compare with that of industrial processes and other experimental studies?
    (b) What are the most important process parameters needed to obtain the maximum productivity?
    (c) What is the effect of heat integration on the overall efficiency of the system?
2. How do the heat losses and mass flow rate of the system compare with the values obtained from simulations?
3. What implications do the results obtained have for future designs of the NCL reactor?

1.4. Thesis Outline

With the background for the thesis and the research questions established in Chapter 1, an overview of the reactor types used for low pressure methanol synthesis is provided in Chapter 2. This is followed by a description of the materials and methods used for the experiments in Chapter 3. The results of the experiments and their discussion is done in Chapter 4. Chapter 5 presents a summary of the work done in this thesis and answers the research questions posed in Chapter 1. Recommendations for future designs of the reactor and its operation are also provided.

2

Literature Review

2.1. History of methanol synthesis

Methanol was first produced in 1661 by wood distillation, with the production volumes being very low (about 20 liters/ton of wood). Because of such limited quantities, methanol as a fuel did not gain much traction until Badische Anilin und Soda Fabriek (BASF) patented a process for its production [15]. BASF produced methanol using Zn based catalysts via coal gasification at high temperatures and pressures. This process was limited by the presence of pollutants in the syngas such as H_2S, CH_4 and other hydrocarbons which caused deactivation of the catalyst. Also, the catalyst produced methanol with only 2-5 wt% selectivity [14]. Improvements in syngas purification (removal of sulfur and chlorine from the gas) and development of a more active Cu catalyst allowed methanol production at low pressures and temperatures. Reactions at these temperatures meant that the production of light hydrocarbons was suppressed. Today, Cu based catalysts are the most widely used for methanol synthesis, with the reactions occurring at low temperatures and pressures, with the process classified as a high pressure (250-300 bar), medium pressure (100-250 bar) or low pressure (50-100 bar) [15]. A brief history of methanol synthesis is tabulated in Table 2.1.

Table 2.1: History of methanol synthesis [7, 11, 14, 15].

Industry	Production method	Catalyst	Operation conditions
BASF (1923) (0.07896 tonnes/day)	Coal gasification	Zn/Cr_2O_3	300-400 °C 250-300 atm
Lonza, Switzerland (1940s)	Reaction of electrolytic H_2 and CO_2, the latter obtained from $Ca(NO_3)_2$ synthesis	ZnO based catalyst	-
ICI (1966) (2500 tonnes/day)	Methane steam reforming	Cu/ZnO	300 °C 100 atm
Lurgi (90000 tonnes/day) [21]	Methane steam reforming	Cu/ZnO	230-250 °C 40-50 atm

2.2. Low pressure methanol synthesis

2.2.1. Sources of methanol

As is evident from Table 2.1, methane steam reforming has replaced coal gasification as the most widely used method for methanol production, mainly because of cleaner syngas output in the former. The syngas composition depends on the source of carbon and the process of production (as can be seen from

Table 2.2), with an ideal ratio of 2 desired for maximum methanol production [15].

$$\text{Stoichiometric Ratio (SN)} = \frac{\text{moles of } H_2 - \text{moles of } CO_2}{\text{moles of } CO_2 + \text{moles of } CO}$$

Table 2.2: Sources of syngas production. A stoicheometric ratio (SN) close to 2 is desired for maximum methanol production. [15].

Source	Process	SN	Drawbacks
Coal and biomass	Gasification	Close to 1	Extensive downstream and upstream cleaning operations
Methane	Steam reforming	Close to 3	High stoicheometric ratio; endothermic process requires high heat input
Methane	Partial oxidation	Close to 2	Exothermic process requiring heat management
Methane	Autothermal reforming	Close to 2	Partial oxidation and steam reforming need to be conducted at different process conditions

Steam reforming, partial oxidation and autothermal reforming have their own disadvantages (the processes are not carbon neutral as methane has 28-34 times the global warming potential of CO_2 and is a major greenhouse gas [22]). Therefore, in the recent years, attention has turned towards biomass and CO_2 as possible candidates for methanol production.

The problem with first generation biomass (any food crop) being used as the source is that it competes with food production for available land and also leads to high handling and transportation costs. Second generation biomass (any non-food crop) on the other hand offers many advantages. It can be grown on land unsuitable for crop production. If the biomass is perennial grass, then it helps to improve the water retention capability of the land as well as prevent soil erosion [23].

While research on making and transportation of fuels from second generation biomass is ongoing, no commercial plants have been developed so far. Also, little research has been done on native lignocellulosic crops in Asia and Africa, while the experience with pilot plants has demonstrated that non-native species threaten the local biodiversity. To conclude, while second-generation biomass offers several advantages, there are many loopholes that need to be closed before it can be used on a large scale for biofuel production, including methanol. [23]. On the other hand, if CO_2 is used as the feedstock, it helps to avoid CO_2 sequestration, which is a very expensive process [24]. Also, a potent greenhouse gas is directly reduced [16, 18].

Methanol synthesis consists of three main reactions with the product formation favoured at high pressures and low temperatures according to Le Chatelier's principle. Equation 2.1 and Equation 2.2 present the CO hydrogenation and CO_2 hydrogenation reactions, respectively, while Equation 2.3 details the water gas shift reaction (WGS).

$$CO + 2H_2 \rightleftharpoons CH_3OH, \qquad \Delta H^o_{298K} = -90.8\,\text{kJ/mole} \tag{2.1}$$

$$CO_2 + 3H_2 \rightleftharpoons CH_3OH + H_2O, \qquad \Delta H^o_{298K} = -49.2\,\text{kJ/mole} \tag{2.2}$$

$$CO + H_2O \rightleftharpoons CO_2 + H_2, \qquad \Delta H^o_{298K} = -41.6\,\text{kJ/mole} \tag{2.3}$$

This process has two major drawbacks [16]:

1. Low conversion to methanol per pass because of thermodynamic limitations necessitating recycle of the feed. The variation of equilibrium conversion to methanol with temperature for a single pass reactor is shown in Figure 2.1 and the parameters for calculation (taken from [25]) are presented in Table A.1.

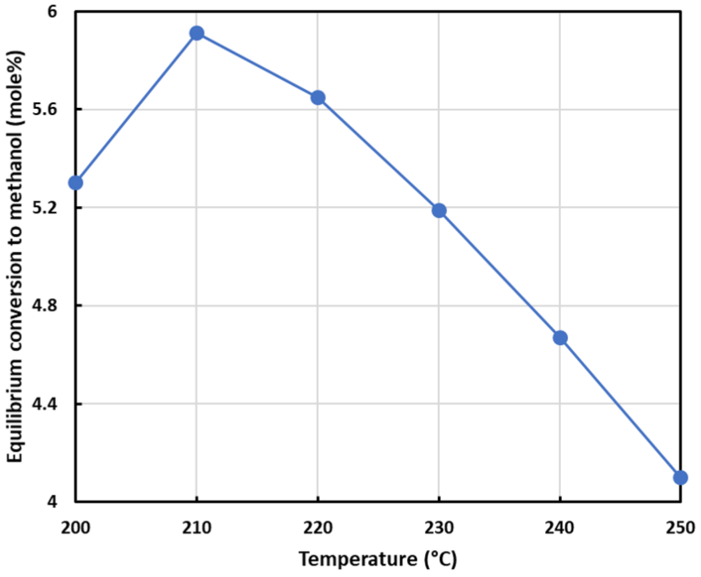

Figure 2.1: Variation of equilibrium conversion to methanol with temperature using syngas as the feed at 50 bar (Mole fraction H_2:CO_2:CO:Ar=0.82:0.03:0.04:0.11).

2. High cooling duty due to exothermic nature of the reactions. This necessitates the use of extra equipment to provide cooling and maintain the reaction temperature and increases the operation cost.

2.2.2. Catalysts for methanol synthesis

Although initial processes produced methanol by the catalytic hydrogenation of CO, most of the authors agree that CO_2 hydrogenation proceeds faster than CO hydrogenation, even if syngas was used as the starting feed [15]. Cu and Zn based catalysts are considered to be among the most selective and active for methanol synthesis from CO_2 and H_2 [26–29], with their composition in the catalyst varying according to the manufacturer and the manufacturing process (2.3) [14].

Table 2.3: Composition of Cu methanol synthesis catalysts from different manufacturers [14].

Manufacturer	Cu (wt%)	Zn (wt%)	Al (wt%)	Other
IFP	45-70	15-35	4-20	Zr-2-18
Synetix (formerly ICI)	20-35	15-50	4-20	Mg
BASF	38.5	48.8	12.9	Rare earth oxide-S
Shell	74	21	12	
Sud Chemie	65	22	31	
DuPont	50	19	17	
United Catalysts	62	21	17	
Haldor Topsoe	>55	21-25	8-10	
Mitsubishi Gas	63.6	33.4	3	
Ammonia Casale	30	50	3	Cr (16)
Lonza	40	20		Zr (40)
AIST, RITE	45.2	27.1	4.5	Zr (22.6) Si (0.6)
YKK Corporation	76.3	11	12.7	

Cu acts as the active phase in these catalysts, with ZnO increasing the sulfur tolerance which gains importance especially if the syngas is produced by coal gasification. Al_2O_3 acts as the support on which CO_2 is dispersed, increasing CO_2 conversion and selectivity to CH_3OH [15, 30, 31].

The catalyst Cu/ZnO/Al_2O_3 is usually prepared by the co-precipitation method, however uncoventional methods of production to improve the Cu/ZnO dispersion have gained interest in recent years [32, 33]. Pd, Au, ZnO, ZrO_2 and SiO_2 are the supports that are proposed for methanol synthesis catalysts [34]. ZrO_2 provides high stability to the catalyst, particularly in oxidizing and reducing atmosphere, but the activity is slightly less than ZnO for methanol synthesis [35]. SiO_2 based catalysts have the problem of low selectivity towards methanol. Several surface modifiers (Rh, Ru, Co, Mo, Mn) could also be added to the catalyst to increase the surface converage of Cu intermediates [36].

The Cu based catalysts are highly suseptible to deactivation via poisoning and thermal sintering [37]. While the problem of poisoning has mostly been eliminated by advances in syngas purification, catalyst sintering remains a problem. A test conducted to check the activity of the catalyst ($CuO/ZnO/Al_2O_3$) after exposure to CO/H_2 stream found that 60% of the activity was lost after 25 hours of operation at 250 °C catalyst bed temperature [38]. Presence of water can also reduce the activity of the catalyst, which is more evident in case of liquid reactors [39].

A schematic of the mechanism for methanol synthesis occuring at the catalyst surface is presented in Figure 2.2.

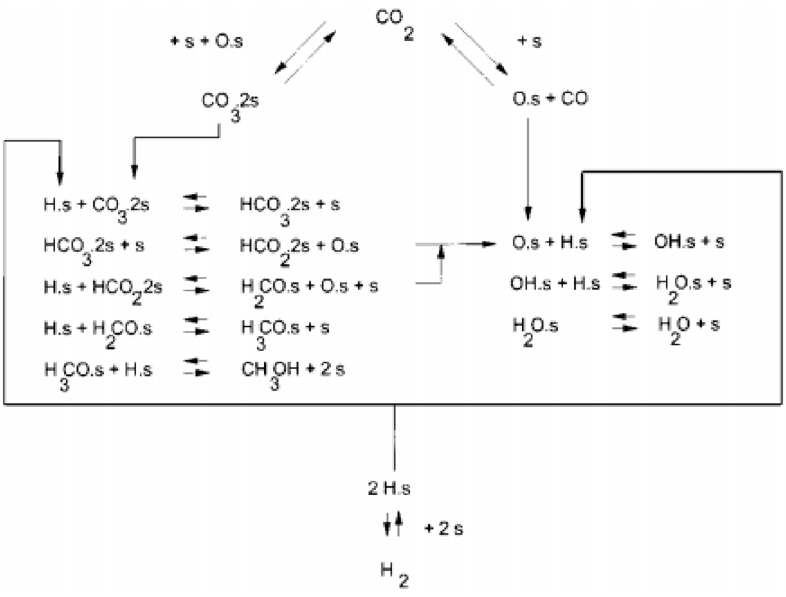
CO2
+ s + O.s
+ s
CO3.2s
O.s + CO
H.s + CO3.2s ⇌ HCO3.2s + s
HCO3.2s + s ⇌ HCO2.2s + O.s
H.s + HCO2.2s ⇌ H2CO.s + O.s + s
H.s + H2CO.s ⇌ H3CO.s + s
H3CO.s + H.s ⇌ CH3OH + 2 s
O.s + H.s ⇌ OH.s + s
OH.s + H.s ⇌ H2O.s + s
H2O.s ⇌ H2O + s
2 H.s
+ 2 s
H2

Figure 2.2: Schematic of the reactions occuring at the catalyst surface. CO_2 and H_2 adsorb dissociatively (on different sites) on Cu. CO_2 is hydrogenated to bicarbonates, then to Cu formate, formaldehyde, methoxy species and finally to methanol. Hydrogenation of the formate is considered to be the rate determing step of the reaction, as formate species is the longest living intermediate [25].

Intra-particle diffusion limitations inside the catalyst assume importance in the case of low pressure methanol synthesis using Cu based catalysts. Numerous studies have been conducted in literature to develop models in order to evaluate the efficiency of the catalyst. Five principles approaches for the same are reported [14]:

1. Dusty gas model,
2. Modified or extended Stefan-Maxwell equations,
3. Multicomponent pore diffusion model combined with convective mass transport,
4. Multicomponent pore diffusion model with constant diffusion coefficients,
5. Model based on Thiele modulus and first order kinetics for methanol and water production.

The Thiele modulus is the ratio of the reaction rate to the diffusion rate in porous catalyst pellets with no mass transfer limitations. It is one of the most widely used methods to determine the effectiveness factor of catalyst pellets as it can be easily implemented in methanol reactor models and reduces the computation time [14].

$$h_T^2 = \frac{\text{Reaction rate}}{\text{Diffusion rate}} \tag{2.4}$$

where,

h_T is the Thiele modulus,

Reaction rate and diffusion rate are expressed in mol/g_{cat}/s.

Thiele modulus is then used to calculate the internal effectiveness factor (η) of the pellets which is defined as [40]:

$$\eta = \frac{\text{Actual rate of the reaction}}{\text{Rate of the reaction if the entire interior surface was exposed to the external pellet surface conditions}} \tag{2.5}$$

where,

Numerator and denominator are expressed in mol/g_{cat}/s.

The internal effectiveness factor is inversely related to the Thiele modulus by the following relation [40]:

$$\eta = \frac{3}{h_T^2} * (h_T^2 * cot(h_T^2) - 1) \tag{2.6}$$

An internal effectiveness factor of 75% was reported at 80 bar pressure and 538 K using 4.2 mm catalyst pellets by Seyfert et al. [41] while Graaf et al. [42] found the effectiveness factor to decrease with increasing temperature (factor varying between 32% and 92%). The factor decreases at a higher temperature as the gases have less time to be adsorbed on the catalyst surface, reducing diffusion. Reducing the catalyst size reduces the diffusion limitations leading to a higher effectiveness factor. The treatment of diffusion limitation is outside the scope of this thesis.

2.2.3. Kinetic Modeling

Even after almost a century of industrial methanol production, there is still a lot of debate regarding the actual source of methanol-CO or CO_2. An analysis of literature studies has been adopted from [15] to find the carbon source of methanol and presented in Table 2.4.

Table 2.4: Carbon source of methanol according to literature. As can be observed, there is little consensus among the authors regarding the source of methanol (table adopted from [15]).

CO	CO_2	CO + CO_2	References
x			[41, 43, 43–47]
	x		[21, 25, 48–58]
		x	[42, 59–69]

As there is no clear solution to the debate regarding the carbon source, kinetic models for methanol synthesis by various authors also differ. Initial models took CO as the source of methanol, with the presence of CO_2 in the feed not taken into account [47, 60]. A rate expression based on the dual-site Langmuir-Hinshelwood-Hougen-Watson (LHHW) mechanism was proposed by Dybkjaer et al. [58], with H_2 and H_2O adsorbed on one site and CO and CO_2 adsorbed on the other.

Graaf et al. [42, 70] proposed that methanol is produced by successive CO and CO_2 hydrogenation with the WGS reaction playing a major role. Their model fitted well with their experimental data and also with other proposed models [41, 43, 58, 60]. They calculated the equilibrium constants for CO hydrogenation and WGS reactions based on partial pressures and based their model on LHHW mechanism, similar to [58]. The equilibrium constants presented by the authors had the following form:

$$\log_{10} K_{\mathrm{pCO}} = 5139/\mathrm{T} - 12.621 \tag{2.7}$$

$$\log_{10} K_{\mathrm{pRWGS}} = -2073/\mathrm{T} + 2.029 \tag{2.8}$$

where,

K_{pCO} is the equilibrium constant for CO hydrogenation in bar^{-2},

K_{pRWGS} is the equilibrium constant for reverse water gas shift (RWGS) reaction,

T is the absolute temperature in K.

Skrzypek et al. [50] conducted experiments with different CO and H_2 feeds and found no production of methanol. They proposed that the role of CO was restricted to CO_2 production via the WGS reaction and removal of H_2O. A few years after Graaf, Bussche and Froment [25] proposed a mechanistic model with CO_2 as the source. They used the equilibrium constants and also based their model on the dual site approach proposed by [42, 58]. According to their model, CO_2 and H_2 undergo dissociation on the catalyst surface (on different sites) and produce methanol, with the rate determining step being the hydrogenation of the formate. The model was developed from literature and experimental studies conducted by the authors on a bench scale setup. The effect of temperature, pressure and ratio of partial pressures of CO and CO_2 on methanol production was investigated. CO_2 was found to be the source of methanol, with CO being produced by the RWGS. The author proposed a ratio of 22 between the reactor diameter and the pellet size for uniform distribution of feed over the reactor section.

The model developed could also predict results outside the experimental window with good agreement. Bussche and Froment validated this model for an adiabatic reactor, Chen et al. [21] validated it for an isothermal reactor while Luyben et al. [71] modeled a methanol synthesis reactor with a distillation column.

A dynamic microkinetic model was proposed by Oversen et al. [72] which was used to reproduce the experimental results of Graaf et al. [42]. The model could explain the behavior of the system under transient conditions. Another microkinetic mechanism consisting of 48 elementary steps was proposed by Lim et al. [67] with the rate-determining step for WGS being the hydrogenation of the formate, similar to [25]. Grabow et al. [68] suggested both CO and CO_2 hydrogenation as the source of methanol using their microkinetic model, with CO_2 being responsible for about 67% of the industrial methanol production.

Kinetics proposed by [42] and [25] are the most widely used today for modeling methanol synthesis processes. Some of the other kinetic models are presented in Table 2.5.

Table 2.5: Kinetic models for methanol synthesis (adapted from [14, 15]).

Operation parameters (P,T)	**Equation rates**	**Reference**
40-50 bar, 493-533 K	$r_{\mathrm{CO}\rightarrow\mathrm{CH_3OH}} = k\left(\frac{p_{CO}^{0.5}\cdot p_{\mathrm{H_2}}}{p_{\mathrm{CH_3OH}^{0.66}}} - \frac{p_{\mathrm{CH_3OH}}^{0.34}}{p_{\mathrm{CO}}^{0.5}\cdot p_{\mathrm{H_2}}\cdot K_2^*}\right)$	[47]
NA	$r_{\mathrm{CO_2}\rightarrow\mathrm{CH_3OH}} = \frac{A_1\cdot A_2\cdot A_3^{0.5}\cdot[f_{\mathrm{CO_2}}\cdot f_{\mathrm{H_2}} - \frac{f_{\mathrm{CH_3OH}}\cdot f_{\mathrm{H_2O}}}{f_{\mathrm{H_2}}^2\cdot K_{eq,\mathrm{CO_2}}}]}{(1+A_2\cdot f_{\mathrm{CO_2}})[1+A_3^{0.3}\cdot f_{\mathrm{H_2}}^{0.5}+A_4\cdot f_{\mathrm{H_2O}}/(A_3\cdot f_{\mathrm{H_2}})^{0.5}]}$ $r_{RWGS} = \frac{A_5\cdot A_2\cdot A_3^{0.5}\cdot[f_{\mathrm{CO_2}}\cdot f_{\mathrm{H_2}}^{0.5} - \frac{f_{\mathrm{CO}}\cdot f_{\mathrm{H_2O}}}{f_{\mathrm{H_2}}^{0.5}\cdot K_{eq,\mathrm{WGS}}}]}{(1+A_2\cdot f_{\mathrm{CO_2}})[1+A_3^{0.5}\cdot f_{\mathrm{H_2}}^{0.5}+A_4\cdot f_{\mathrm{H_2O}}/(A_3\cdot f_{\mathrm{H_2}})^{0.5}]}$	[58]
15-50 bar, 483-518 K	$r_{\mathrm{CO}\rightarrow\mathrm{CH_3OH}} = \frac{k_1\cdot K_{\mathrm{CO}}\cdot[f_{\mathrm{CO}}\cdot f_{\mathrm{H_2}}^{1.5} - f_{\mathrm{CH_3OH}}/(f_{\mathrm{H_2}}^{0.5}\cdot K_1^{eq})]}{(1+K_{CO}\cdot f_{\mathrm{CO}}+K_{\mathrm{CO_2}}\cdot f_{\mathrm{CO_2}})[f_{\mathrm{H_2}}^{0.5}+(K_{H2O}/k_{\mathrm{H_2}}^{0.5}\cdot f_{\mathrm{H_2O}})]}$ $r_{RWGS} = \frac{k_2\cdot K_{\mathrm{CO_2}}\cdot[f_{\mathrm{CO_2}}\cdot f_{\mathrm{H_2}} - f_{\mathrm{H_2O}}\cdot f_{\mathrm{CO}}/(K_2^{eq})]}{(1+K_{CO}\cdot f_{\mathrm{CO}}+K_{CO2}\cdot f_{\mathrm{CO_2}})[f_{\mathrm{H_2}}^{0.5}+(K_{H2O}/k_{\mathrm{H_2}}^{0.5}\cdot f_{\mathrm{H_2O}})]}$ $r_{\mathrm{CO_2}\rightarrow\mathrm{CH_3OH}} = \frac{k_3\cdot K_{\mathrm{CO_2}}\cdot[f_{\mathrm{CO_2}}\cdot f_{\mathrm{H_2}}^{1.5} - f_{\mathrm{CH_3OH}}\cdot f_{\mathrm{H_2O}}/(f_{\mathrm{H_2}}^{1.5}\cdot K_3^{eq})]}{(1+K_{CO}\cdot f_{\mathrm{CO}}+K_{\mathrm{CO_2}}\cdot f_{\mathrm{CO_2}})[f_{\mathrm{H_2}}^{0.5}+(K_{\mathrm{H_2O}}/k_{\mathrm{H_2}}^{0.5}\cdot f_{\mathrm{H_2O}})]}$	[42]
15-51 bar, 453-553 K	$r_{\mathrm{CO_2}\rightarrow\mathrm{CH_3OH}} = \frac{k_{5a}'\cdot K_2'\cdot K_3\cdot K_4\cdot K_{\mathrm{H_2}}\cdot p_{\mathrm{CO_2}}\cdot p_{\mathrm{H_2}}\cdot[1-(1/K^*)\cdot p_{\mathrm{H_2O}}\cdot p_{\mathrm{CH_3OH}}/(p_{\mathrm{CO_2}}\cdot p_{\mathrm{H_2}}^3)]}{(1+(K_{\mathrm{H_2O}}/(K_8\cdot K_9\cdot K_{\mathrm{H_2}}\cdot(p_{\mathrm{H_2O}}/p_{\mathrm{H_2}}+\sqrt{K_{\mathrm{H_2}}\cdot p_{\mathrm{H_2}}}+K_{\mathrm{H_2O}}\cdot p_{\mathrm{H_2O}}))))^3}$ $r_{RWGS} = \frac{k_1'\cdot p_{\mathrm{CO_2}}\cdot[1-K_3^*\cdot p_{\mathrm{H_2O}}\cdot p_{\mathrm{CO}}/(p_{\mathrm{CO_2}}\cdot p_{\mathrm{H_2}})]}{(1+(K_{\mathrm{H_2O}}/(K_8\cdot K_9\cdot K_{\mathrm{H_2}}\cdot(p_{\mathrm{H_2O}}/p_{\mathrm{H_2}}+\sqrt{K_{\mathrm{H_2}}\cdot p_{\mathrm{H_2}}}+K_{\mathrm{H_2O}}\cdot p_{\mathrm{H_2O}}))))}$	[25]
49 bar, 473-548 K	$r_{\mathrm{CO_2}\rightarrow\mathrm{CH_3OH}} = \frac{k_M\cdot p_{\mathrm{CO_2}}\cdot p_{\mathrm{H_2}} - p_{\mathrm{CH_3OH}}\cdot p_{\mathrm{H_2O}}/[K_M\cdot p_{\mathrm{H_2}}^2]}{[1+K_{\mathrm{CO_2}}\cdot p_{\mathrm{CO_2}}+K_{\mathrm{H_2O}}\cdot p_{\mathrm{H_2O}}^2]}$ $r_{RWGS} = \frac{k_R\cdot p_{\mathrm{CO_2}}\cdot p_{\mathrm{CO}} - p_{\mathrm{H_2O}}\cdot p_{\mathrm{H_2O}}/[K_M\cdot p_{\mathrm{H_2}}^2]}{[1+K_{\mathrm{CO_2}}\cdot p_{\mathrm{CO_2}}+K_{\mathrm{H_2O}}\cdot p_{\mathrm{H_2O}}^2]}$	[53]
50-90 bar, 503-613 K	$r_{\mathrm{CO}\rightarrow\mathrm{CH_3OH}} = \frac{k_{r_{\mathrm{CO}\rightarrow\mathrm{CH_3OH}}'}'\cdot K_{\mathrm{CO}}\cdot[f_{\mathrm{CO}}\cdot f_{\mathrm{H_2}}^{0.5} - f_{\mathrm{CH_3OH}}/(f_{\mathrm{H_2}}^{0.5}\cdot K_{Pr_{\mathrm{CO}\rightarrow\mathrm{CH_3OH}}})]}{(1+K_{\mathrm{CO}}\cdot f_{\mathrm{CO}})(1+K_{\mathrm{H_2}}^{0.5}\cdot f_{\mathrm{H_2}}^{0.5}+K_{\mathrm{H_2O}}\cdot f_{\mathrm{H_2O}}}$ $r_{RWGS} = \frac{k_{RWGS}'\cdot K_{\mathrm{CO_2}}\cdot[f_{\mathrm{CO_2}}\cdot f_{\mathrm{H_2}} - f_{\mathrm{CO}}\cdot f_{\mathrm{H_2O}}/K_{Pr_{RWGS}}]}{(1+K_{\mathrm{CO}}\cdot f_{\mathrm{CO}})(1+K_{\mathrm{H_2}}^{0.5}\cdot f_{\mathrm{H_2}}^{0.5}+K_{\mathrm{H_2O}}\cdot f_{\mathrm{H_2O}})}$ $r_{\mathrm{CO_2}\rightarrow\mathrm{CH_3OH}} = \frac{k_{r_{\mathrm{CO_2}\rightarrow\mathrm{CH_3OH}}'}'\cdot K_{\mathrm{CO_2}}\cdot[f_{\mathrm{CO_2}}\cdot f_{\mathrm{H_2}}^{1.5} - f_{\mathrm{CH_3OH}}\cdot f_{\mathrm{H_2O}}/(f_{\mathrm{H_2}}^{1.5}\cdot K_{Pr_{\mathrm{CO_2}\rightarrow\mathrm{CH_3OH}}})]}{(1+K_{\mathrm{CO}}\cdot f_{\mathrm{CO}})(1+K_{\mathrm{H_2}}^{0.5}\cdot f_{\mathrm{H_2}}^{0.5}+K_{\mathrm{H_2O}}\cdot f_{\mathrm{H_2O}}}$	[69]
52 bar, 513 K	$r_{\mathrm{CO_2}\rightarrow\mathrm{CH_3OH}} = \frac{k_3\cdot p_{\mathrm{H_2}}\cdot(1-\frac{p_{\mathrm{H_2O}}\cdot p_{\mathrm{CH_3OH}}}{K_{p(\mathrm{CH_3OH}}\cdot p_{\mathrm{H_2}}^3\cdot p_{\mathrm{CO_2}}})}{(1+K-2\cdot p_{\mathrm{H_2O}}+K-2\cdot p_{\mathrm{H_2O}}/(K_1\cdot p_{\mathrm{CO_2}})}$	[66]

2.2.4. Reactor types for methanol production

Since the reactions for methanol synthesis are exothermic in general, any reactor chosen must have effective temperature control to maintain the temperature and maximize the yield per pass. A simplified flow diagram for methanol synthesis is presented in Figure 2.3.

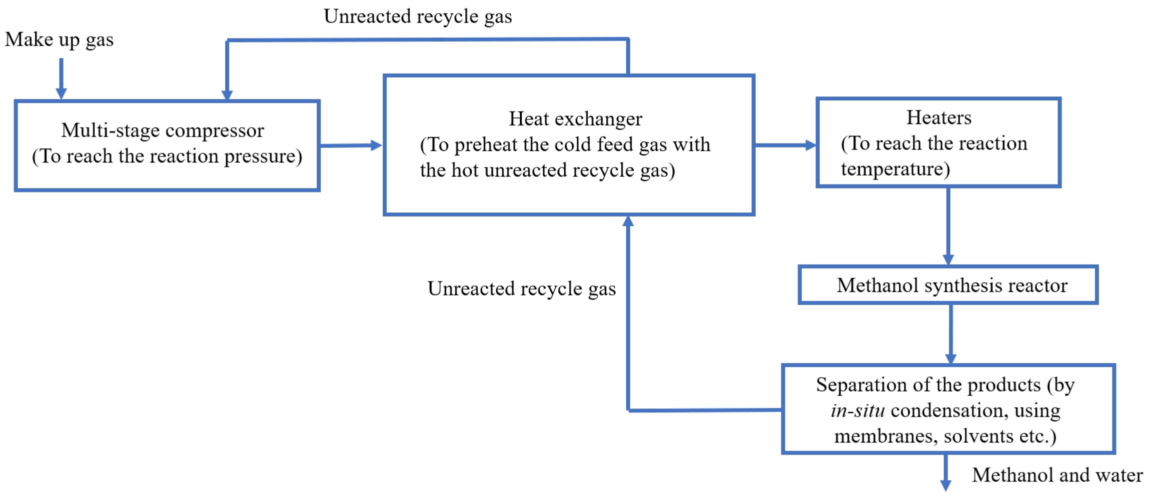
Unreacted recycle gas
Make up gas
Multi-stage compressor
(To reach the reaction pressure)
Heat exchanger
(To preheat the cold feed gas with the hot unreacted recycle gas)
Heaters
(To reach the reaction temperature)
Methanol synthesis reactor
Unreacted recycle gas
Separation of the products (by *in-situ* condensation, using membranes, solvents etc.)
Methanol and water

Figure 2.3: Simplified flow diagram for methanol synthesis reactors. The feed gas is first compressed after which it exchanges heat with the unreacted recycled gas. The gas mixture is then heated to the reaction temperature and fed to the reactor. The products are then separated using membranes, solvents or *in-situ* condensation while the unreacted gas is recycled back [14].

The reactors for methanol synthesis fall into two major categories-adiabatic and isothermal, which are summarized in Table 2.6 and in Table 2.7 respectively with the liquid reactor technologies presented in Table 2.8 [15].

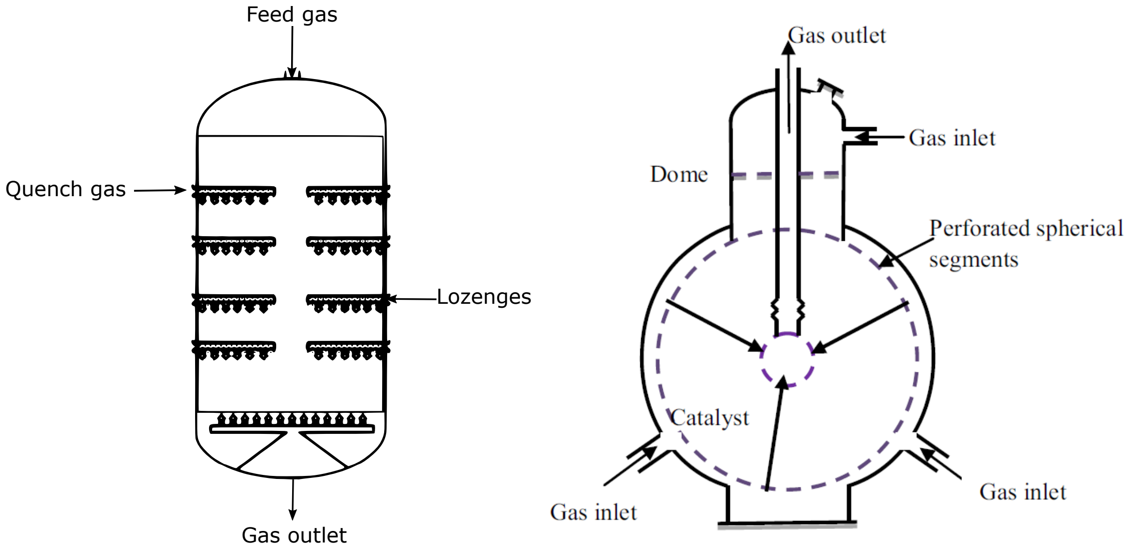
Feed gas
Quench gas
Lozenges
Gas outlet
Gas outlet
Gas inlet
Dome
Perforated spherical segments
Catalyst
Gas inlet
Gas inlet

(a) Quench reactor [15, 73] **(b)** Kellogg, Brown and Root reactor [15, 74]

Figure 2.4: Examples of adiabatic reactors used for methanol synthesis: (2.4a) Quench reactor and (2.4b) Kellogg, Brown and Root reactor.

Table 2.6: Adiabatic reactor technologies for methanol synthesis.

Reactor	Features	Advantages	Reference(s)
Quench reactor (ICI) (Figure 2.4a)	1.Multiple adiabatic beds in a shell 2.Catalyst loaded in one bed 3.Reaction temperature controlled using syngas feed from lozenges	1.Simple and reliable design 2.Easy catalyst loading and unloading 3.Heat of reaction recovered	[15, 73]
Kellogg, Brown and Root reactor (Figure 2.4b)	1.Series of adiabatic, fixed bed reactors 2.Catalyst placed in annulus of two shells	1.Installation, manufacturing cost lower due to low wall thickness 2.Less recycle stream needed 3.Low pressure drop due to radial syngas flow	[15, 74]
Advanced Reactor Concept (Casale) (Figure 2.5a)	Adiabatic bed section separated using distribution plates	1. Efficient and reliable design 2. 20 % increase in yield compared to quench reactors	[15]
Collect-Mix-Distribute (CMD) (Used by Haldor Topsoe) (production up to 10000 tonnes/d)	1.Series of catalyst beds separated by vertical beams 2.Syngas fed at the bottom travels upwards and mixes with cold feed at the top, and then travels downwards	1.Effective temperature control achieved 2.Improved carbon conversion and catalyst life	[15]
MRF-Z (developed by Toyo Engineering Corporation) (Figure 2.5b)	1. Multi-stage radial flow reactor 2.Catalyst loaded in concentric beds	1. Easy scale up 2. Less pressure drop due to radial flow 3. Efficient heat recovery	[15]

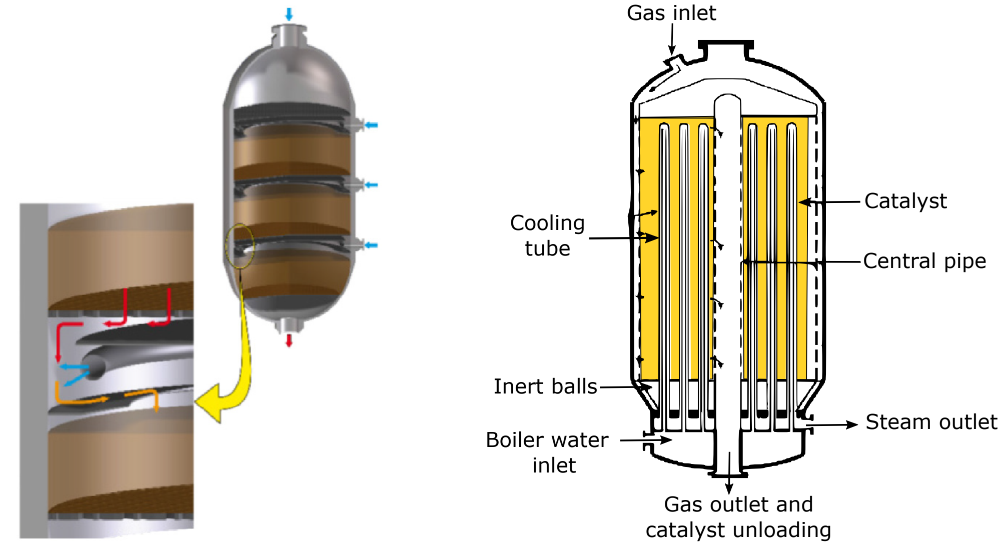
Gas inlet
Cooling tube
Catalyst
Central pipe
Inert balls
Steam outlet
Boiler water inlet
Gas outlet and catalyst unloading

(a) Advanced Reactor Concept [15] **(b)** MRF-Z reactor [15]

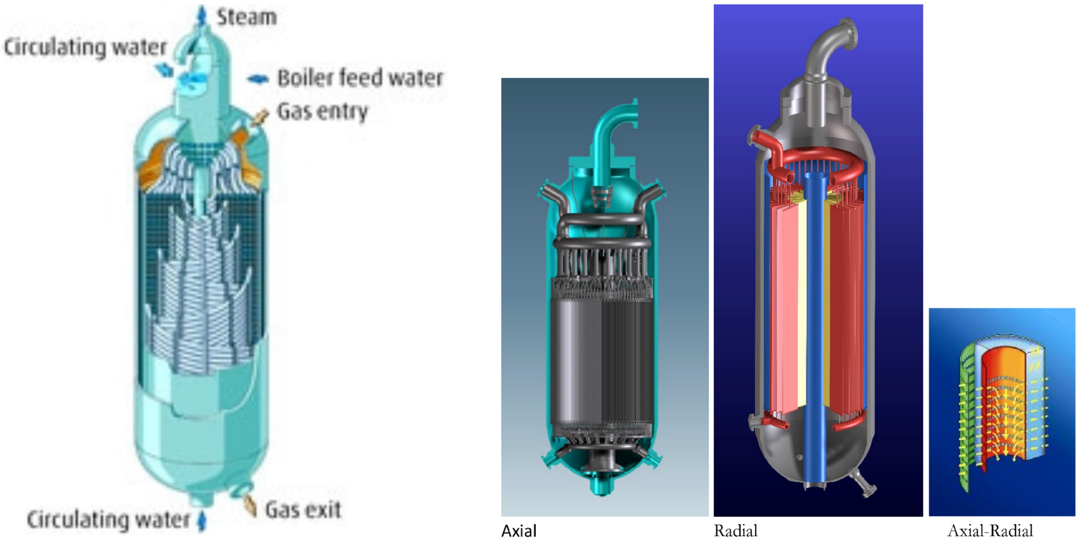
Steam
Circulating water
Boiler feed water
Gas entry
Circulating water
Gas exit
Axial
Radial
Axial-Radial

(c) Linde isothermal reactor [15, 75] **(d)** Isothermal Methanol Converter [15]

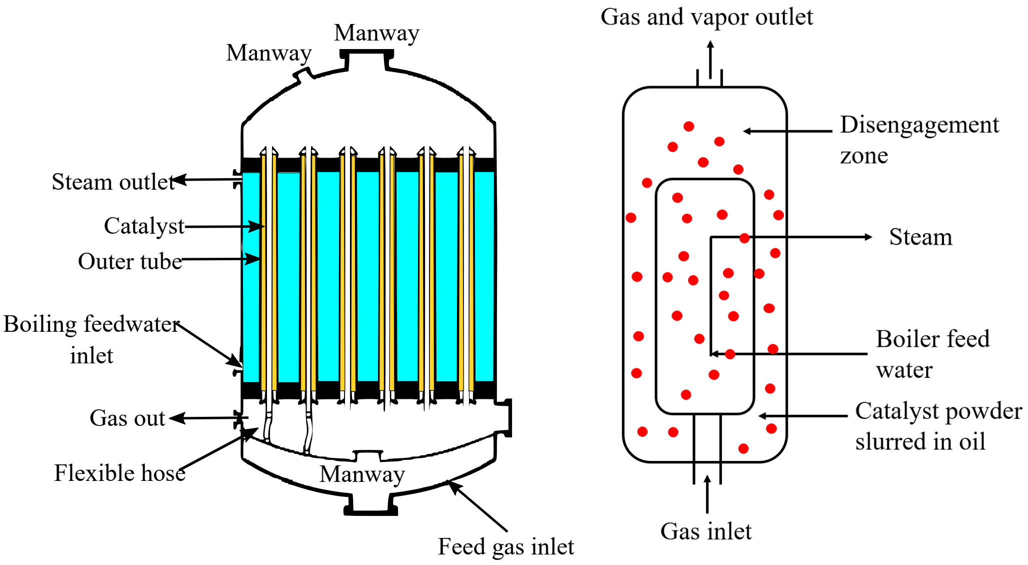
Manway
Manway
Steam outlet
Catalyst
Outer tube
Boiling feedwater inlet
Gas out
Flexible hose
Manway
Feed gas inlet
Gas and vapor outlet
Disengagement zone
Steam
Boiler feed water
Catalyst powder slurred in oil
Gas inlet

(e) Mitsubishi Reactor (Isothermal) [15, 76] **(f)** LPMEOH™reactor (Liquid) [15, 77]

Figure 2.5: Examples of reactors used for methanol synthesis.

Table 2.7: Isothermal reactors used for methanol synthesis.

Reactor	Features	Advantages	Reference(s)
Linde reactor (Figure 2.5c)	Consists of helical tubes in catalyst bed which carry the cooling fluid	1.Reduced thermal stresses due to helical tubes 2.Longer material life, efficient heat transfer, optimum reaction temperature 3.Reduced reaction and catalyst volume due to good heat transfer	[15, 75]
Lurgi reactor	1.Shell and tube design with catalyst inside the tubes and boiling water on the outside 2.Reaction temperature controlled by water pressure	1.Good temperature control 2.High yield and low recycle ratio 3.Availability of high pressure steam which can be used in other applications	[15, 78–80]
Mitsubhishi Gas Chemical and Mitsubhishi Heavy Industry (MGC/MHI) superconverter (Figure 2.5e)	1.Shell and tube design with double walled tubes 2.Catalyst loaded in tube annulus 3.Gas flows through the inside tube and enters the catalyst bed 4.Cooling water on the outside maintains the reaction temperature	1.High conversion per pass (14% methanol production) 2.Safe operation and high mechanical stability	[15, 76]
Isothermal Methanol Converter (IMC) (developed by Casale SA) (Figure 2.5d)	1.Series of plates arranged radially surrounded by the catalyst 2.Cooling fluid flows inside the plates to maintain reaction temperature	1.Good temperature and reaction rate control 2.Easy loading and unloading of catalysts 3.Small pressure drop	[15]
Fluidized bed converter technology (Developed by NEDO)	1.Gas fed into the reactor bottom fluidizes the catalyst bed 2.Catalyst temperature controlled using cooling pipes	1.Good temperature and reaction rate control 2.Easy loading and unloading of catalysts	[15]

Table 2.8: Summary of liquid based reactors used for methanol synthesis.

Reactor	Operation Principle	Advantages	Reference(s)
Slurry liquid phase technology (LPMEOH™) (developed by Air Products) (Figure 2.5f)	The reactor consists of catalyst particles suspended in a bed of inert oil, with the gas and liquid flowing co-currently	1.High conversion per pass with significantly less recycle 2.Heat of reaction recovered and reused 3.Can be operated as a continuous or a batch process 4.High production capacity of 3E5 L/d of methanol	[15, 77]
Brookhaven National Laboratory, USA	The reactor produced methanol via the methyl formate pathway	1.Low temperature and pressure of operation 2.High conversions of about 90% leading to lower recycles	[15]
Pittsburg University	Co-current slurry based process using the methyl formate pathway	1.Low temperature operation (170-200 °C) 2.High conversions and high selectivity achieved	[15]

One of the major drawbacks of liquid based reactors compared to the gas based ones is the quick deactivation of catalysts. This is due to decomposition of oil used to suspend the catalyst and also because of carbon deposition. [81, 82].

Even though some of the reactor designs mentioned in Tables 2.6, 2.7 and 2.8 have the advantage of reduced feed recycle, their equilibrium yield of methanol is still low (see Figure 2.1). One way of improving this yield is by shifting the equilibrium towards the product side using either membranes, solvents, maintaining a temperature gradient or by in-situ condensation (also called ”separation enhanced equilibrium approach”) [16–18, 83–90]. As mentioned by [16], using membranes or solvents necessitates the use of extra equipment and increases the processing cost. Very high pressures are also not suitable to increase the yield as they require the use of special high pressure resistant equipments and add to the operating costs.

2.2.5. Brilman Reactor

Brilman et al. [16] proposed a method for driving the equilibrium to the right in the reactor by in-situ condensation of products. The authors calculated the dew point temperatures of the gases at different reaction temperatures by varying the pressure. According to Figure 2.6, if the reaction temperature is high (523 K), then a very high pressure (>150 bar) is required to condense the products at the reaction temperature. If the reaction temperature is kept low (473 K), then a decrease of temperature is needed in the reactor to achieve condensation (dew point temperature of 423 K), if the reactor is operated at low pressure (50 bar). Therefore, the authors chose 50 bar as the pressure of operation.

At 473 K reaction temperature, the temperature difference available for driving the flow (reaction temperature - dew point temperature) is 50 K, which increases when the reaction temperature is increased (about 80.27 K for 498 K and 112.57 K for 523 K). The authors then postulated that a minimum temperature difference of 70 K is required to drive the flow (50 K difference for the 473 K case plus an addition 20 K temperature difference is desired to ensure effective heat and mass transfer in accordance with practical condensation manuals [91]).

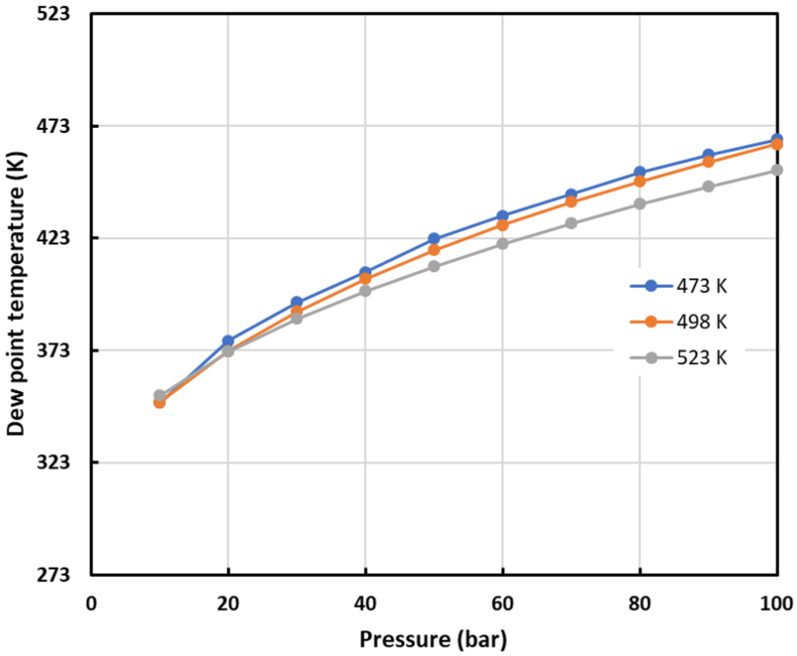

Figure 2.6: Dew point temperature of the gas mixture as a function of the reaction pressure and temperature (H_2:CO_2=3:1). At a high temperature (523 K), a very high pressure is required to condense the gases at the reaction temperature. At lower pressures (50 bar) and temperatures (473 K), a decrease of temperature is required to initiate condensation. At these pressures, a temperature gradient can be achieved in the reactor to drive the flow.

The reactor design of [16] is presented in Figure 2.7. The reaction zone consists of two tubes with the catalyst placed in the tube annulus. A gas buffer is filled with the feed gas (mixture of CO_2 and H_2 in the volume ratio 1:3) upto a pressure of 100 bar and is connected to the reactor inlet. The reactor itself is operated in a semi-continuous mode, keeping the pressure in the reactor constant at 50 bar. From the buffer vessel, the feed flows through the inside tube into the annulus region containing the catalyst. 5 mm catalyst pellets are used, with a catalyst bed volume of 97713 mm^3. The reaction temperature is maintained using a temperature controlled heating jacket. After reacting on the catalyst bed, the products are condensed at the top of the reactor and collected in a collection vessel. The condensation is achieved by flowing tap water through cooling coils. The condensation temperature was varied between 358 K and 413 K for the duration of the experiment (which is lower than the dew point of approximately 423 K at a reaction temperature of 483 K and pressure of 50 bar), while the catalyst outlet temperature was set at 483 K. Hence a temperature difference of atleast 70 K was maintained between the reaction and the condensation zone. To improve circulation, a fan was placed at the bottom of the vessel. This concept was named as Liquid Out Gas In Concept (LOGIC) and it provided a simple way to achieve high carbon conversion and methanol yield, while negating the external recycle of products and circumventing thermodynamic equilibrium limitations.

The authors performed two sets of experiments-one varying the condensation temperature and the other varying the fan speed. In the former case, lowering the condensation temperature increased the yield of methanol as more liquid product was condensed per pass leading to higher carbon conversion. The methanol productivity was measured in terms of mmole $CH_3OH/g_{cat}/h$ and was found to be about 4.3 mmole $CH_3OH/g_{cat}/h$ for a condenser temperature of 363 K compared to about 19.4 mmole $CH_3OH/g_{cat}/h$ for an industrial scale reactor (see Appendix C for the calculation procedure) [21]. The industrial yield was higher as the reactor was operated at a higher pressure of 69.7 bar with a higher feed flow rate and a feed temperature of 225 °C.

When the fan was used, productivity increased at slow fan speeds (around 7.5 mmole $CH_3OH/g_{cat}/h$) as a result of improved circulation, but higher speeds decreased the catalyst bed temperature leading to lower productivity.

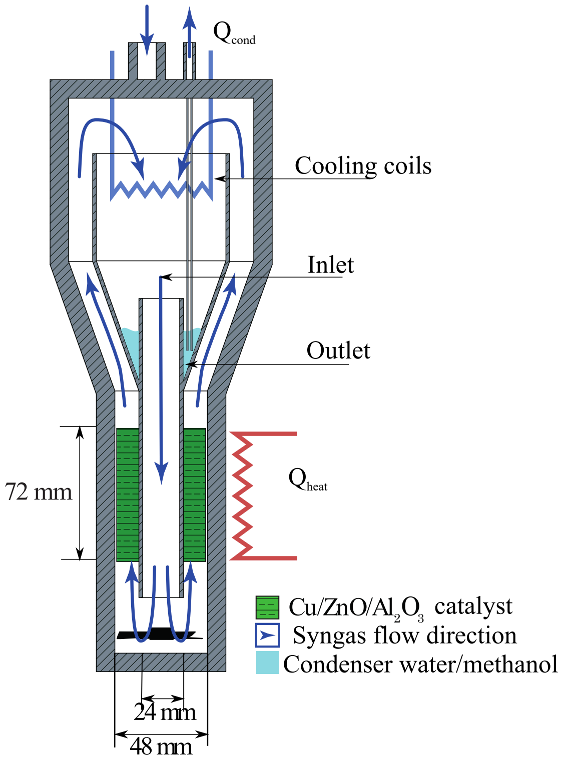

Figure 2.7: Design of the reactor proposed by [16]. The feed gas enters through the inlet and flows through the inner tube before passing through the tube annulus which contains the catalyst. The catalyst bed is maintained at the reaction temperature using an oven. Methanol and water mixture are then condensed at the top using a cooling coil. The liquids formed are tapped out at regular intervals.

The authors identified the feed of CO_2 and H_2 as the more efficient route to produce methanol than using CO and H_2. This was because although the minimum energy required to remove oxygen from CO_2 and H_2O is the almost the same (Eq 2.9 and Eq 2.10, respectively), water electrolysis is much more advanced and efficient than the former process [16, 92]. Several methanol plants around the world are currently working on CO_2 to methanol conversion (Table 2.9).

$$\mathrm{CO_2} \rightleftharpoons \mathrm{CO} + 1/2\mathrm{O_2}, \qquad \Delta H_{298\,\mathrm{K}} = 283\ \mathrm{kJ/mole} \tag{2.9}$$

$$\mathrm{H_2O} \rightleftharpoons \mathrm{H_2} + 1/2\mathrm{O_2}, \qquad \Delta H_{298\,\mathrm{K}} = 286\ \mathrm{kJ/mole} \tag{2.10}$$

Inspite of the advantage of almost complete carbon conversion to methanol and no external recycle, this reactor was comparatively energy inefficient (The energy input was about three times the higher heating value (HHV) of methanol) [16]. In order to improve this efficiency, Lammerink in his MSc thesis proposed the use of a heat exchange system to transfer heat between the reaction and the condensation zone [93]. Since the driving force for flow in this reactor is the temperature difference (and ultimately, the density difference) between the two zones, Lammerink evaluated some factors which could improve the efficiency of the system while increasing the mass flux of the fluid at the same time. These parameters are given in Table 2.10.

Table 2.9: Plants working on CO_2 to methanol conversion.

Plant	Features	Capacity	References
Laboratory pilot plant, Japan	High methanol selectivity (about 99.8%)	50 kg/day	[7, 11, 26]
Carbon Recycling International, Iceland	CO_2 captured from exhaust of geothermal/aluminium smelting plants H2 produced from water electrolysis using geothermal energy	10 (metric) MT/day	[7, 11]
Mitsui Chemicals	CO_2 obtained as an industrial by-product H_2 obtained from photochemical splitting of water	100 (metric) MT/year	[7, 11, 94]
Blue Fuel Energy, Canada	CO_2 obtained from natural gas H_2 produced via electrolysis using hydroelectricity	2.5 million liters/day	[7, 11, 95]
Sunfire, Germany	CO_2 obtained from direct air capture or industrial emissions; H_2 obtained from electrolysis using renewable energy CO_2 and H_2 will be converted to different fuels using a fuel cell	Proposed (8000 tonnes/year)	[7, 11, 96]

Table 2.10: Parameters affecting the mass flux [93].

Parameter	Effect on mass flux	Reason
Length	Increases and then stabilizes	Additional frictional losses decrease with increasing length. The mass flux will increase till these losses become negligible and then become constant.
Diameter	Increases and then stabilizes	Initial increase is due to reducing wall friction per unit volume. Then this friction becomes negligible as compared to other losses like internal friction because of developing flow.
Pressure	Increases	Pressure is directly correlated with density.
Absolute temperature difference (ΔT)	Increases	Increasing absolute temperature difference increases the density difference.
Average temperature difference ($\Delta(<T>)$)	Decreases	$\Delta\rho = \frac{1}{T_c+\Delta(<T>)} - \frac{1}{T_h+\Delta(<T>)}$. The first term in the denominator decreases faster than the second term with increasing $\Delta(<T>)$ leading to reduced density difference.

If the pressure of the system is kept constant, then increasing the absolute temperature difference between the heating and the cooling zones increases the mass flux (observe Table 2.10). Based on this result, Lammerink proposed two heat exchanger designs for improving the mass flux.

Internal heat exchange can be achieved using plate and fin or plate and shell heat exchangers. However, having such an arrangement would decrease the difference in average temperature between the two zones and thus lead to lower mass flux (see Table 2.10), in addition to increasing the frictional losses due to increased heat transfer area. External heat exchangers on the other hand can increase the mass flux by increasing the absolute temperature difference between the condenser and reaction zones through simultaneous cooling of the hot fluid and heating of the cold fluid. According to the authors, an external cooling fluid would be required to transfer heat in this case [93].

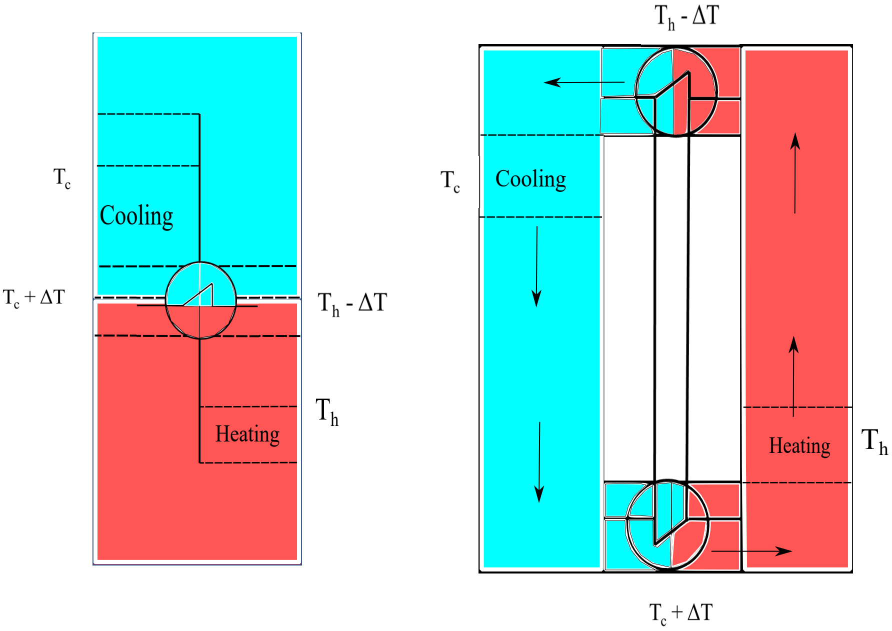

Figure 2.8: Internal heat exchange (shown on the left) and external heat exchange design (shown on the right) with arrows showing the syngas flow direction. An internal heat exchange system would decrease the average temperature difference between the heating and the cooling zones, decreasing the mass flux. An external heat exchange system on the other hand increases the absolute temperature difference between the two zones, increasing the mass flux. The latter is used in this thesis.

3

Experiments

This chapter describes the experimental setup used for the project. Section 3.1 details the MATLAB convection model and the process model in COCO to dimensionalize the reactor. This work was done as part of the internship project of the author. Section 3.2 describes the various components in the experimental setup. Section 3.3 discusses the operating procedure of the reactor while Section 3.4 presents the test plan of the experiments.

3.1. Reactor Design and Fabrication

ZEF specified 135 grams per day as the production capacity of the methanol synthesis reactor. Assuming that one day meant five hours of operation, the methanol production rate should be close to 27 grams per hour. Apart from the methanol production rate, the outside dimensions too were specified as it needed to fit on the back of a solar panel.

A process model of the reactor was then made in COCO (CAPE-OPEN to CAPE-OPEN-an open source process simulator similar to Aspen Plus™) [2]. The reactor was simulated as a plug flow reactor using the kinetics of Bussche and Froment [25]. The dimensions of the catalyst bed were varied until the methanol production rate from the reactor was close to the desired value of 27 g/h. The condenser wall temperature was kept at 40 °C and the reaction wall temperature at 210 °C to have enough driving force for the flow.

A convection model was built in MATLAB and the heat needed to be released to maintain the temperature difference of 170 K was calculated. Using the catalyst bed dimensions obtained above, the area required for heat transfer was obtained using the MATLAB model. Since the area was quite large compared to the outer dimensions available, it was decided to have small flow channels in the blocks to enhance their area. This area was divided into six blocks made of aluminium. Six blocks were chosen as they would be easier to manufacture and to assemble considering the number of seals that would be required to maintain the leak tightness of the system.

Hence, in the end, it was decided to use six blocks to enhance the surface area for heat transfer along with the block where the reaction would take place (reaction zone) and the block to condense the products (condensation zone).

This design of the reactor and its fabrication was done during the internship project of the author.

3.2. Experimental System

Before describing different components, a process and instrumentation diagram of the experimental system is first presented.

3.2.1. Process and Instrumentation Diagram

The experimental system consists of the reactor assembly, gas cylinders, electrical and data logging circuit and the apparatus used to analyze the gas and liquid components (density measurement apparatus and the gas chromatograph). The process and instrumentation diagram for the experiment is presented in Figure 3.1.

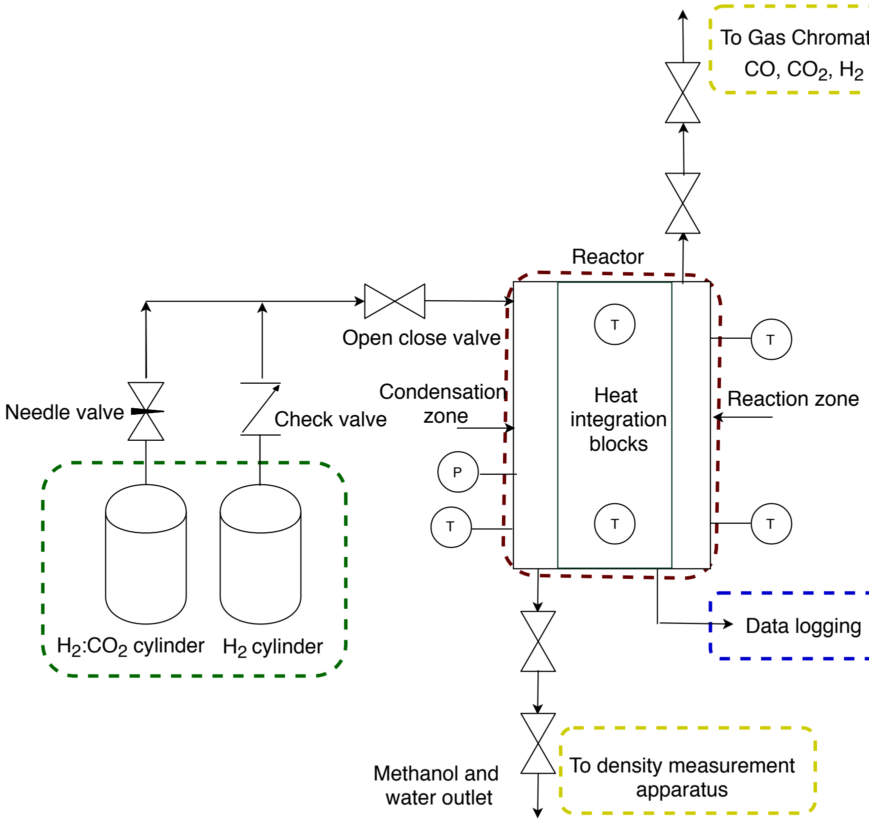
To Gas Chromatograph
CO, CO_2, H_2
Reactor
Open close valve
T
T
Heat integration blocks
Condensation zone
Reaction zone
Needle valve
Check valve
P
T
T
T
H_2:CO_2 cylinder
H_2 cylinder
Data logging
Methanol and water outlet
To density measurement apparatus

Figure 3.1: Process and instrumentation diagram of the methanol synthesis reactor setup. The gas cylinders (highlighted in green), the reactor (in red), the data logging circuit (in blue) and the instruments used for analysis (in yellow) can be clearly seen.

3.2.2. Reactor

Modified Brilman Reactor

As discussed in Section 2.2.5, Brilman et al [16] demonstrated a reactor concept where the external recycle of the feed stream was negated and complete carbon conversion was achieved using in-situ condensation of products (see Figure 2.7). Since the reactor was comparatively low on energy efficiency, a new reactor design was developed by the author to improve the efficiency of the system by adding heat integration blocks between the reaction and the condensation zones. The presence of heat integration blocks would enable the hot fluid flowing to the condenser to cool down by heating the cold fluid going to the reaction zone. This design, although similar to one proposed by Lammerink [93], was developed independently. This updated version of the reactor was called the Modified Brilman Reactor (MBR). MBR coupled the advantages of the natural circulation loop of the Brilman reactor with a heat integration system. The schematics of the Brilman reactor and MBR are presented in Figure 3.2.

Reactor Assembly

The reactor assembly is shown in Figure 3.3, while Figure 3.4 shows the reactor assembly as used in the experiment.

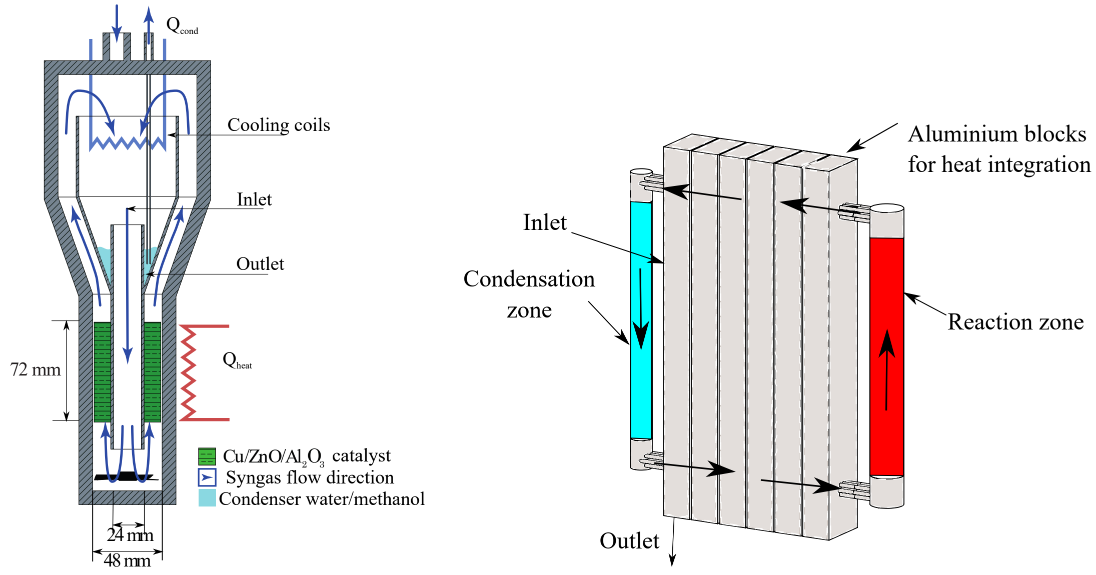
Q_cond
Cooling coils
Inlet
Outlet
72 mm
Q_heat
Cu/ZnO/Al2O3 catalyst
Syngas flow direction
Condenser water/methanol
24 mm
48 mm
Aluminium blocks
for heat integration
Inlet
Condensation
zone
Reaction zone
Outlet

(a) Brilman reactor

(b) Modified Brilman Reactor (MBR)

Figure 3.2: Schematic of the Brilman reactor (3.2a) and the MBR (3.2b) as used in this thesis.

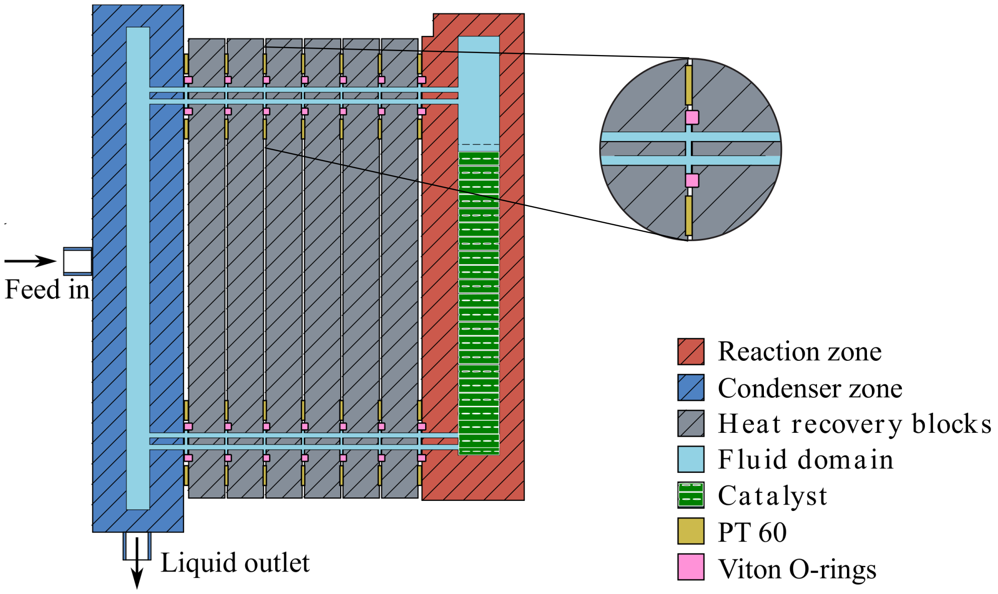
Feed in
Liquid outlet
Reaction zone
Condenser zone
Heat recovery blocks
Fluid domain
Catalyst
PT 60
Viton O-rings

Figure 3.3: Schematic of the complete reactor assembly. The six heat integration blocks are placed between the reaction zone on the right and the condensation zone on the left. Viton™ O-rings and PT 60 papers are placed between each block to provide effective sealing and reduce axial conduction of heat respectively.

As can be seen from Figure 3.4, the entire assembly containing the reaction zone, heat integration blocks and the condenser is mounted at a height of 20 cm on a wooden base using two support plates (and fixed using bolts). Such a mounting makes sluicing of liquid components easier using gravity. Glass wool is used as the insulation material since it can withstand temperatures up to 250 °C and has a very low thermal conductivity of 0.04 W/m-K [97]. All components except the condenser (the leftmost block in Figure 3.4) are insulated.

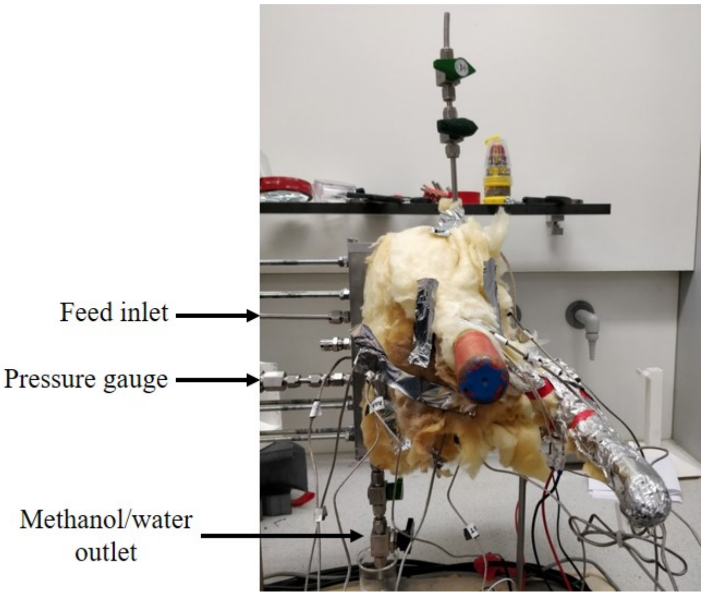
Feed inlet
Pressure gauge
Methanol/water outlet

Figure 3.4: Reactor assembly as used in the experiment. Glass wool is used as the insulation material. The thermocouple connections can be clearly seen. The feed input is from the left and the methanol and water mixture is tapped from the bottom using the two open close valves.

Reaction zone

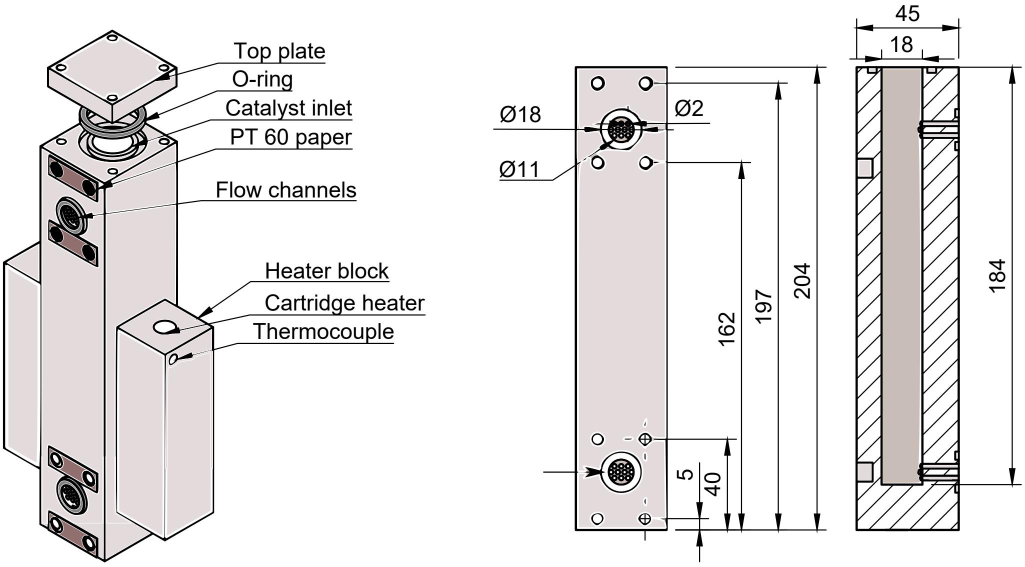
Top plate
O-ring
Catalyst inlet
PT 60 paper
Flow channels
Heater block
Cartridge heater
Thermocouple
Ø18
Ø2
Ø11
45
18
162
197
204
184
5
40

(a) Isometric view **(b)** Front and sectional view

Figure 3.5: Isometric view of the reaction zone (left) and front and sectional view (on the right). The reaction zone consists of a cylindrical channel where the catalyst in inserted. All the dimensions are in mm.

The reaction zone (Figure 3.5) is a cylindrical channel drilled inside an aluminium block. The channel is drilled from the top and provides an opening to feed the catalyst pellets. The top is sealed using a Viton^{TM} O-ring and covered with a plate of aluminium. Viton^{TM} is used as the material for O-rings as it has a "fair" compatibility with methanol [98] and can withstand temperatures up to 230 °C [99]. Two cartridge heaters (80/20 NiCr heated wire, the maximum operating temperature of 400 °C, sourced from TC Direct, Netherlands) are placed inside two small aluminium blocks (heater blocks) which are then fixed on either side of the reaction zone using a clamp to provide uniform heating to the system. K-type thermocouples (sourced from TC Direct; maximum operating temperature 1024 °C; the accuracy of ± 1.5 °C) are used to measure the temperature of the heaters and at the top and bottom section of the reaction zone.

Small flow channels in the block (at the top and bottom) provide an increased surface area for heat transfer to the fluid. Two Viton^{TM} O- rings are placed in the groove surrounding these channels to provide effective sealing. Four pieces of paper (PT 60) are placed near the bolt holes to reduce the axial conduction of heat between the blocks. The dimensions of the various components in the reaction zone summarized in Table B.1 in the appendix.

The reaction zone is filled with $Cu/ZnO/Al_2O_3$ catalyst used in this experiment, up to a height of 14 cm (just below the flow channels at the top). This catalyst is the most widely used in the industry for methanol synthesis because of its high methanol selectivity and low temperature operation (see Section 2.2.2). The catalyst is sourced from Riogen, USA and is in the form of cylindrical pellets of 5 mm diameter and 6 mm height (see Figure 3.6) [100].

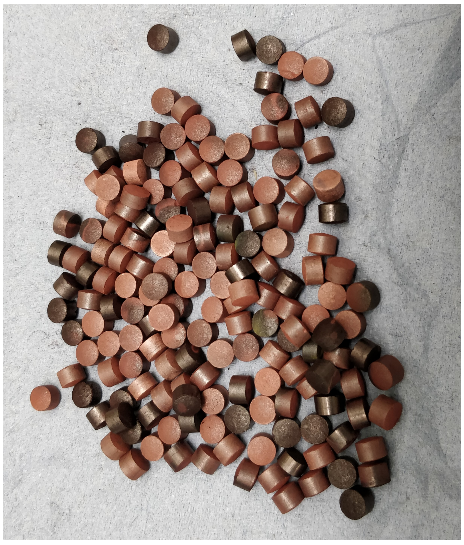

Figure 3.6: Catalyst pellets as sourced from the manufacturer (The red colour of some of the pellets is due to prior reduction with H_2).

Heat integration blocks

The heat integration blocks (Figure 3.7) like the reaction zone, have flow channels at the top and bottom of 2 mm diameter each. The blocks are solid and provide means for achieving heat integration. Aluminium is used as the block material because of its high thermal conductivity, light weight and ease of machining.

Thermocouples placed at the top and bottom of each block provide means for estimating this heat transfer. Like in the reaction zone, Viton^{TM} O-rings are placed around the flow channels for sealing purposes. The relevant dimensions of the block are summarized in Table B.2 in the appendix.

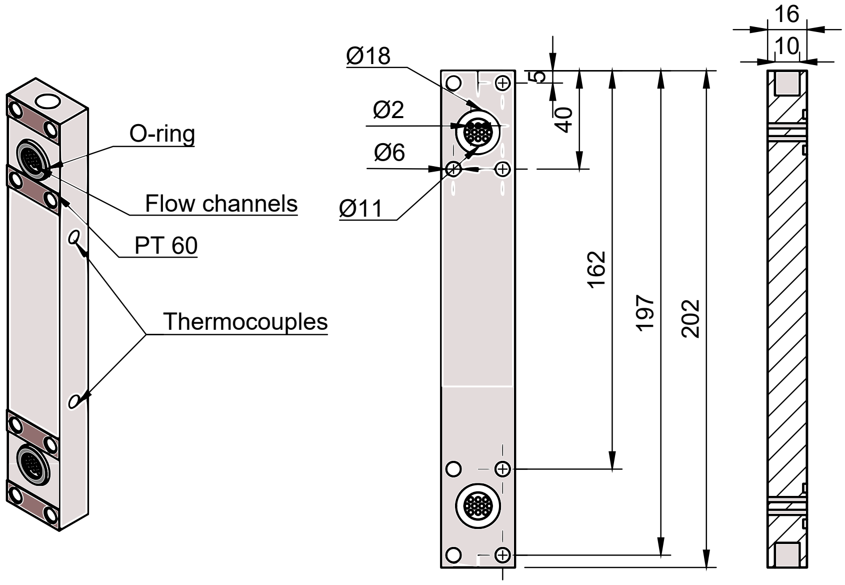
O-ring
Flow channels
PT 60
Thermocouples
Ø18
Ø2
Ø6
Ø11
5
40
162
197
202
16
10

Figure 3.7: Schematic of the heat integration block with the isometric view on the left, the front view in the middle and the sectional view on the right. All the dimensions are in mm.

Condensation zone

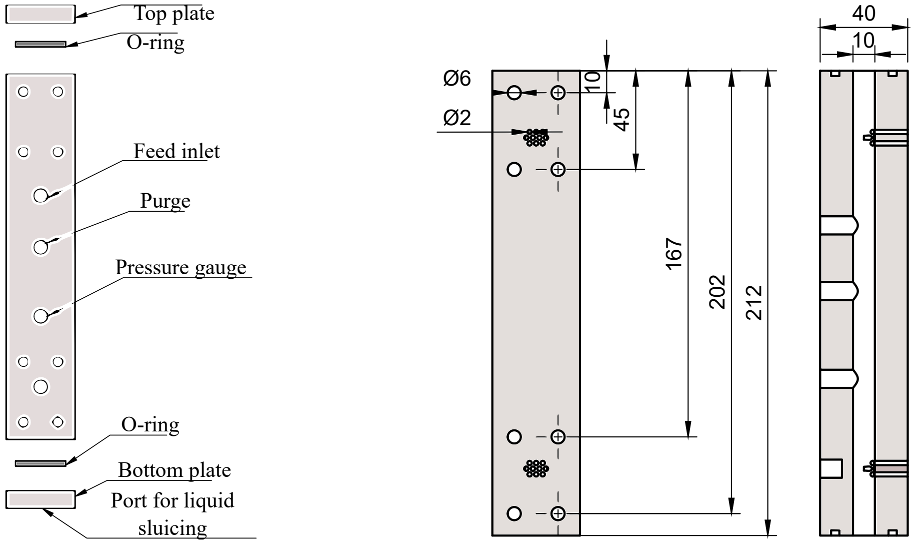
Top plate
O-ring
Feed inlet
Purge
Pressure gauge
O-ring
Bottom plate
Port for liquid sluicing
Ø6
Ø2
10
45
167
202
212
40
10

(a) Back view **(b)** Front and sectional view

Figure 3.8: Condenser block.

The condenser block (Figure 3.8) has a cylindrical channel drilled through which serves to condense the methanol and water mixture for collection at the bottom port. One side of the condenser has 2 mm flow channels at the top and bottom, while the other side has holes for mounting the pressure sensor (ADZ-SML-37.0 with an operating range of -1 to 50 bar and accuracy of ± 1E-2 bar), purge valve (Swagelok; maximum operating pressure 275 bar) and the connections for the inlet feed.

The methanol and water mixture is sampled from the bottom using a combination of two open-close valves (see Figure 3.1). Like the reaction zone, this block is also sealed at the top and bottom using Viton^{TM} O-rings and aluminium plates of 10 mm thickness. The relevant dimensions of the condensation zone are summarized in Table B.3 in the appendix.

3.2.3. Gas cylinders

Two gas cylinders (sourced from Linde, Netherlands) are used in this experiment-one of pure H_2 and the other containing the feed gas (24.9 ± 0.1 vol% of CO_2 in H_2). The pure H_2 cylinder is used during the activation of the catalyst, while the feed gas is used to carry out the reaction.

3.2.4. Electrical circuits and data logging

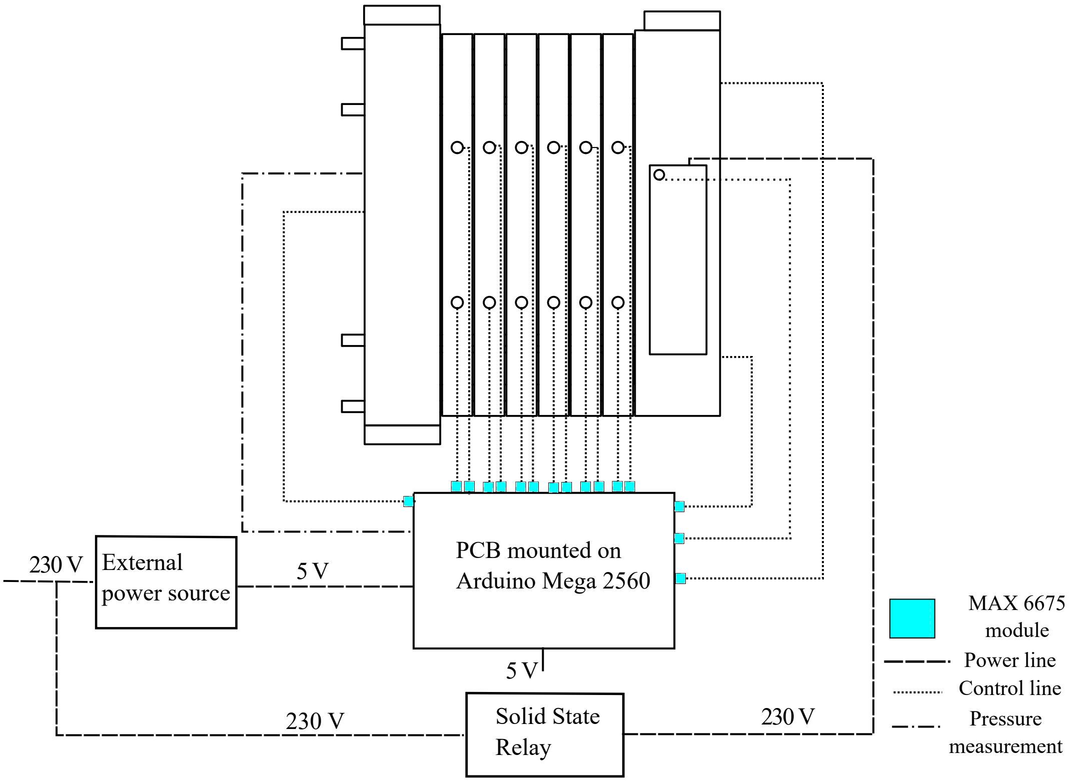

Figure 3.9: Schematic of the electrical circuit for the reactor.

An electric circuit is constructed in order to capture the values of essential parameters like temperature, pressure and heat input. A total of seventeen K-type thermocouples are used in the setup-twelve in the heat integration blocks (two per block-one at the top and one at the bottom), two in the reaction zone (one each at the top and bottom of the catalyst bed), two to control the heater temperature and one to measure the surface temperature of the condenser block. The position of the sensors in the reactor assembly is shown in Figure 3.9.

A pressure sensor is placed in the condensation zone to have a measure of the reaction pressure. All the thermocouples and the pressure sensor are then placed on a printed circuit board (PCB) specifically designed for this setup, with the PCB placed over an Arduino Mega 2560 and powered by an external power source.

The power to the heaters is regulated with the help of a solid state drive (SSD) relay. A code is developed in the Arduino open source compiler and linked with the Processing tool for data collection. The output of the Processing tool is a comma separated value (CSV) file, which is then analyzed to provide the processed results.

The electrical connections were first made using a breadboard and later using a PCB (Figure 3.10). PCB was used during the experiments as it eliminated a lot of wiring.

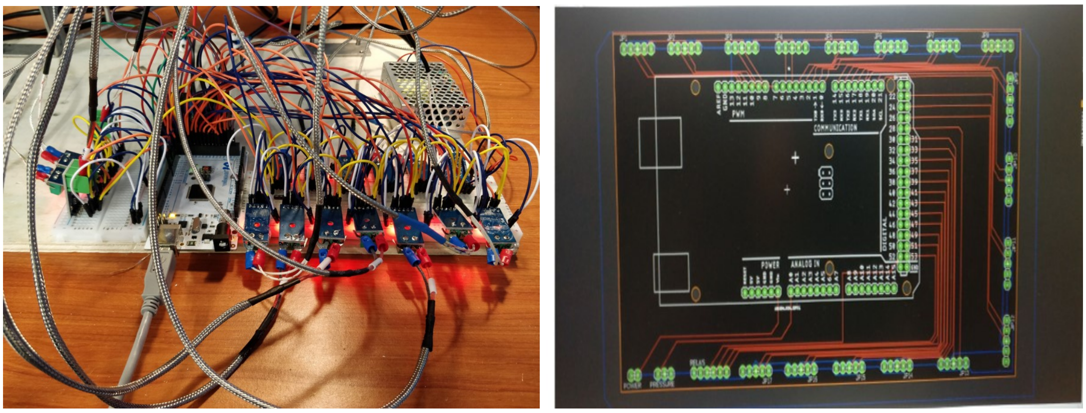

(a) Electrical wiring using a breadboard **(b)** Printed circuit board

Figure 3.10: Electrical circuit for the reactor made using a breadboard and then using a PCB.

3.2.5. Instruments used for analysis

A total of three instruments were used for analysis of the gas and liquid components of the reaction- weight balance (Mettler Toledo; accurate upto 1E-4 grams), a density measurement apparatus (Anton Parr DMA 5000 density meter, accurate upto 1E-5 kg/L) and a micro gas chromatograph (Varian CP-4900 Micro-GC3) with a 1 m CP-COX column (carrier gas-N_2; column temperature-100 °C; run time-240 s). The column could separate gases like CO, CO_2 and H_2 but detection of methanol in gaseous state was not possible using the current setup [101]. A more accurate thermal conductivity detector (TCD) can help analyze the methanol and water composition in the gaseous phase.

3.3. Reactor Operating Procedure

The reactor start-up procedure is depicted in Figure 3.11.

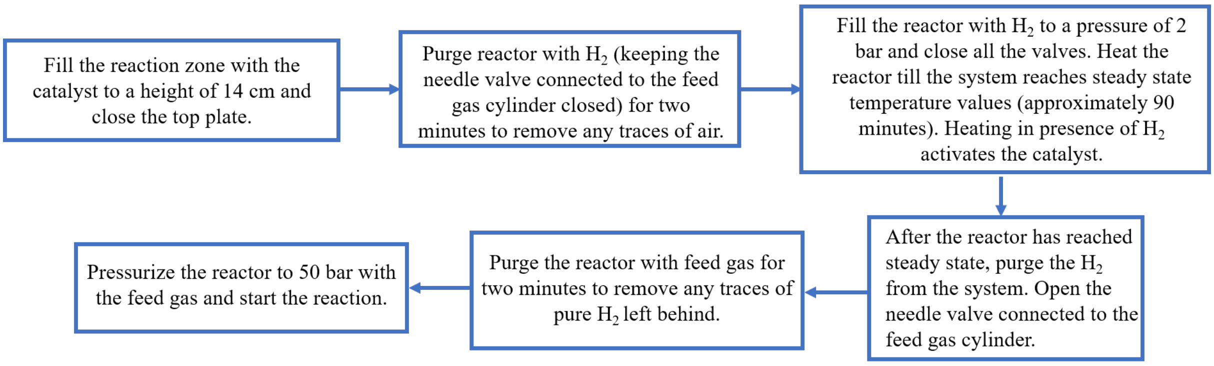
Fill the reaction zone with the catalyst to a height of 14 cm and close the top plate.
Purge reactor with H_2 (keeping the needle valve connected to the feed gas cylinder closed) for two minutes to remove any traces of air.
Fill the reactor with H_2 to a pressure of 2 bar and close all the valves. Heat the reactor till the system reaches steady state temperature values (approximately 90 minutes). Heating in presence of H_2 activates the catalyst.
After the reactor has reached steady state, purge the H_2 from the system. Open the needle valve connected to the feed gas cylinder.
Purge the reactor with feed gas for two minutes to remove any traces of pure H_2 left behind.
Pressurize the reactor to 50 bar with the feed gas and start the reaction.

Figure 3.11: Reactor start-up procedure.

The catalyst was activated in a reducing environment by flowing H_2 in the reaction zone for a period of two hours before the start of the reaction. This was done as the system temperatures take a long time (approximately 90 minutes) to reach steady state on account of the high thermal mass. The experiments are performed in a semi-continuous mode with a continuous amount of feed gas entering the reactor to maintain the pressure at 50 bar (The pressure in the reactor would reduce due to condensation of the products). The pressure sensor used in this reactor is calibrated using the pressure gauge on the feed gas cylinder. The temperature drop over the catalyst bed is measured using the two thermocouples placed on the reaction zone while the thermocouple in the condenser block gives an estimate of its surface temperature. All the thermocouples are placed in holes drilled 14 mm into the blocks and therefore, measure the surface temperature and not the flow temperature.

Gas samples taken at regular intervals are analyzed using the gas chromatograph. The liquid samples obtained are first weighed using the weight balance and then analyzed in the density measurement apparatus to get its density. This density value is then used as an input for an online calculation tool (the website www.handymath.com) to get the weight fraction of methanol in the liquid [102].

In order to stop the reaction, all the gas mixture inside is purged out and the reactor is filled with H_2 to store the catalyst in a reducing atmosphere. The results obtained are then analyzed. The heat input to the reactor from the heaters is calculated based on the amount of time the heater was switched on during the course of the experiment. Heat integration and mass flow rate of the gases are evaluated using the procedure outlined in Section 3.3 and 3.3.

Heat integration Calculation

A schematic of a heat integration block is reproduced in Figure 3.12.

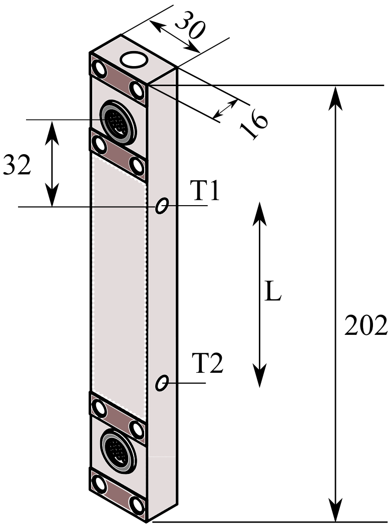

Figure 3.12: Heat integration block. All dimensions are in mm.

The heat integration achieved in one block is calculated using the Fourier Law of heat conduction assuming that the thermal conductivity of aluminium does not change with temperature. The temperatures measured are at the surface of the block and not in the fluid.

$$Q_1 = \frac{k_{Al} * A_{Al} * (T_1 - T_2)}{L} \tag{3.1}$$

where,

Q_1 is the heat integration achieved in one block in W,

k_{Al} is the thermal conductivity of aluminium in W/m-K,

A_{Al} is the cross sectional area of the heat integration block in m^2,

L is the distance between the two thermocouples in m,

T_1 and T_2 are the temperatures at the top and bottom surface respectively of the aluminium block.

The values used for calculation are given in Table 3.1.

Table 3.1: Parameter values used to estimate heat integration for one block.

Parameter	Value	**Unit**
L	8.50E-01	m
A	4.80E-04	m^2
k_{Al} [103]	237	W/m-K
T_1	185	°C
T_2	175	°C
Q_1	13.4	W

This process is repeated to calculate the heat integration of all the other blocks and the values are then added together to give the heat integration for the entire system.

Mass Flow Rate Calculation

Heat integration values derived from the previous section (Section 3.3) were used to estimate the mass flow rate as there was no direct method for its calculation. Schematic of the reactor for mass flow rate calculations is shown in Figure 3.13.

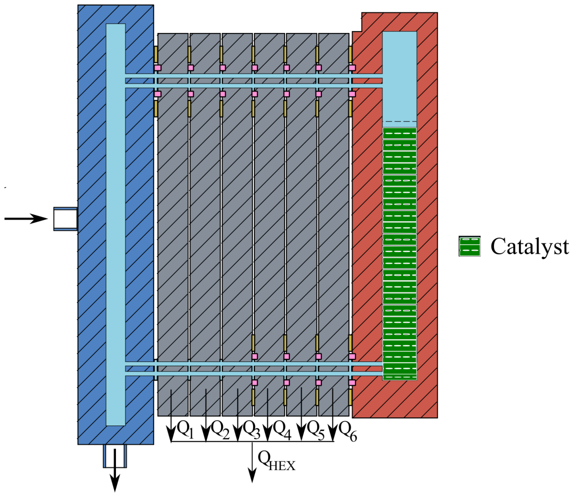
Catalyst
Q_1
Q_2
Q_3
Q_4
Q_5
Q_6
Q_{HEX}

Figure 3.13: Heat integration in each block.

where,

Q_{1-6} are the heat integration values for each block in W,

Q_{HEX} is the total heat integration for the reactor in W.

The process for calculating the mass flow rate is depicted in Figure 3.14 and a sample calculation is performed in Table 3.2.

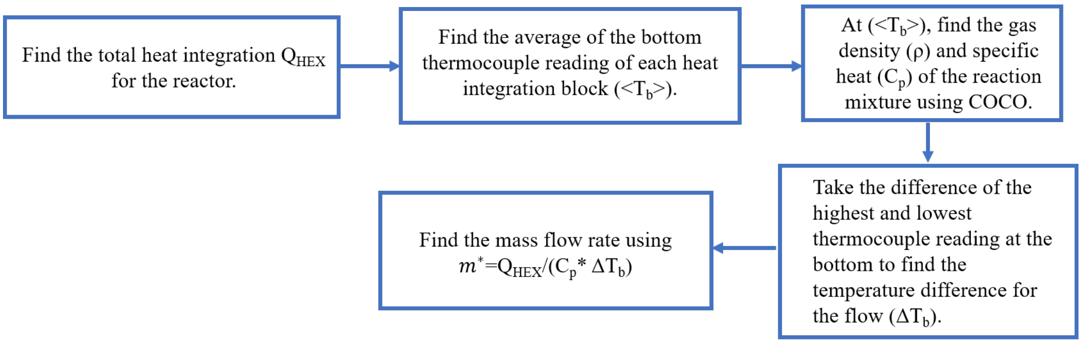
Find the total heat integration Q_{HEX} for the reactor.
Find the average of the bottom thermocouple reading of each heat integration block ($<T_b>$).
At ($<T_b>$), find the gas density (ρ) and specific heat (C_p) of the reaction mixture using COCO.
Take the difference of the highest and lowest thermocouple reading at the bottom to find the temperature difference for the flow (ΔT_b).
Find the mass flow rate using $m^* = Q_{HEX}/(C_p * \Delta T_b)$

Figure 3.14: Schematic of the procedure to calculate the mass flow rate.

Since the temperatures measured here are at the surfaces of the block, it is assumed that the surface temperature profiles are the same as that of the fluid temperature. In this way, ΔT_b and $<T_b>$ for the two cases remains the same.

Table 3.2: Sample calculation to estimate the mass flow rate.

Block Temperatures (°C)						
Top	**Bottom**	**Heat integration (W)**	**$<T_b>$ (°C)**	**C_p (J/kg-K)**	**ΔT_b (°C)**	**$\dot{m}$ (kg/s)**
183.96	174.85	11.8	123.01	1091	102.21	4.12E-04
158.73	153.73	6.5				
138.42	131.75	8.7				
119.25	113.58	7.4				
96.29	91.52	6.2				
76.75	72.65	5.3				
	Q_{HEX}	**45.9**				

3.4. Experimental Test Plan

After the reactor assembly was complete and the electrical connections done, a test plan to perform the experiments was made.

Experiments with N_2 were performed first to get an estimate of the mass flow rate and the heat input to the system when using an inert gas. The reaction temperature was chosen as 210 °C (since it gave the maximum conversion to methanol-observe Figure 1.2 and 42 °C was maintained as the condenser temperature using an external fan). These temperatures were chosen to get a high driving force for the gases.

Four reaction process scenarios were tested-without any catalyst, with the catalyst, with internal fins and finally, with the flow completely blocked in the reactor using aluminium foil. In these four tests, the flow was increasingly blocked and the effect on heat input and the mass flow rate due to this increased blockage was observed.

Once the tests with N_2 were completed, tests with the feed gas were performed at the same temperatures as the previous case. However, these tests gave a low methanol yield. This yield was less than the minimum quantity required by the density measurement apparatus to analyze the composition. Hence a fault tree analysis was constructed (explained in detail in Chapter 4) to identify the source of low methanol yield and correct it.

Once this problem of low yield was solved, experiments were performed with the feed gas using 5 mm pellets (as sourced from the manufacturer). Three parameters were identified as affecting the methanol production, assuming that the reaction pressure is held constant at 50 bar-catalyst particle size, sampling time of the liquids from the reactor and the reaction temperature. The procedure presented below was followed to identify the influence of these three parameters on the methanol yield:

- Keep the catalyst size fixed,
- Keeping the reaction temperature as constant, optimize the sampling time of the liquid mixture,
- Once the optimum sampling time has been found, keep this time fixed and vary the reaction temperature to see its effect on methanol production,
- Change the catalyst size (5 mm pellets cut into two halves along the central axis and crushed pellets) to see the effect of catalyst diameter change on methanol production and repeat steps 2 and 3.

After performing the experiments with different catalyst sizes, a COCO model of the process including the effect of heat integration developed by Guttierez-Neri [104] was worked on and the experimental results using the 5 mm catalyst were compared with the simulation results.

4

Results and Discussion

4.1. Experiments using N_2 as the fluid

The reactor schematics while experimenting with N_2 as the fluid are presented in Figure 4.1.

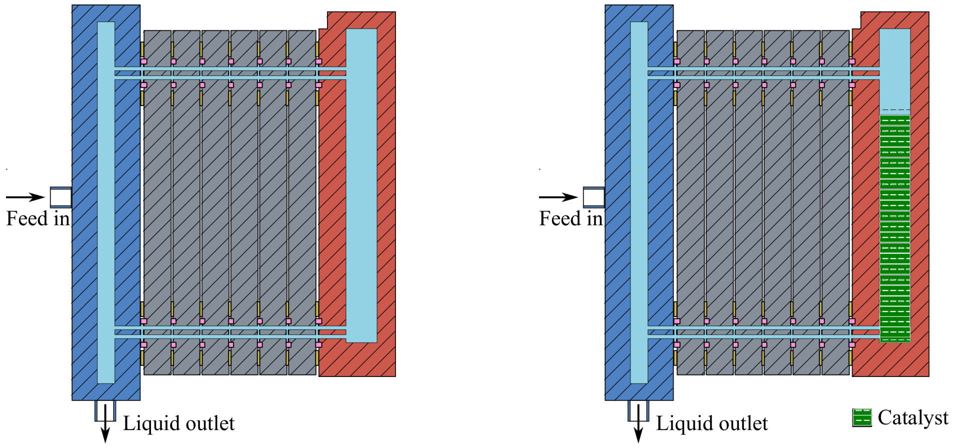
Feed in
Liquid outlet
Feed in
Liquid outlet
🟩 Catalyst

(a) Flow without catalyst

(b) Flow with catalyst

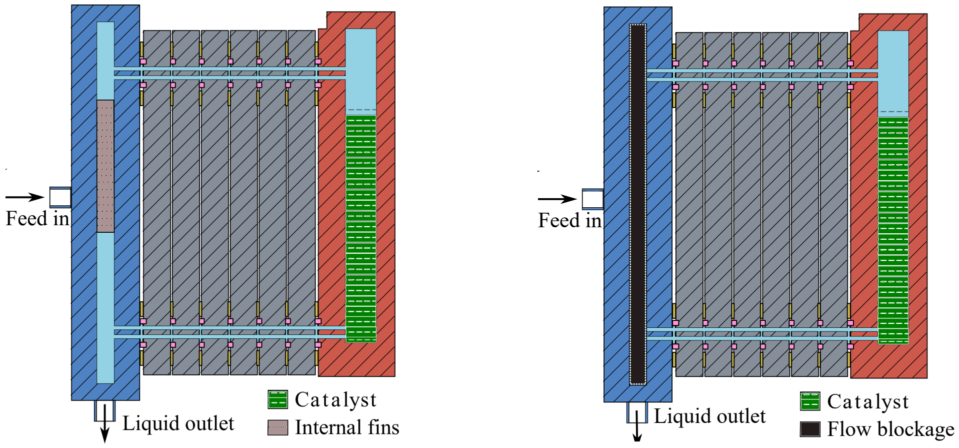
Feed in
Liquid outlet
🟩 Catalyst
▨ Internal fins
Feed in
Liquid outlet
🟩 Catalyst
■ Flow blockage

(c) Flow with internal fins

(d) Flow blockage using aluminium foil

Figure 4.1: Schematics of the reactor during experiments with N_2 as the fluid. The reactor without catalyst (Figure 4.1a), with catalyst (Figure 4.1b), with catalyst and internal fins (Figure 4.1c) and with the flow completely blocked (Figure 4.1d) can be seen.

Experiments were performed using N_2 as the fluid to understand the temperature profile in the reactor when no reaction was taking place. The reaction wall temperature was kept at 208 °C (Average temperature of the two thermocouples at the top and bottom of the catalyst bed) as it gave the highest single pass conversion to methanol (see Figure 2.1) and the condenser wall temperature was set at 42 °C using the fan placed near the condenser block. The condenser temperature was kept low so as to have a high driving force between the two zones.

Four different tests were performed (as mentioned in Section 3.4)- one without any catalyst (to simulate a condition of no flow blockage-Figure 4.1a), a second with the catalyst (Figure 4.1b), third with the catalyst and internal fins on the condenser side (Figure 4.1c) and the last with the catalyst and the flow completely blocked on the condenser side (Figure 4.1d).

Each successive test introduced more flow blockage in the reactor. Therefore, the mass flow rate of the gas inside the reactor should decrease with each successive case. As the heat input and the heat integration are related to the mass flow rate, these should also go down. This is what is observed in the results of Table 4.1. The mass flow rate and heat input are the highest for the case without the catalyst and the lowest for the completely blocked flow case. The heat integration also follows the same trend except in the last case where its value is higher than the internal fins case. This is because even though the flow is completely blocked, the gas can still flow from the top of the reaction zone to the condenser and from the bottom of the condenser to the bottom of the reaction zone, giving the "impression" of flow and correspondingly a higher heat integration.

The case without catalyst was simulated in Fluent by Guttierez-Neri [104]. The difference in the mass flow rates between the experiments and the Fluent model is due to the fact that higher heat integration was achieved in the experiments as compared to the latter case because of inaccuracies in the thermocouples used. The mass flow rates differ since the heat integration is directly related to it (see Section 3.3).

Table 4.1: Details of the experiments performed with N_2 as the fluid. Only the first test without the catalyst was simulated by Guttierez-Neri [104] in Fluent.

Test condition	Heat input (W)	Heat integration (W)	$\dot{m}$ (kg/s)	
			Experiments	Fluent
Flow without catalyst (Figure 4.1a)	51.8	46.0	4.12E-04	2.09E-04
Flow with catalyst (Figure 4.1b)	46.2	18.8	1.54E-04	-
Flow with internal fins (Figure 4.1c)	45.7	13.2	1.04E-04	-
Flow blockage using aluminium foil (Figure 4.1d)	43.0	16.0	1.26E-04	-

4.2. Experiments using feed gas

Once the experiments with N_2 were completed, experiments using the feed gas (refer Section 3.2.3) were done. The reactor, in this case, consisted only of the catalyst with no internal fins or flow blockage on the condenser side (Figure 4.1b). No/low liquid production was achieved using 208 °C reaction temperature and 42 °C condenser temperature. Therefore, a fault tree analysis was done to find the solutions to the problem of low liquid production.

4.3. Fault Tree Analysis

A fault tree analysis was done as no/low liquid production was achieved using the feed gas mixture. Four probable causes were the identified-high fluid temperature in the condenser, no reaction of the gases, no liquid accumulation at the bottom port and no gas flow. The likely causes for each of these problems were identified and solutions proposed and acted upon. Each of these problems and their solutions is described in the subsequent subsections.

4.3.1. High fluid temperature in the condenser

One of the causes of low liquid yield of the reactor could be insufficient heat transfer in the condenser block which could cause the fluid temperature to be at or above the dew point of the mixture. In order to find the true fluid temperature, a small K-type thermocouple (1 mm tip diameter; sourced from TC Direct; maximum temperature 1024 °C; accuracy ± 1.5 °C) was inserted into the flow channel in the condenser by making a groove in the top plate. Nitrogen at a pressure of one bar was circulated inside the reactor, with the reaction zone temperature maintained at 210 °C. Ideally, this test should have been conducted at the reaction pressure (50 bar), but leaks in the top plate meant that the test had to performed at one bar.

The modifications to the top plate of the condenser zone, the thermocouple and the result from the experiment are shown in Figure 4.2.

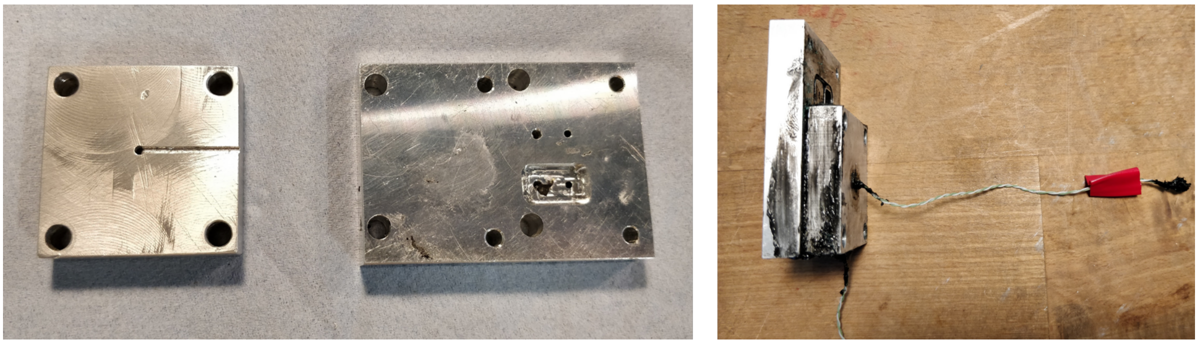

(a) Modifications to the top plate for measuring the fluid temperature (shown on the left) and the top plate with the thermocouple (shown on the right)

Figure 4.2: Fluid temperature measurement in the condenser. The difference between the condenser surface and fluid temperature is a maximum of 5.5 °C using 1 bar N_2.

The maximum temperature difference between the surface and the fluid temperatures was found to be 5.5 °C. The maximum condenser surface temperature during this test was 45.75 °C and the fluid temperature was 51.25 °C, well below the dew point of the mixture (dew point temperature is around 80.16 °C for a feed of 3:1 ratio by volume of H_2 and CO_2 with 210 °C as the reaction temperature and 50 bar as the pressure). However, this test was performed at one bar and using N_2 as the fluid, which does not simulate the reaction conditions exactly, since the temperature profiles would be different when another fluid was used (like the feed gas) and if the pressure was higher. Therefore, a test at the reaction conditions would give an exact measure of the correct temperature profiles. For the time being, it was assumed that high fluid temperature in the condenser was not the cause of low liquid production.

4.3.2. No reaction in the catalyst zone

Another reason for no liquid production could be that there is no reaction taking place in the catalyst zone. Some of the reasons for this and the solutions are given in the flowchart below (Figure 4.3).

- **Air inside the reactor:** As mentioned in Section 3.3, the reactor was filled with H_2 and heated to the reaction temperature. Once steady state temperature profiles were reached, H_2 was purged out (using the purge valve) and the feed gas mixture was circulated through the reactor. The reactor was pressurized with this gas after being circulated for around two minutes. The gas composition at this point was analyzed using the gas chromatograph and was found to contain

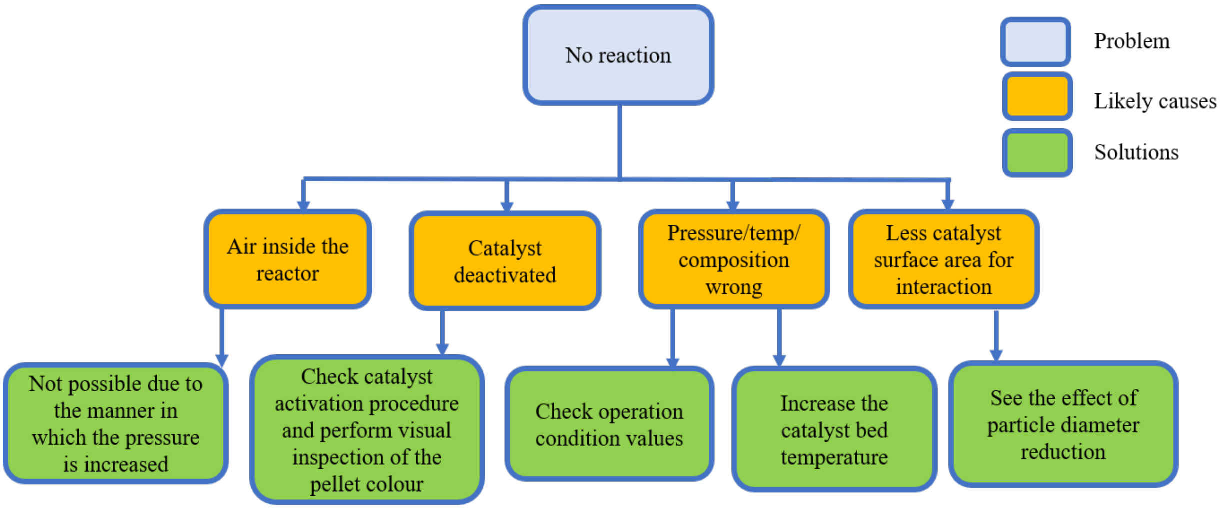
No reaction
Problem
Likely causes
Solutions
Air inside the reactor
Catalyst deactivated
Pressure/temp/ composition wrong
Less catalyst surface area for interaction
Not possible due to the manner in which the pressure is increased
Check catalyst activation procedure and perform visual inspection of the pellet colour
Check operation condition values
Increase the catalyst bed temperature
See the effect of particle diameter reduction

Figure 4.3: Causes for no reaction taking place in the catalyst zone with their solutions.

no oxygen, removing air inside the reactor as one of the causes of low liquid production.

- **Catalyst deactivated:** The catalyst was activated before the start of every experiment at 230 °C reaction zone wall temperature using H_2 (Literature proposes using a mixture of 90-95% N_2, He or Ar in H_2 for activation [37, 38, 105, 106]. The inert gas is present only as a carrier gas and to dilute the H_2 concentrations for safety purposes. Pure H_2 was used in this case as ZEF would not have access to N_2 when they deploy the system in the field). Visual inspection of the catalyst was carried out just after reduction, and the colour of the catalyst was found to be reddish, which indicates the presence of metallic copper, suggesting proper activation.

- **Pressure/temperature/gas composition wrong:** Wrong operating conditions can also lead to no/limited liquid production. However, the working of the thermocouples was verified with that of the ice-water mixture and boiling water (100 °C at one bar pressure) while the readings of the pressure sensor in the reactor were found to be the same as the pressure set using the feed gas cylinder pressure gauge. The pressure sensor in the reactor was calibrated using the gauge in the cylinder (see Section 3.3). The gas composition from the cylinder was also analyzed in a gas chromatograph and found to be very close to the composition mentioned in the gas cylinder. Therefore, wrong parameter values was also ruled out as one of the reasons for low liquid production.

  The experiments up to this point were performed at 208-210 °C reaction temperature (temperature of the catalyst bed). At this temperature, the reaction might be kinetically limited (the catalyst becomes active for reaction around 200 °C). Therefore, it was decided to increase the reaction temperature and observe whether the methanol production was increased. However, increasing the reaction temperature also yielded an almost negligible liquid amount.

- **Less catalyst surface area for reaction:** If the catalyst pellets are large, then there is less outer surface area per unit volume available for the reactions to take place. On the other hand, small catalyst size increases the pressure drop across the catalyst bed and therefore, decreases the flow. Hence there is a trade-off between the size of the catalyst and the pressure drop. While the experiments in this project were done with 5 mm catalyst pellets up to this point, it was decided to also experiment with smaller catalyst sizes and then compare the results of the two. However, lowering the catalyst size did not improve the reaction yield and led to very low methanol production.

4.3.3. No liquid accumulation

The likely causes of this problem and its solutions are presented in the flowchart (Figure 4.4).

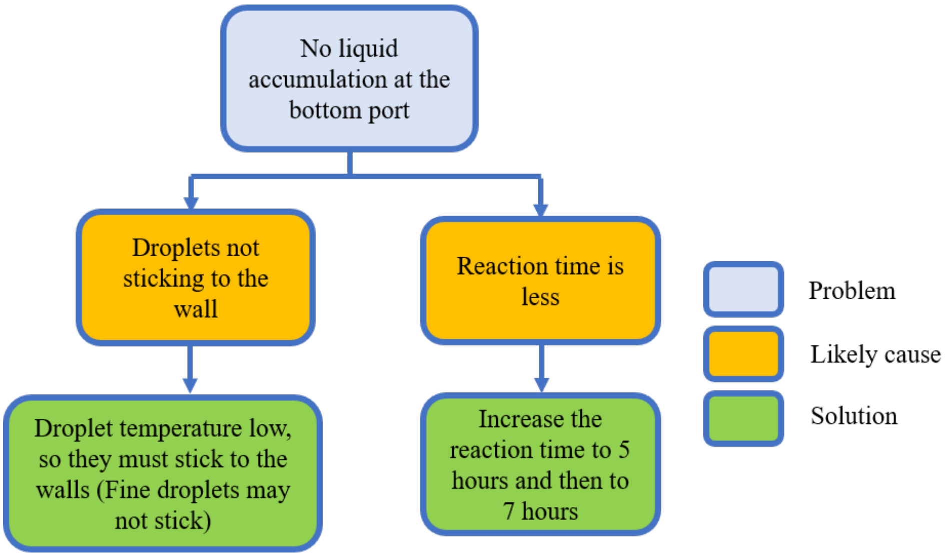
No liquid accumulation at the bottom port
Droplets not sticking to the wall
Reaction time is less
Droplet temperature low, so they must stick to the walls (Fine droplets may not stick)
Increase the reaction time to 5 hours and then to 7 hours
Problem
Likely cause
Solution

Figure 4.4: Causes for insufficient liquid accumulation in the bottom port of the condenser and their solutions.

- **Droplets not sticking to the wall:** One possible reason for low liquid accumulation can be the inability of droplets formed to stick to the walls. However the surface tension in these droplets would cause them to stick to the walls as the mass flow rate of the gases is too low to carry them (see Table 4.1). The exception here is very fine droplets, which may not stick because of low surface tension. However, there was no way to verify these claims during the experiment.
- **Less reaction time:** Methanol synthesis is a slow reaction, especially at temperatures of around 210 °C, at which the reaction was run initially. Hence less reaction time could well be a reason for low liquid output (The outlet port was checked for liquid presence till this point after about 3 hours of reactor operation). Therefore, it was decided to increase the reaction time to five and/or even seven hours to see if there was any methanol formation. However, even after doing this, the methanol production was negligible.

4.3.4. No gas flow in the reactor

Even if the catalyst is activated, the gas composition is as expected and the temperature and pressure match the reaction conditions, the reaction progression can still be hindered by no gas flow inside the reactor. Some of the possible causes for this are mentioned in Figure 4.5.

- **Flow blockage by catalyst particles:** If the flow is blocked in the catalyst bed, then there would be no reaction and hence no/very little formation of the products. In order to check this hypothesis, a flow outlet channel was made on top of the catalyst bed to analyze the gas as shown in Figure 4.6. On analysis, the gas mixture showed the presence of CO, thereby confirming that the reaction was taking place and catalyst particles (5 mm particles were used up to this point) were not blocking the flow.

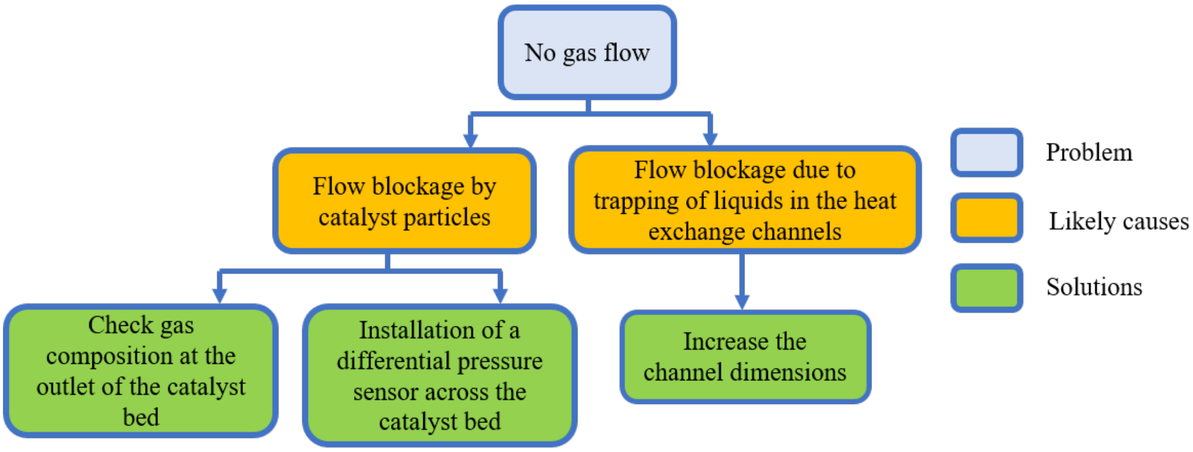
No gas flow
Flow blockage by catalyst particles
Flow blockage due to trapping of liquids in the heat exchange channels
Check gas composition at the outlet of the catalyst bed
Installation of a differential pressure sensor across the catalyst bed
Increase the channel dimensions
Problem
Likely causes
Solutions

Figure 4.5: Causes for no gas flow in the reactor and their solutions.

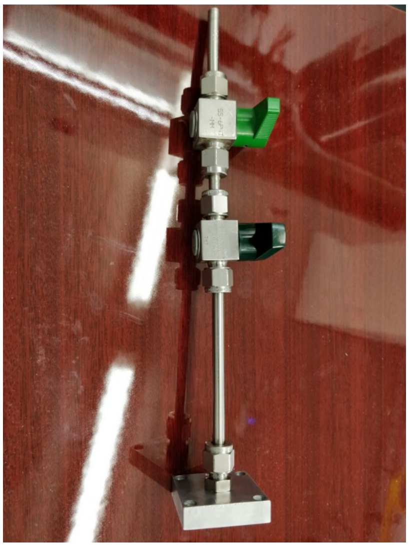

(a) Modification to the top plate

Figure 4.6: Modification at the outlet of the catalyst bed to measure the gas composition. Two open close valves were used to enable gas sampling.

- **Installation of a differential pressure sensor:** A differential pressure sensor can give an estimation of the pressure drop across the catalyst bed. However, such a sensor was not used during the experiment and hence there was no way to measure the pressure drop experimentally.

- **Flow blockage due to premature condensation in the heat integration blocks:** The flow can be blocked due to trapping of liquids in the heat exchanger blocks due to premature condensation. Once the channels are clogged with the liquid, the droplets remain in place due to the strong capillary forces.

  An experiment was done using the feed gas by increasing the average catalyst bed temperature to 225 °C (about 15 °C higher than that used previously) as per one of the solutions mentioned in Section 4.3.2. The temperatures at the top and bottom of the heat integration blocks are shown in Table 4.2.

Table 4.2: Temperatures at the top and bottom thermocouple of the heat integration blocks at the reaction temperature of 225 °C. Block 1 is closest to the reaction zone and Block 6 to the condensation zone.

	Thermocouple readings (°C)	
	Top	**Bottom**
Block 1	197.51	192.03
Block 2	173.01	170.89
Block 3	150.13	146.32
Block 4	130.82	118.57
Block 5	104.74	102.98
Block 6	80.17	80.07

The dew point of the gas mixture at 225 °C (498 K) is around 127.38 °C (from COCO-using the model described in Section 4.7). From Table 4.2 it can be seen that the temperatures of block 4-6 fall below that dew point. This could result in some liquid getting trapped in the flow channels and blocking the flow.

In order to prove that liquid was indeed trapped in the flow channels, a batch process was performed with six heat integration blocks and then with three heat integration blocks. In this experiment, the reactor was fed with the feed gas at 50 bar and the needle valve connected to the feed gas cylinder (see Figure 3.1) was closed. The experiment was continued till the pressure in the reactor stabilized (the pressure would fall because of reaction and subsequent condensation of the products) and the process was repeated again twice. The pressure profiles for this experiment are presented in Figure 4.7. A higher pressure drop in time in Figure 4.7b indicates less flow blockage.

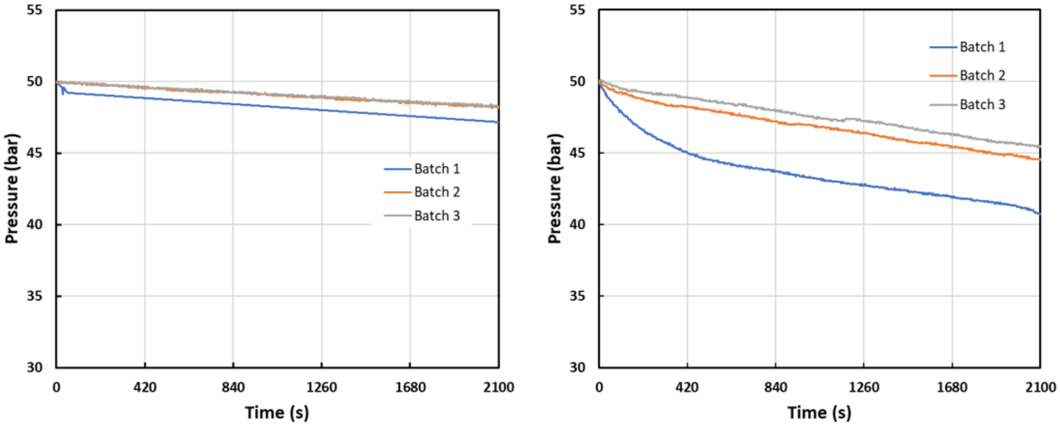

(a) Six heat integration blocks

(b) Three heat integration blocks

Figure 4.7: Pressure drop using (4.7a) six heat integration blocks and (4.7b) three heat integration blocks. Premature condensation in the case of six blocks was the cause of low liquid production and thus low pressure drop in time.

Following this result, subsequent experiments were performed with three heat integration blocks. Even with three blocks, enough liquid was not produced to be analyzed in the density measurement apparatus. This pointed to the fact that some liquid might still be trapped there.

To check this hypothesis, the flow channels were made larger by enlarging the holes from 2 mm to 6.5 mm as shown in Figure 4.8. This size was chosen because that was the largest diameter that could be drilled into the blocks without damaging the grooves for the O-rings. Tests performed using heat integration blocks with bigger holes yielded a significant amount of liquid, pointing to the fact that it was indeed condensation in the small flow channels that was blocking the flow and

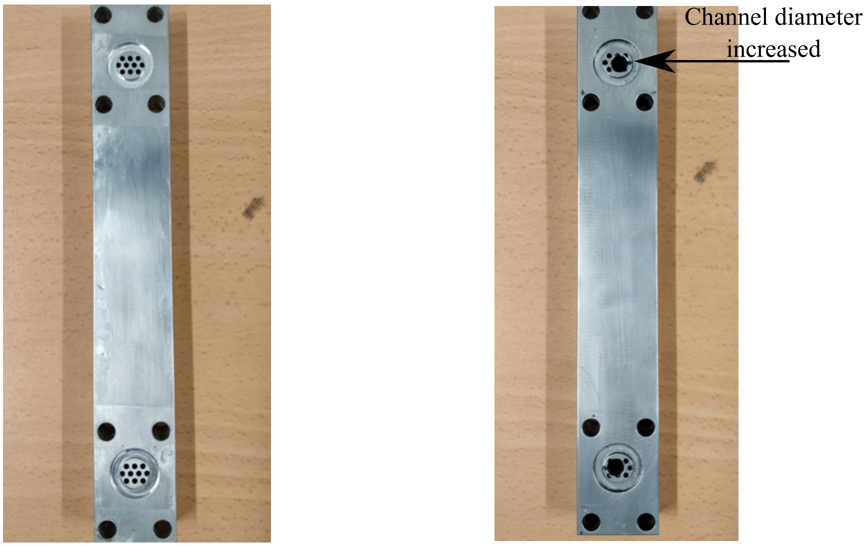

(a) Aluminium blocks with 2 mm channels **(b)** 6.5 mm flow channels

Figure 4.8: Change in flow channel dimensions to solve the problem of flow blockage due to liquid condensation.

leading to less liquid output.

Once the problem of the too low methanol output was solved, a series of experiments were performed to calculate the reactor productivity, which are detailed in the subsequent sections.

4.4. Experiments with 5 mm catalyst pellets

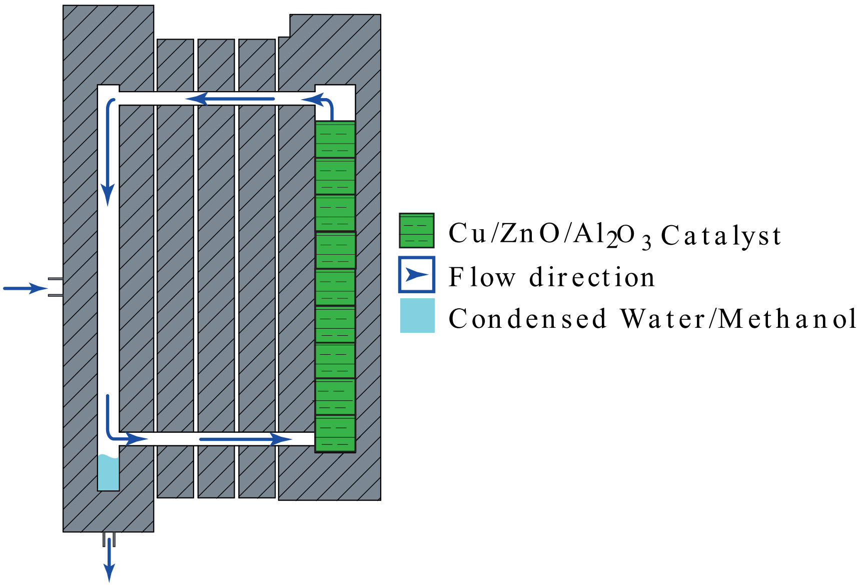

Figure 4.9: Schematic of the Small Modified Brilman Reactor (SMBR) used for the experiments. The reactor now consists of the reaction zone, three heat integration blocks (with larger flow channels) and a condensation zone.

Based on the results obtained in Section 4.3.4, three heat integration blocks were removed and the channel dimensions in the remaining three blocks were increased from 2 mm to 6.5 mm. This reactor was called the Small Modified Brilman Reactor (SMBR) and is shown in Figure 4.9. 45 grams of 5 mm catalyst pellets (as sourced from the manufacturer) were put into the reactor.

4.4.1. Sampling time optimization

Once the catalyst size was fixed, the reactor wall temperature was set at 235 °C and the condenser wall temperature at 62 °C using an external fan. A higher temperature was chosen to achieve faster kinetics. The sampling time of the liquids (the time after which the liquid mixture of methanol and water is taken out from the reactor) was then optimized.

Initial tests (mentioned in Section 4.3.3) had yielded negligible amounts of liquid even if the liquid was sampled every three hours. Therefore, in this test, the liquid was first sampled every 3 hours. Since a significant amount of methanol was produced this time, the sampling time was then reduced to one hour. Even after one hour, almost the same amount of liquid as that obtained at 3 hours was sampled. Therefore, the liquid sampling time was continually lowered to 30 , 15 , 10 and ultimately 5 minutes. The methanol production rate was expressed in mmole$CH_3OH/g_{cat}/h$ (as the same was done by Brilman et al.[16]) and calculated using the procedure outlined in Figure 4.10.

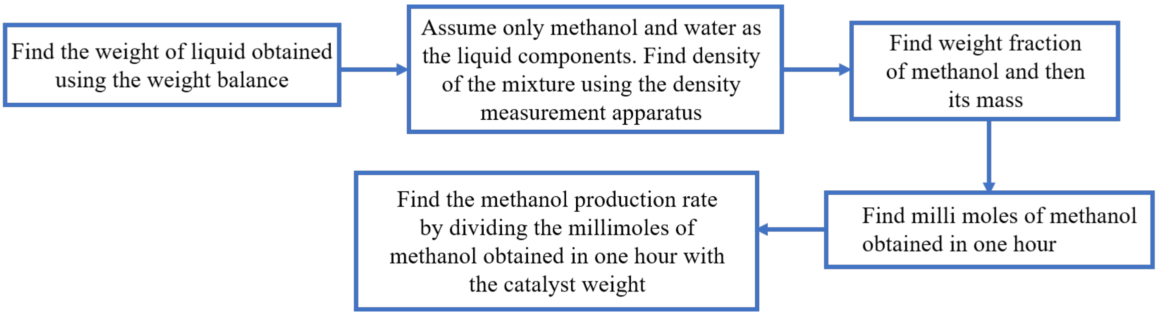
Find the weight of liquid obtained using the weight balance
Assume only methanol and water as the liquid components. Find density of the mixture using the density measurement apparatus
Find weight fraction of methanol and then its mass
Find milli moles of methanol obtained in one hour
Find the methanol production rate by dividing the millimoles of methanol obtained in one hour with the catalyst weight

Figure 4.10: Procedure followed for calculating the methanol production rate in mmole $CH_3OH/g_{cat}/h$.

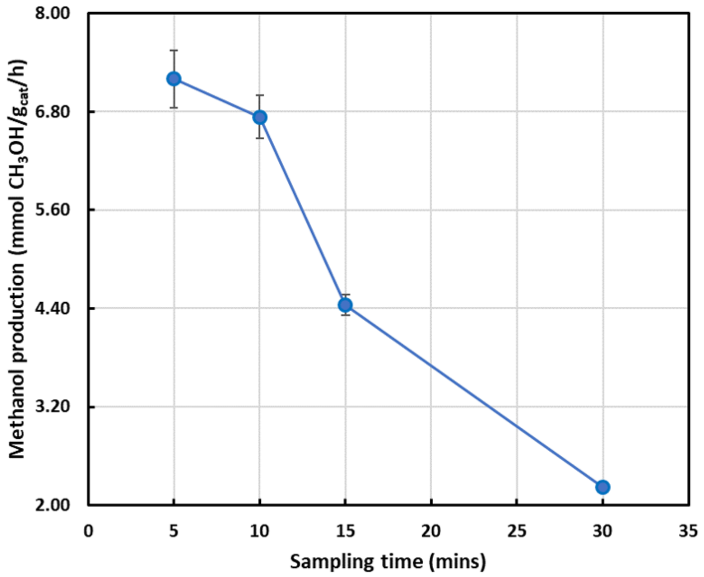

Figure 4.11: Variation in methanol production with sampling time at 235 °C for 5 mm catalyst pellets.

The variation in methanol production rate with sampling time is shown in Figure 4.11. The methanol production at 30 mins of sampling time was 2.2 mmole $CH_3OH/g_{cat}/h$, while at 15 mins was 4.4 mmole

$CH_3OH/g_{cat}/h$, since the liquid was sampled four times for 15 minutes and two times for 30 minutes. This signified that the reaction reached equilibrium at or before 15 minutes. Lowering the sampling time to 10 minutes further increased the production, signifying that equilibrium was attained at or before 10 minutes. Finally, the liquid was sampled every five minutes. This did not increase the methanol yield by a proportional amount, suggesting that the reaction did not reach equilibrium at 5 minutes. Therefore, 10 minutes was chosen as the optimum sampling time.

The error bars for 5 and 10 mins of sampling time are larger than at the other two times as more number of samples were taken in the former case.

4.4.2. Reaction temperature optimization

Once the sampling time was optimized, it was kept fixed and the reaction temperature was varied. Tests were first conducted at 235 °C (the temperature at which the sampling time was optimized). The reactor wall temperature was then lowered in steps to 228 °C, 220 °C and finally to 213 °C. Higher and lower temperatures than 240 °C and 210 °C were not chosen. This is because at higher temperatures, the Viton™ O-rings fail and the reaction is kinetically limited at lower temperatures. The condenser wall temperature was maintained at 62 °C for all the cases.

Mass Balance

A mass balance was conducted prior to analyzing results from the temperature test. This was done to estimate the feed flow rate of the mixture into the reactor. The inlet and outlet streams into the reactor along with their relevant process parameters were defined (Figure 4.12).

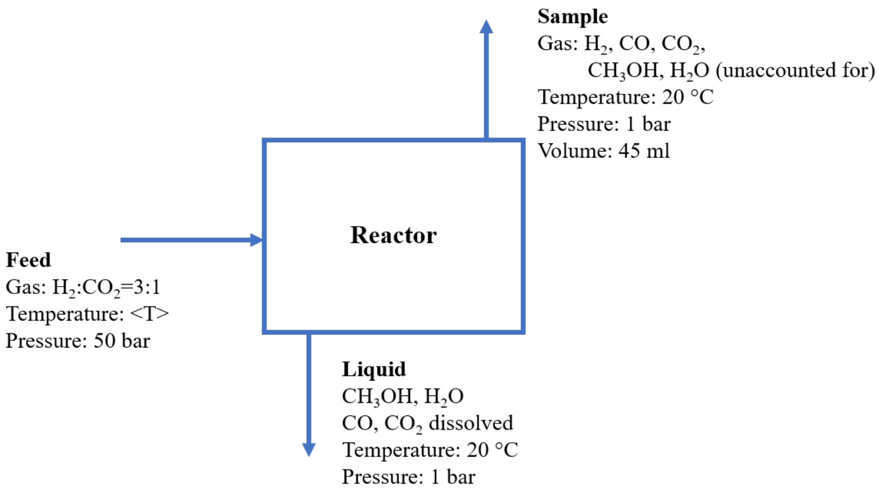

Figure 4.12: Schematic of the reactor showing the inlet and outlet streams.

1. **Feed**: This is the feed gas mixture that is fed into the reactor at a pressure of 50 bar. The temperature of the feed stream is taken as the average temperature in the reactor (<T>), ie, the average of the reaction and condensation zone temperatures.
2. **Sample**: This stream represents the gas sample that is taken at the outlet of the catalyst bed (see Figure 4.2a). Although the sample is intially at a high temperature (temperature of the catalyst bed), it is analyzed when its temperature is around 20 °C. It was not possible to detect CH_3OH and H_2O in this stream using the current gas analysis setup. However using a more accurate TCD can solve this problem.
3. **Liquid**: This stream is the liquid that is sluiced out from the reactor periodically. Methanol and water are considered as the only liquid outlet components (the catalyst is quite selective to methanol

production and produces other components only in trace amounts [16]) with some CO and CO_2 dissolved [107, 108]. The liquid components are analyzed in a density measurement apparatus with CO and CO_2 solubility in the liquid mixture calculated using the reactor model developed in COCO (Section 4.7).

Once the inlet and outlet streams have been defined, the moles of various components at these locations are found using the steps outlined in Figure 4.13.

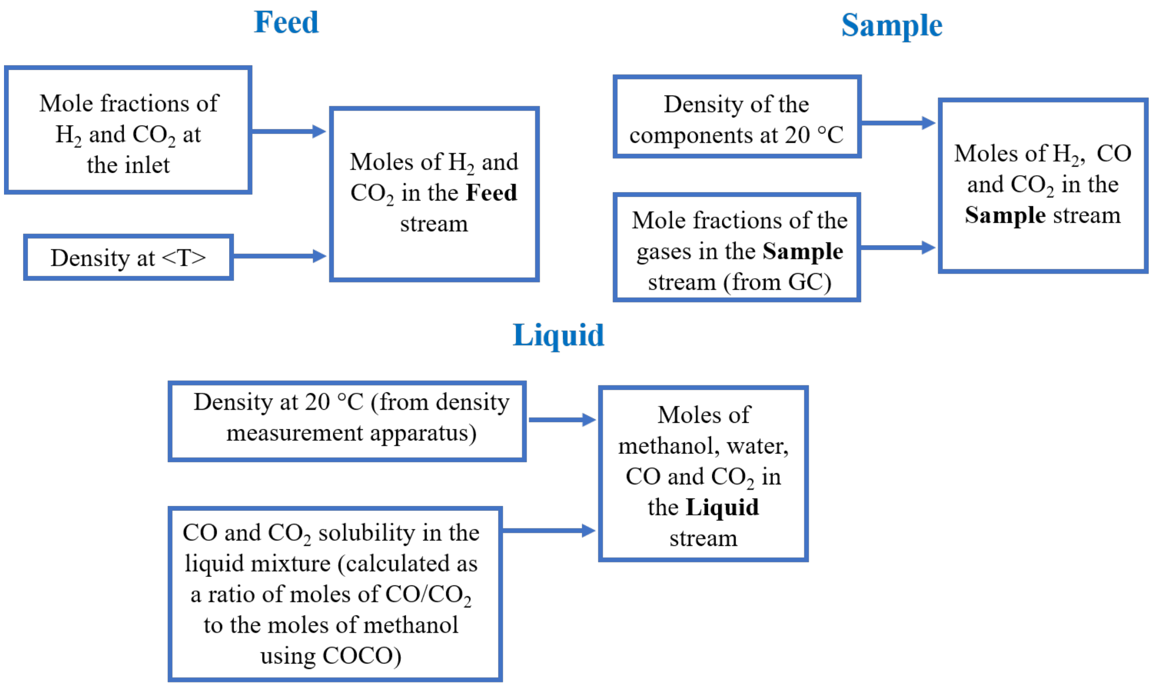
Feed
Mole fractions of H_2 and CO_2 at the inlet
Density at <T>
Moles of H_2 and CO_2 in the **Feed** stream
Sample
Density of the components at 20 °C
Mole fractions of the gases in the **Sample** stream (from GC)
Moles of H_2, CO and CO_2 in the **Sample** stream
Liquid
Density at 20 °C (from density measurement apparatus)
CO and CO_2 solubility in the liquid mixture (calculated as a ratio of moles of CO/CO_2 to the moles of methanol using COCO)
Moles of methanol, water, CO and CO_2 in the **Liquid** stream

Figure 4.13: Procedure to calculate the moles of gaseous components in the reactor.

The moles found using the above steps are then used to find the carbon conversion, selectivity and feed flow rate of the gas into the reactor using the steps mentioned in Figure 4.14.

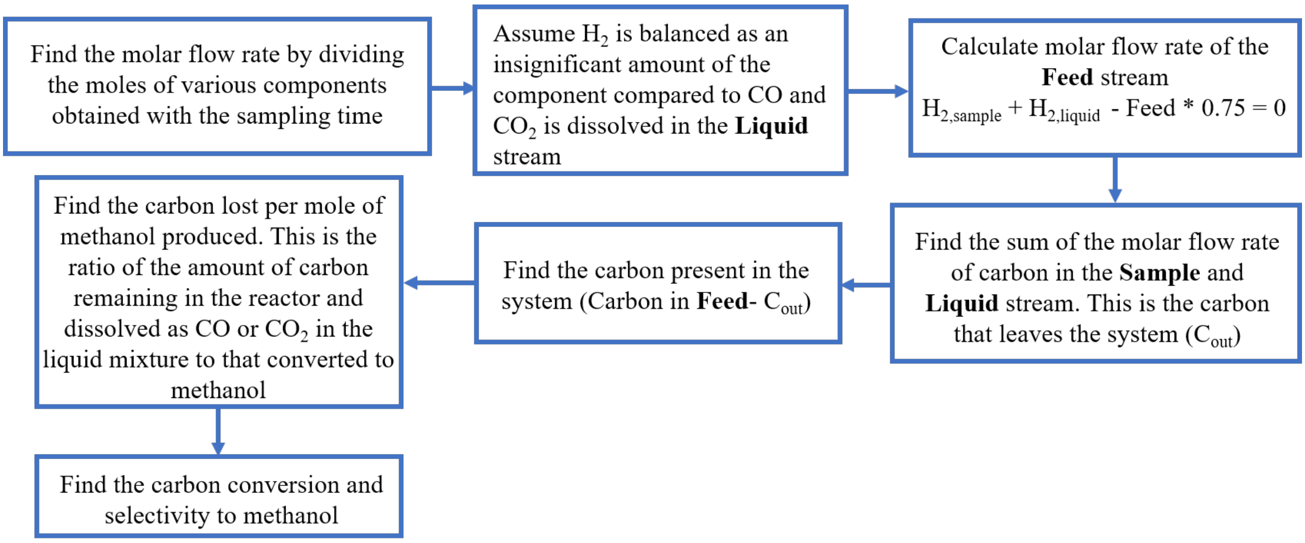
Find the molar flow rate by dividing the moles of various components obtained with the sampling time
Assume H_2 is balanced as an insignificant amount of the component compared to CO and CO_2 is dissolved in the **Liquid** stream
Calculate molar flow rate of the **Feed** stream $H_{2,sample} + H_{2,liquid}$ - Feed * 0.75 = 0
Find the sum of the molar flow rate of carbon in the **Sample** and **Liquid** stream. This is the carbon that leaves the system (C_{out})
Find the carbon present in the system (Carbon in **Feed**- C_{out})
Find the carbon lost per mole of methanol produced. This is the ratio of the amount of carbon remaining in the reactor and dissolved as CO or CO_2 in the liquid mixture to that converted to methanol
Find the carbon conversion and selectivity to methanol

Figure 4.14: Flowchart for mass balance calculations.

where,

$H_{2,sample}$ is the molar flow rate of H_2 in the **Sample** stream,

$H_{2,liquid}$ is the molar flow rate of H_2 in the **Liquid** stream,

C_{out} is the molar flow rate of carbon leaving the system.

The molar flow rates, carbon conversion and selectivity calculated using the procedure outlined in Figure 4.13 and Figure 4.14 are presented in Table 4.3 and Table 4.4.

Table 4.3: Molar flow rate of the components at the outlet of the reactor for 5 mm pellets at 228 °C reaction temperature, presented as an example.

	Molar flow rate (moles/s)		
Gas	**Sample**	**Liquid**	**Outlet (Sample + Liquid)**
H_2	2.74E-06	0	2.74E-06
CO_2	4.72E-07	9.30E-07	1.40E-06
CO	1.38E-07	7.83E-09	1.46E-07
CH_3OH	0	8.45E-05	8.45E-05
H_2O	0	8.84E-05	8.84E-05

Table 4.4: Estimation of carbon conversion and selectivity for 5 mm pellets at different temperatures.

	Value				
Parameter	**213 °C**	**220 °C**	**228 °C**	**235 °C**	**Unit**
Feed flow rate	2.72E-04	3.09E-04	3.47E-04	3.42E-04	moles/s
H_2 feed flow	2.04E-04	2.31E-04	2.60E-04	2.56E-04	moles/s
CO_2 feed flow	6.80E-05	7.71E-05	8.68E-05	8.55E-05	moles/s
Carbon conversion	99.0	99.1	99.2	99.2	%
Selectivity	98.7	98.8	99.0	98.9	%

The carbon and oxygen balance was found to be within $\pm 1.5\%$ for all the cases. Hydrogen was assumed to be completely balanced (observe Figure 4.14).

The carbon conversion and selectivity increase with temperature to 228 °C, after which they stabilize. This is because, at lower temperatures, the solubility of CO and CO_2 in the liquid mixture is higher [107, 108]. So more carbon is lost since it is dissolved in the mixture and therefore, less carbon is available for conversion to methanol. At 235 °C, carbon is also being increasingly converted to CO, since its formation is favoured at high temperature, in addition to losing some CO and CO_2 in the liquid mixture. Carbon is also lost at all temperatures in the **Sample** stream since methanol detection was not possible using the current gas analysis setup.

Brilman et al. [16] obtained a selectivity higher than 99.5% as their condenser temperature was higher (about 85 °C) compared to 62 °C in this experiment. Operation at this temperature meant that the solubility of CO_2 and CO in the methanol and water mixture was less [107, 108].

Efficiency calculation

Once the mass balance calculations are done and the feed flow rates of H_2 and CO_2 determined, the efficiencies are calculated using Equation 4.1, Equation 4.2 and Equation 4.3. The maximum theoretical efficiency of the system [109] is defined considering methanol production only by CO_2 hydrogenation (Equation 2.2).

The overall efficiency, energy efficiency and maximum theoretical efficiency [109] of the system are defined as:

$$\text{Maximum theoretical efficiency} = \frac{n_{CH_3OH} \cdot HHV_{CH_3OH}}{HHV_{H_2} + Q_{in}} \tag{4.1}$$

$$\text{Overall efficiency} = \frac{\dot{m}_{CH_3OH} \cdot HHV_{CH_3OH}}{Q_{in} + \dot{m}_{H_2} \cdot HHV_{H_2}} \tag{4.2}$$

$$\text{Energy efficiency} = \frac{\dot{m}_{CH_3OH} \cdot HHV_{CH_3OH}}{Q_{in} + \dot{m}_{H_2} \cdot HHV_{H_2} + n_{H_2} \cdot \Delta H_{CO_2\,\text{hydrogenation}}} \tag{4.3}$$

where,

$n_{CH_3OH} \cdot HHV_{CH_3OH}$ is the product of number of moles of CH_3OH produced per mole of H_2 and the HHV of CH_3OH in W,

HHV_{H_2} is the higher heating value of one mole of H_2 in W,

Q_{in} is heat input from the heaters in W,

$\dot{m}_{H_2} \cdot HHV_{H_2}$ is the chemical heat content of H_2 consumed in the reaction in W,

$\dot{m}_{CH_3OH} \cdot HHV_{CH_3OH}$ is the chemical heat content of CH_3OH produced in W,

$n_{H_2} \cdot \Delta H_{CO_2\,\text{hydrogenation}}$ is the heat released by H_2 consumption in W.

The variation of these values and of methanol production with temperature for 5 mm catalysts is presented in Figure 4.15 and the results are tabulated in Table 4.5.

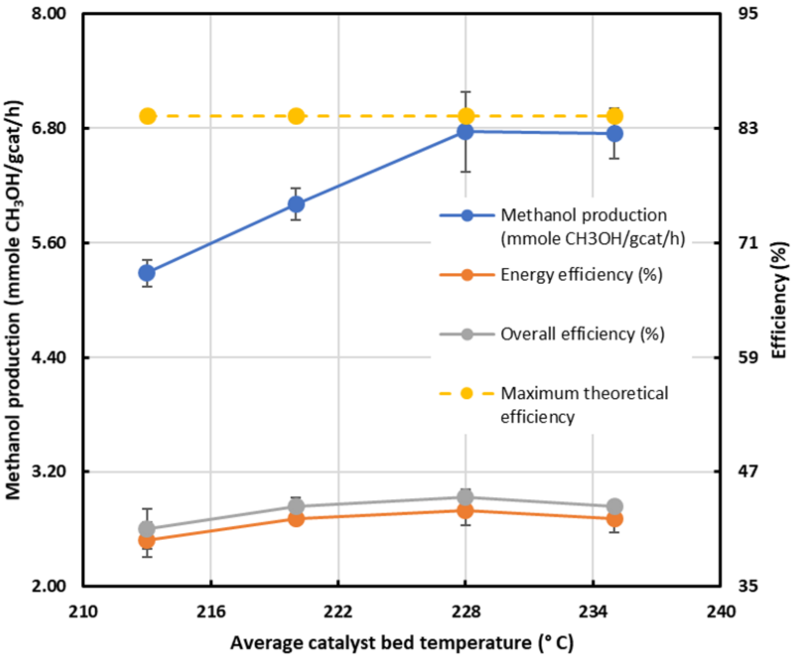

Figure 4.15: Variation in methanol production, energy efficiency and overall efficiency with time for 5 mm pellets. Methanol production, overall and energy efficiency of the system are found to increase with temperature (till 228 °C), and then start to decrease. 228 °C was identified as the optimum temperature to produce methanol in the SMBR using 5 mm pellets.

The methanol production increases when the temperature is increased to 228 °C as the reaction is kinetically favoured. At temperatures above 228 °C, the thermodynamic limitations of the reactions (the reaction is more favoured at lower temperatures) lead to less methanol production as CO formation is favoured.

A similar trend is observed for energy efficiency and overall efficiency curves. The heat content of methanol produced increases faster than the heat input from the heaters and the heat released by hydrogen consumption till 228 °C, after which the heat content of methanol starts to drop as less amount of the component is produced.

Based on these results, 228 °C was identified as the reaction temperature for methanol production using 5 mm pellets and given the current reaction zone dimensions.

The methanol composition in the liquid mixture did not change with temperature and was found to be 48.3 ± 1.9 mol% of methanol in water, while the expected theoretical ratio is 50 mol% of methanol in water. The difference is probably due to some methanol loss during sampling as it is volatile [16].

Table 4.5: Results of the experiment with 5 mm catalyst at 228 °C and 10 minutes of sampling time.

Parameter	Value				Unit
	213 °C	220 °C	228 °C	235 °C	
$\dot{m}_{CH_3OH}$	7.61E-03	8.64E-03	9.74E-03	9.60E-03	kg/h
$\dot{m}_{H_2}$	1.43E-03	1.62E-03	1.83E-03	1.80E-03	kg/h
$\dot{m}_{CO_2}$	1.05E-02	1.19E-02	1.34E-02	1.32E-02	kg/h
$n_{H_2} \cdot \Delta H_{CO_2\ \mathrm{hydrogenation}}$	3.3	3.7	4.2	4.1	W
Q_{in}	59.2	60.1	64.8	66.9	W
Heat integration	6.7	9.9	11.1	11.4	W
$\dot{m}_{CH_3OH} \cdot HHV_{CH_3OH}$	47.3	53.8	60.6	59.7	W
$\dot{m}_{H_2} \cdot HHV_{H_2}$	56.1	63.8	71.9	70.8	W
Energy efficiency	39.9	42.2	43.0	42.1	%
Overall efficiency	41.0	43.4	44.3	43.4	%
Maximum theoretical efficiency	84.3	84.3	84.3	84.3	%

Since the maximum methanol production was obtained at 228 °C, these results were then compared to those obtained by Brilman et al. [16] as the catalyst pellet size was similar in both cases (Table 4.6).

Table 4.6: Comparison of the results of the current study with those of Brilman et al [16].

	Reaction temperature (°C)	Condenser temperature (°C)	Methanol production (mmole $CH_3OH/g_{cat}/h$)	Reaction heat (W)	Energy input (MJ/kg_{CH_3OH})
Present study	228	62	6.8	4.2	24
Brilman et al	210	85	4.3	8.5	75

In the present study, the reactor was operated at a higher reaction temperature and a lower condensation temperature than the Brilman reactor. This leads to higher kinetic rates (due to higher reaction temperature) and higher methanol condensation (due to lower condenser temperature). However, the mass of the catalyst in the Brilman reactor was almost four times higher than in this case ((about 172 grams compared to 45 grams). Therefore, in terms of mass, the methanol produced is higher in the case of Brilman, which results in a higher reaction heat, but a lower methanol productivity because of high catalyst mass. The major drawback of high energy input in the Brilman reactor was overcome in this study mainly due to the presence of heat integration. This is the reason why the energy demand in the current reactor is almost a third of the Brilman reactor.

4.5. Experiments with crushed catalyst particles

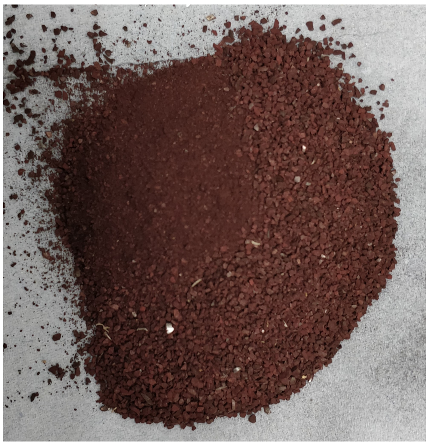

Figure 4.16: Crushed catalyst pellets.

After experiments with 5 mm pellets, crushed catalyst particles were used to see whether a reduction in catalyst size would increase the methanol production. 228 °C was set as the catalyst bed temperature and 10 minutes as the sampling time (since these were the optimum values obtained using the 5 mm pellets). The condenser wall temperature was maintained at 62 °C.

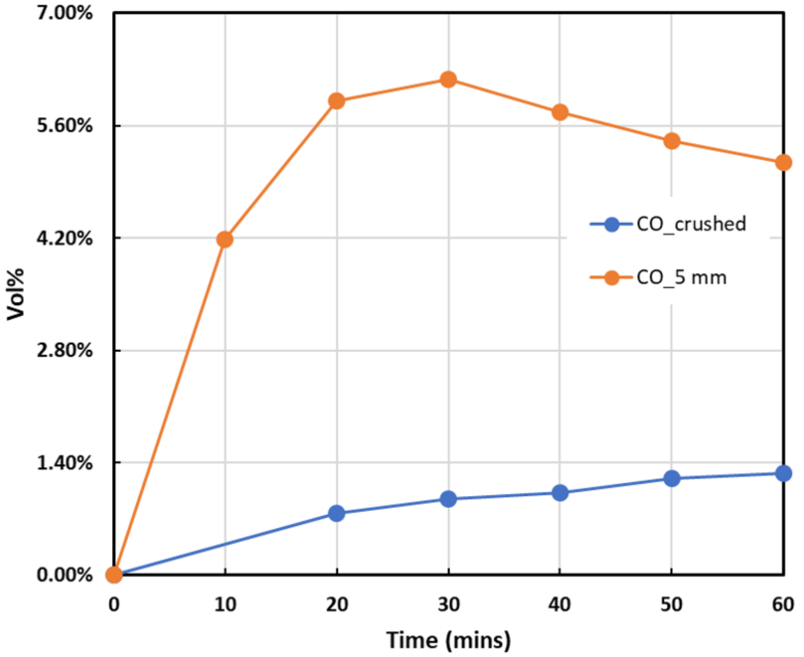

Figure 4.17: Variation in CO formation with time for 5 mm and crushed catalyst pellets. Reduction in catalyst size did not lead to increased methanol production as the flow rate was restricted as a result of high pressure drop caused by the small particle size.

Tests with crushed pellets did not yield any liquid even after an hour of operation. This could be due to flow blockage due to high catalyst packing, resulting in no reaction. In order to check this hypothesis, the gas composition was analyzed in the gas chromatograph. Indeed, it was found that the maximum CO concentration using crushed pellets was only 1.27% after an hour of reaction time compared to 6.17% for 5 mm pellets (see Figure 4.17). This confirmed the hypothesis that the high pressure drop caused reduced flow of the gases leading to almost negligible reaction. Since the crushed pellets did not yield any methanol, the next series of experiments were performed with the 5 mm pellets cut into two halves along the central axis (2.5 mm diameter).

4.6. Experiments with 5 mm pellets cut into two halves

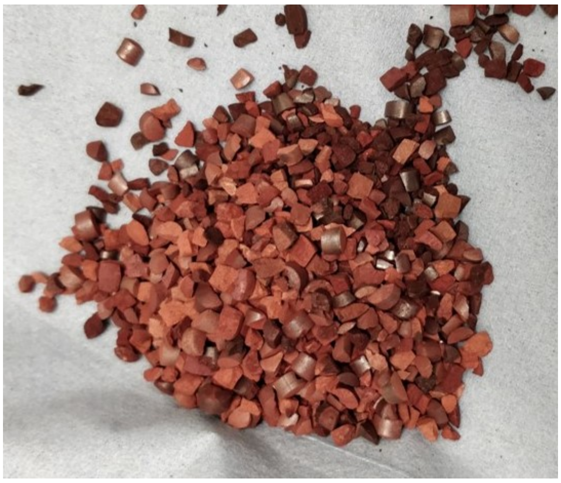

Figure 4.18: 5 mm catalyst pellets cut into two halves along the central axis.

The 5 mm pellets were cut into two halves along the central axis (Figure 4.18) to observe whether this catalyst size would result in increased methanol production without increasing the pressure drop by a large amount.

A methodology similar to Section 4.4 was followed. First the temperature of the catalyst bed was fixed and the sampling time of the liquids was optimized. The result of this experiment is presented in Figure 4.19.

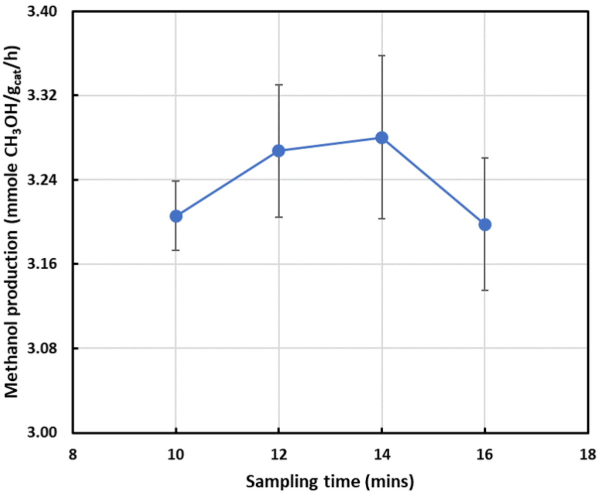

Figure 4.19: Variation in methanol production with sampling time. Maximum production is observed at 14 minutes of sampling compared to 10 minutes using 5 mm pellets, pointing towards flow limitations imposed by a higher pressure drop.

14 minutes was found as the optimum sampling time in this case compared to 10 minutes for 5 mm pellets (see Figure 4.11). The increase in sampling time to get the maximum amount of methanol in this

case can be attributed to reduced flow due to increased pressure drop. This meant that the gas needed more time to reach the equilibrium composition in the latter case. This is also evident in the maximum production of 3.3 mmole $CH_3OH/g_{cat}/h$ using these pellets compared to 6.8 mmole $CH_3OH/g_{cat}/h$ using 5 mm pellets.

Experiments were then performed by keeping the sampling time fixed at 14 minutes and varying the temperature. The results are presented in Figure 4.20. The methanol production as well as the efficiency values for these pellets do not show a decrease with temperature beyond 230 °C as was the case when using 5 mm pellets (observe Figure 4.15). This again points towards reduced mass flow in the reactor with these pellets, which means that the gas mixture is yet to reach equilibrium within the sampling time of 14 minutes. Increasing the temperature increases the mass flow rate (see Table 2.10), thereby driving the gas mixture closer towards equilibrium and increasing the methanol production. The results of these tests are tabulated in Table 4.7.

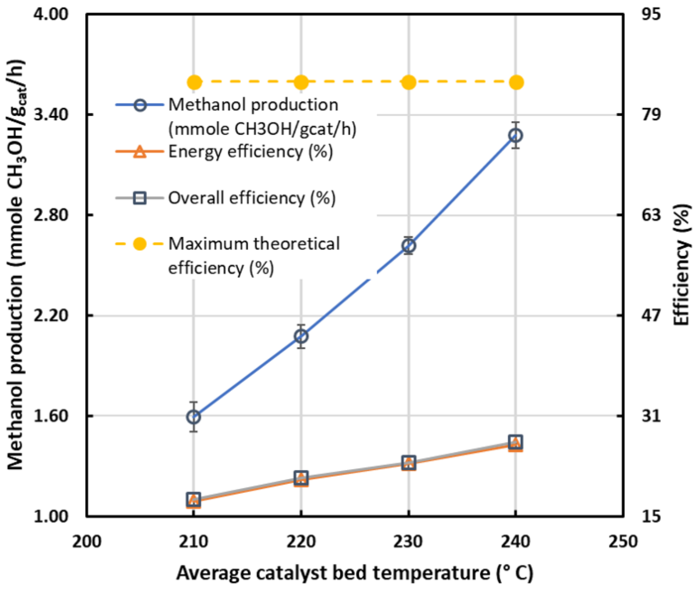

Figure 4.20: Variation of overall efficiency and methanol production with reaction temperature.

Table 4.7: Results of the experiments performed using 5 mm pellets cut into two halves at 14 minutes of sampling time. The methanol production and efficiency are lower compared to the results obtained using 5 mm pellets.

Parameter	Value				Unit
	210 °C	220 °C	230 °C	240 °C	
$\dot{m}_{CH_3OH}$	2.38E-03	3.09E-03	3.90E-03	4.89E-03	kg/h
$\dot{m}_{H_2}$	4.46E-04	5.80E-04	7.31E-04	9.17E-04	kg/h
$\dot{m}_{CO_2}$	3.27E-03	4.25E-03	5.36E-03	6.72E-03	kg/h
$n_{H_2} \cdot \Delta H_{CO_2\ \text{hydrogenation}}$	1.0	1.3	1.7	2.1	W
Q_{in}	68.8	71.5	78.5	82.8	W
Heat integration	8.4	8.5	8.6	8.6	W
$\dot{m}_{CH_3OH} \cdot HHV_{CH_3OH}$	14.8	19.2	24.3	30.4	W
$\dot{m}_{H_2} \cdot HHV_{H_2}$	17.6	22.8	28.8	36.1	W
Energy efficiency	17.5	20.9	23.5	25.2	%
Overall efficiency	17.7	21.2	23.6	25.6	%
Carbon conversion	96.0	96.0	96.9	98.7	%
Selectivity	96.6	97.4	98.0	98.5	%

4.7. Comparison of experimental results with simulations in COCO and Fluent

A process model developed by Gutierrez-Neri [104] in COCO was worked on to match the simulation results with those of the experiments. The model took into account the effect of heat integration.

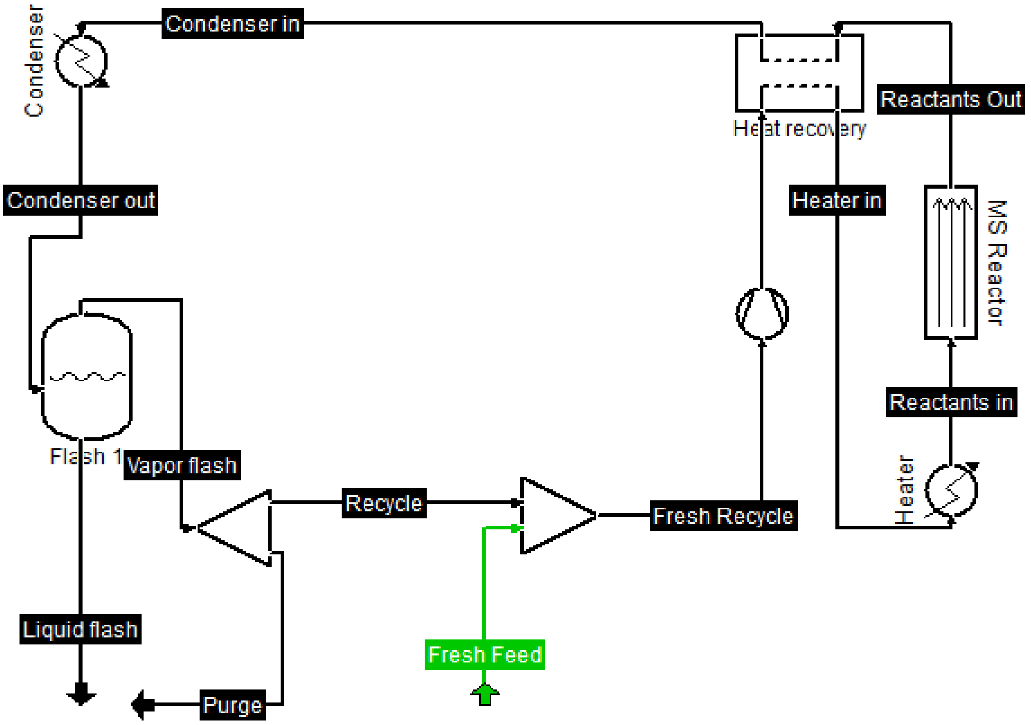
Condenser
Condenser in
Heat recovery
Reactants Out
Condenser out
Heater in
MS Reactor
Reactants in
Flash 1
Vapor flash
Recycle
Fresh Recycle
Heater
Liquid flash
Fresh Feed
Purge

Figure 4.21: Simulation model developed in COCO by Guttierez-Neri [104] incorporating the heat integration achieved by the aluminium blocks.

The model consists of a fresh feed of the feed gas which mixes with the recycle stream. The feed is then compressed and heated after which it reacts in an isothermal plug flow reactor, which has the kinetics of Bussche and Froment [25]. The inlet and outlet streams of the reactor pass through a heat integration block, after which the feed is cooled in the condenser and flashed to give a liquid and vapor stream. Methanol and water mixture is obtained in the liquid stream while the vapor products are recycled after purging. Purging is done to keep the concentration of CO in the reactor low.

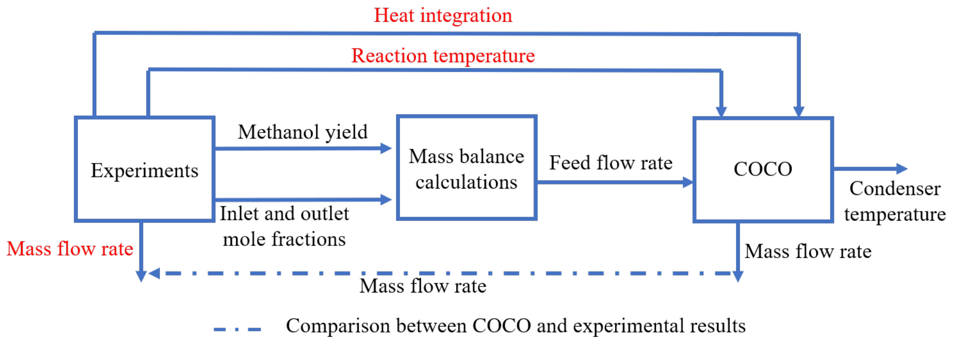
Heat integration
Reaction temperature
Experiments
Methanol yield
Inlet and outlet mole fractions
Mass balance calculations
Feed flow rate
COCO
Condenser temperature
Mass flow rate
Mass flow rate
Mass flow rate
Comparison between COCO and experimental results

Figure 4.22: Steps to compare experimental and simulation results obtained from COCO. Red font indicates possible sources of error in the measurement.

In order to compare the experimental results with those of COCO, the steps outlined in Figure 4.22 are followed. The methanol yield, as well as the inlet and outlet mole fractions of the components obtained from the experiments, are used in the mass balance calculations to obtain the feed flow rate of the gases in the reactor. This calculation is quite accurate since the methanol yield and mole fractions are measured using precise instruments.

During the simulation, the feed flow rate of the gases, the heat integration and the reaction temperature obtained from the experiments are fixed. These last two values have some sources of error as they are both calculated using surface temperatures and not using the actual flow temperatures. The condenser temperature is varied until the methanol yield obtained from simulations matches that of the experiments. The value of the temperature so obtained gives a measure of the fluid temperature in the condenser. The parameters for simulating the reaction in COCO are given in Table 4.8. The experimental results using 5 mm pellets at 228 °C reactor wall temperature are compared with COCO since they gave the best results.

Table 4.8: Simulation parameters for the COCO model for 5 mm pellets at 228 °reaction temperature.

Parameter	Value	Unit
Catalyst		
Diameter	5	mm
Density	1263	kg/m^3
Void fraction	0.29	
Heat integration		
Heat integration	11.1	W
Reaction zone		
Reaction temperature	228	°C
Length	0.14	m
Diameter	0.018	m
Condenser		
Condenser temperature	62	°C

The mass flow rate value obtained from the experiments differs slightly from those of the simulations. This is because there was a difference between the gas composition measured during the experiments and obtained from the simulation study. This led to a difference in the specific heat of the mixture, resulting in difference in mass flow rates. The result is presented in Table 4.9.

Table 4.9: Comparison of mass flow rate obtained from experiments and simulations.

Parameter	Experiments	COCO	Fluent	Unit
Mass flow rate	4.61E-5	3.27E-5	3.06E-5	kg/s

To make a comparison between the heat transferred to the condenser from the experiments and simulations, a heat exchange network was constructed to account for the system losses.

4.8. Heat Exchange Network

A heat exchange network (shown in Figure 4.23) was constructed based on the experimental results using 5 mm catalyst pellets at 228 °C reactor wall temperature to account for the losses of the system.

During steady state operation of the reactor, the heat transferred from the heaters should be released thorough the condenser. However, losses from the reactor mean that these two values are not the same. The heat input and losses from the system are summarized in Table 4.10. This value of heat obtained from the experiments was then compared with the results from COCO (Table 4.11). The two values have a close agreement with each other. The difference is due to inaccuracies in temperature

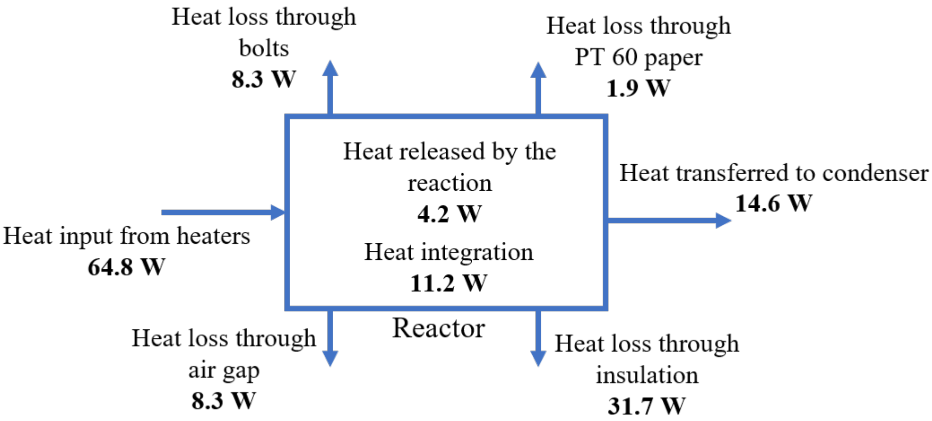
Heat loss through
bolts
8.3 W
Heat loss through
PT 60 paper
1.9 W
Heat released by the
reaction
4.2 W
Heat integration
11.2 W
Heat transferred to condenser
14.6 W
Heat input from heaters
64.8 W
Reactor
Heat loss through
air gap
8.3 W
Heat loss through
insulation
31.7 W

Figure 4.23: Heat exchanging network depicting the pathway of heat loss in the reactor. Loss through the insulation is the highest suggesting that selection of proper insulation material should be a priority for future experimental designs.

measurements during the experiments.

Table 4.10: Heat losses in the system.

Parameter	Value	Unit
Heat input	64.8	W
Heat loss through bolts	8.3	W
Heat loss through air gap	8.3	W
Heat loss through PT 60	1.9	W
Heat loss through insulation	31.7	W
Heat transferred to the condenser	14.6	W
Heat integration	11.2	W
Heat released by the reaction	4.2	W

Table 4.11: Comparison of heat transferred to the condenser based on experimental and simulation results.

Parameter	Experiments	COCO	Unit
Heat transferred to the condenser	14.6	14.1	W

Once this comparison was done, different scenarios were postulated for the heat exchange network to estimate whether autothermal operation of the reactor was possible (Figure 4.24).

In the first case, the values of the heat input and the losses calculated from experimental findings are shown. In the next case ("Perfect insulation"), the insulation is assumed to be perfect with no heat loss to the surroundings. This leads to a decrease in heat input needed to maintain the reaction temperature. In subsequent cases ("Perfect insulation + Air gap insulated" and "Perfect insulation + Air gap insulated + Insulated bolt spacers"), the losses from the air gap, PT 60 and from the bolts are also assumed to be zero. It can be seen that even though the heat released by the reaction and the heat integration achieved are 4.2 W and 11.2 W, respectively, 14.6 W of heat needs to be applied at the input externally to maintain the reaction temperature. Therefore, autothermal operation of the reactor is possible if an additional 14.6 W (and in total 25.8 W) of heat integration is achieved, given the current rate of methanol production. The calculation procedure for the same is presented in Appendix F.

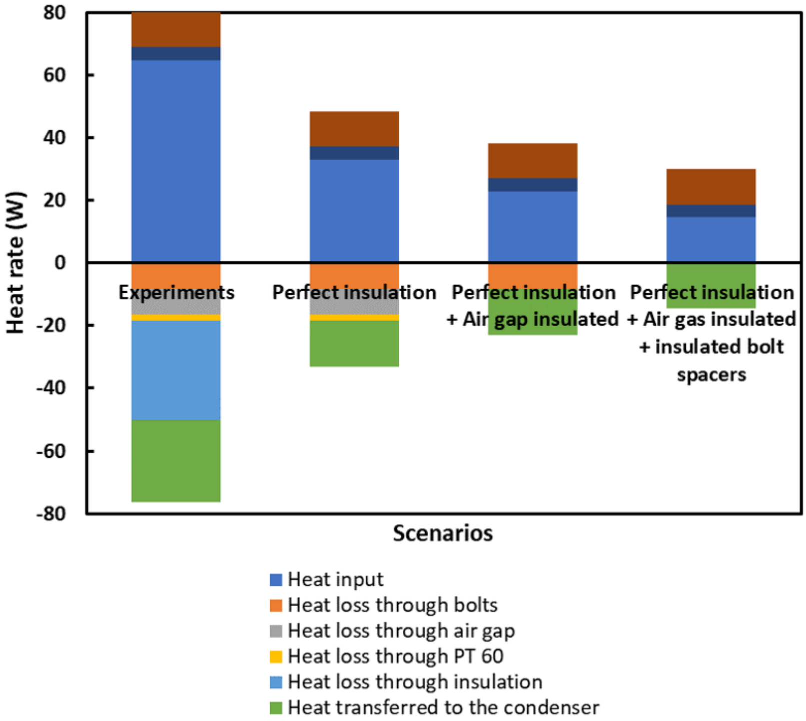

Figure 4.24: Scenarios for estimating the performance of the reactor in case of no heat losses. Autothermal reactor operation is possible if an additional 14.6 W of heat is generated from the system. This can be achieved using higher heat integration or by producing more methanol.

5

Conclusions and Recommendations

5.1. Conclusions

The objective of this thesis was to experimentally characterize a novel small-scale natural circulation loop methanol synthesis reactor with internal heat recovery. To that end, the reactor with six heat integration blocks having 2 mm flow channels developed at the end of the internship project of the author was modified to include additional sensors to measure the heat integration and pressure. A data logging circuit was built to enable easy data collection.

Experiments were first performed with N_2 to get an estimate of the mass flow rate and heat input to the system when using an inert gas. The data obtained was compared with the simulation results in Fluent by Gutierrez-Neri [104]. After these tests, experiments with the feed gas were performed which yielded no/very less liquid output. A fault tree analysis was done to identify possible causes of this low yield. It was ultimately found that premature condensation of the liquid in the channels was the problem and therefore, three heat integration blocks were removed and the flow channel dimensions increased from 2 mm to 6.5 mm. Significant methanol yield was obtained after these modifications.

Experiments were then performed using 5 mm catalyst pellets as they were obtained from the manufacturer. The sampling time of the liquids was optimized and the methanol production variation with temperature was studied. Tests were performed using the 5 mm pellets cut into two halves as well as crushed pellets. They did not yield much liquid since the pressure drop caused by the smaller catalyst sizes was high compared to the driving force available to the flow due to natural convection.

Based on the experimental results using 5 mm pellets, a mass balance calculation was done to estimate the feed flow rate of the gases into the reactor. A process model incorporating heat integration developed by Gutierrez-Neri [104] was then worked on to compare the experimental results with those of the simulations in COCO. Finally, a heat exchange network was built to identify the losses in the system and to determine whether autothermal operation of the reactor was feasible.

Three main research questions were posed at the beginning of this thesis. Having studied the process, the questions can now be answered.

What is the maximum methanol productivity and overall system efficiency that can be obtained experimentally using the reactor given the process conditions?

A maximum methanol productivity of 6.8 mmole $CH_3OH/g_{cat}/h$ was obtained at 228 °C reactor wall temperature using 5 mm catalyst pellets. While this value is more than that obtained by Brilman et al. [16] because of a higher reaction temperature (faster kinetics) and lower condensation temperature (more methanol condensed) in this study, it is less than the industrial value of 19.4 mmole $CH_3OH/g_{cat}/h$ obtained by Chen et al. [21]. This is because Chen simulated the industrial process at higher pressure (66.7 bar) and with higher feed flow rates. The methanol production is also lower compared to what the reactor was initially designed for (18.8 mmole $CH_3OH/g_{cat}/h$-Section 3.1). This limitation is mainly because the liquid sampling was done at fixed intervals rather than when the liquid collection tube at the bottom of the reactor was filled up.

The optimum reactor wall temperature using 5 mm pellets has been found to be 228 °C. The other important parameters to obtain high methanol productivity are the condenser temperature, the heat integration achieved and the liquid sampling time. Lowering the condenser temperature ensures that all the methanol and water that is produced is condensed. A lower condenser temperature also increases the driving force available to the flow (See Appendix G). Increased heat integration leads to a higher mass flow rate which results in more methanol production. Optimum liquid sampling time ensures that the liquid is sampled when the liquid collection tube is full and not at specific time intervals (as done in this study).

Heat integration has an indirect impact on the overall efficiency of the system. This is because a high value of heat integration lowers the heat input required from the heaters to maintain the reaction temperature. This in turn increases the overall system efficiency. In the case of experiments using 5 mm pellets at 228 °C, the heat input, heat integration and overall efficiency of the system were 64.8 W, 11.2 W and 44.3%, respectively. If there were no heat integration, the overall efficiency would have been 41.0% instead of 44.3%.

How do the heat losses and mass flow rate of the system compare with the values obtained from simulations?

The simulations of the process done in COCO by the author assume perfect heat transfer (no losses). Therefore, comparison of heat losses obtained from the experiments to those from simulations was not directly possible. A heat exchange network was developed which accounted for all the heat losses in the system. These losses were subtracted from the heat input to give the heat transferred to the condenser and it was this value that was compared with the simulation results. The experimental and COCO values showed a close match (observe Table 4.11). Heat transfer to the condenser obtained from the Fluent model developed by Guttierez-Neri [104] accounted only for the sensible heat loss (and not the latent heat loss) and therefore was not compared with the values obtained from experiments and COCO.

The mass flow rates differed slightly due to the different gas compositions measured during the experiments and obtained from the Fluent simulation study. This led to a difference in specific heat of the mixture and ultimately, different mass flow rates.

What implications do the results obtained have for future designs of the NCL reactor?

The heat exchange network developed provided valuable insights regarding future reactor designs. If all the losses of the system are assumed to be zero (an ideal case), then an additional 14.6 W of heat is required to achieve autothermal reactor operation for the current system. This additional heat can be obtained by increasing the methanol production (which is an exothermic reaction and releases heat) and by improving the heat integration that can be achieved. The next section discusses how this can be done.

5.2. Recommendations

While this study provided valuable insights into the working of a small-scale reactor, there are still many areas of improvement.

The mass of the reactor used in this study was close to five kilograms. This resulted in the system taking a long time to reach steady state in terms of temperature profiles (close to 90 minutes). Such a time frame will not be feasible when this system is deployed in the field. Therefore, the weight of the reactor should be reduced. This can be done by reducing the thicknesses of the reaction and condensation zone blocks (which are currently overdimensioned). Replacing the heat integration blocks made of aluminium with copper heat pipes would reduce the weight as well as improve the heat transfer significantly.

Although aluminium was chosen as the material of construction in this study, it has a "fair" (not too good) tolerance to methanol. Over the course of the experiments, the author found that the area near the flow channels which came in contact with the liquid methanol was starting to corrode (see Appendix H). Therefore, some other material compatible with methanol must be chosen. Stainless steel lined aluminium can be an alternative.

An experiment was conducted using N_2 as the fluid with the flow on the condenser side completely blocked. The reactor wall and the condenser wall temperature were maintained as 210 °C and 42 °C. The heat input in this case was obtained as 43.0 W (Table 4.1). The heat exchange network predicted 50.2 W of heat losses from the system (Section 4.8). However this test was done at a higher temperatures (228 °C and 62 °C respectively for the two zones). Since the N_2 test gives a heating value in case of no flow (which ideally translates to heat loss since there is no flow, and hence no energy is transferred to the flow), an experiment conducted with N_2 at the operation parameters used in the experiment should give a heat input close to 50 W. This would help in correlating the experimental and analytical results better.

Based on the results of the heat exchange network constructed, the losses of the system need to be reduced to achieve autothermal operation. Loss through insulation was identified as the major component. Therefore, choosing an appropriate insulation material becomes paramount. Silica aerogels can be the material of choice as they have a very low thermal conductivity (about 0.005 W/m-K [110]) and can withstand very high temperatures.

Loss through the air gaps can be reduced by having some space between the blocks, which is only 1 mm in the current design and therefore not feasible to insulate. Placing an insulation material like silica aerogel between the gap can help reduce the axial heat loss to almost zero.

Eight bolts connect the reactor components together. Since these are made of stainless steel, they also conduct heat. Having plastic spacers in the places where these bolts touch the metal components of the reactor can help reduce this heat loss. Vespel® can be used as the plastic material because of its high temperature resistance.

Once all these losses are reduced, autothermal operation of the reactor can be possible if an additional 14.6 W of heat is available (based on the results obtained using 5 mm pellets at 228 °C). This heat can be achieved in two ways-either by increasing the methanol production (which results in more heat released by the reaction) or by increasing the heat integration. Increasing the heat integration can be done by adding more blocks to the reactor. For the current design, an experiment with six heat integration blocks-three with 2 mm flow channels placed close to the reaction zone followed by three blocks with 6.5 mm flow channels close to the condensation zone would increase the heat integration even more, and thereby the overall efficiency. Improving the heat integration would help to improve methanol production as the mass flow rate would then be increased.

Reducing the condenser temperature would also help to improve the methanol production. To this end, the COCO process model shown in Figure 4.21 was used to evaluate the effect of changing this parameter changes on methanol yield. It was found that reducing the condenser temperature to 35 °C (the condenser wall temperature in the experiments was 62 °C) can greatly improve the methanol yield (Appendix G). Reduction of the condenser fluid temperature can be done using external fins. If internal fins are used, they can limit the flow rate in the reactor by adding resistance to the flow. Also flow blockage can result due to condensation of the liquid droplets in the flow channels. Increasing the catalyst bed diameter can also lead to more methanol production (because of higher mass of the catalyst). But the heat transfer from the walls to the fluid in case of large diameters needs to be investigated as the possibility of hot spot formation is high.

The methanol yield was also limited by the size of the collection zone (the tube at the bottom of the condenser block where the liquid used to accumulate before being sluiced). Therefore, future designs need to have a level sensor whereby the liquid is sampled when the collection tube becomes full and not at specified time intervals (determined by the sampling time measurements in this study). This would help increase the productivity. If the tube having the level sensor is transparent, then the liquid accumulation can also be observed.

One of the sources of error in the measurements came from the fact that surface temperatures were measured and not the fluid temperatures. Therefore, to improve the accuracy, fluid temperatures need to be measured using precise thermocouples since the ones used in this study were not very accurate. In addition, two thermocouples should be placed at the inlet and outlet of the condenser block to have a measure of the temperature gradient (only one was used in this study).

A differential pressure gauge placed across the catalyst bed can give an accurate measure of the pressure drop developed due to the flow. This can be useful when using smaller catalyst pellets. Smaller pellets increase the outer surface area available for the reaction and also take the ratio of the diameter of the channel to the those of the pellets closer to 22, which was suggested by Bussche and Froment [25] as the optimum to achieve uniform flow. However in this study, using smaller pellets led to low production due to increased pressure drop. A differential pressure sensor would help to get a measure of this value.

This study was conducted using H_2 and CO_2 in the molar ratio of 3:1. Tests also need to be conducted with different feed ratios to test the system response under various inlet compositions.

Bibliography

[1] Aspen plus, .

[2] Cape open to cape open simulation environment, .

[3] Matlab, .

[4] Kyoto protocol: United nations framework convention on climate change, .

[5] Paris agreement: United nations framework convention on climate change, .

[6] R. Pidcock, Analysis: What global emissions in 2016 mean for climate change goals, (2016).

[7] A. Goeppert, G. A. Olah, and G. S. Prakash, Toward a sustainable carbon cycle: the methanol economy, in Green Chemistry (Elsevier, 2017) pp. 919–962.

[8] Global ccs institute: Projects database, .

[9] Lake nyos: Deadliest lake in the world suffocated over 1,746 people in one night, .

[10] I. Statistics, Key world energy statistics 2017, International Energy Agency (2017).

[11] A. Goeppert, M. Czaun, J.-P. Jones, G. S. Prakash, and G. A. Olah, Recycling of carbon dioxide to methanol and derived products–closing the loop, Chemical Society Reviews **43**, 7995 (2014).

[12] Annual worldwide methanol supply and demand balance, .

[13] Ihsg: Global methanol market review, (2012).

[14] A. Basile and F. Dalena, Methanol: Science and Engineering (Elsevier, 2017).

[15] G. Bozzano and F. Manenti, Efficient methanol synthesis: perspectives, technologies and optimization strategies, Progress in Energy and Combustion Science **56**, 71 (2016).

[16] M. J. Bos and D. W. F. Brilman, A novel condensation reactor for efficient CO_2 to methanol conversion for storage of renewable electric energy, Chemical engineering journal **278**, 527 (2015).

[17] B. Xu, R. Yang, F. Meng, P. Reubroycharoen, T. Vitidsant, Y. Zhang, Y. Yoneyama, and N. Tsubaki, A new method of low temperature methanol synthesis, Catalysis surveys from Asia **13**, 147 (2009).

[18] J. Van Bennekom, R. Venderbosch, J. Winkelman, E. Wilbers, D. Assink, K. Lemmens, and H. Heeres, Methanol synthesis beyond chemical equilibrium, Chemical Engineering Science **87**, 204 (2013).

[19] A. MacCarley, Methanol fuel safety-a practical guide, (2013).

[20] Zero emission fuels, .

[21] L. Chen, Q. Jiang, Z. Song, and D. Posarac, Optimization of methanol yield from a lurgi reactor, Chemical engineering & technology **34**, 817 (2011).

[22] United states environmental protection agency: Understanding global warming potentials, .

[23] A. Eisentraut, Sustainable production of second-generation biofuels, (2010).

[24] G. A. Olah, Beyond oil and gas: the methanol economy, Angewandte Chemie International Edition **44**, 2636 (2005).

[25] K. V. Bussche and G. Froment, A steady-state kinetic model for methanol synthesis and the water gas shift reaction on a commercial $Cu/ZnO/Al_2O_3$ catalyst, Journal of Catalysis **161**, 1 (1996).

[26] M. Saito, R&d activities in japan on methanol synthesis from CO_2 and H_2, Catalysis Surveys from Asia **2**, 175 (1998).

[27] Y. Amenomiya, Infrared study of methanol synthesis from CO_2+ H_2 on supported copper-zinc oxide catalysts, in Proc. of 8th Int. Congress on Catal, Vol. 2 (1984) pp. 557–567.

[28] T. Tagawab, G. Pleizier, and Y. Amenomiya, Methanol synthesis from CO_2+ H_2 i. characterization of catalysts by tpd, Applied catalysis **18**, 285 (1985).

[29] T. Tagawa and Y. Amenomiya, An infrared spectroscopy system for catalytic reaction at elevated pressure and temperature, Applied spectroscopy **39**, 358 (1985).

[30] H. Arakawa, Recycling technology of emitted CO_2.-selective synthesis of methanol from CO_2 by catalytic hydrogenation over $Cu-ZnO/SiO_2$, Shokubai (Catalyst) **33**, 103 (1991).

[31] K. Okabe, K. Sayama, N. Matsubayashi, K. Shimomura, and H. Arakawa, Selective hydrogenation of carbon dioxide to methanol on $Cu-ZnO/SiO_2$ catalysts prepared by alkoxide method, Bulletin of the Chemical Society of Japan **65**, 2520 (1992).

[32] Y. Zhang, Q. Sun, J. Deng, D. Wu, and S. Chen, A high activity $Cu/ZnO/Al_2O_3$ catalyst for methanol synthesis: Preparation and catalytic properties, Applied Catalysis A: General **158**, 105 (1997).

[33] M. Pori, B. Likozar, M. Marinšek, and Z. C. Orel, Preparation of cu/zno-based heterogeneous catalysts by photochemical deposition, their characterisation and application for methanol synthesis from carbon dioxide and hydrogen, Fuel Processing Technology **146**, 39 (2016).

[34] X.-M. Liu, G. Lu, Z.-F. Yan, and J. Beltramini, Recent advances in catalysts for methanol synthesis via hydrogenation of CO and CO_2, Industrial & engineering chemistry research **42**, 6518 (2003).

[35] G. Bonura, F. Arena, G. Mezzatesta, C. Cannilla, L. Spadaro, and F. Frusteri, Role of the ceria promoter and carrier on the functionality of cu-based catalysts in the CO_2-to-methanol hydrogenation reaction, Catalysis Today **171**, 251 (2011).

[36] J. S. Lee, K. I. Moon, S. H. Lee, S. Y. Lee, and Y. G. Kim, Modified $Cu/ZnO/Al_2O_3$ catalysts for methanol synthesis from $CO_{2/}H_2$ and CO/H_2, Catalysis letters **34**, 93 (1995).

[37] M. B. Fichtl, D. Schlereth, N. Jacobsen, I. Kasatkin, J. Schumann, M. Behrens, R. Schlögl, and O. Hinrichsen, Kinetics of deactivation on $Cu/ZnO/Al_2O_3$ methanol synthesis catalysts, Applied Catalysis A: General **502**, 262 (2015).

[38] J. T. Sun, I. S. Metcalfe, and M. Sahibzada, Deactivation of $Cu/ZnO/Al_2O_3$ methanol synthesis catalyst by sintering, Industrial & engineering chemistry research **38**, 3868 (1999).

[39] X. Zhai, J. Shamoto, H. Xie, Y. Tan, Y. Han, and N. Tsubaki, Study on the deactivation phenomena of cu-based catalyst for methanol synthesis in slurry phase, Fuel **87**, 430 (2008).

[40] H. S. Fogler et al., Elements of chemical reaction engineering, (1999).

[41] W. Seyfert and G. Luft, Untersuchungen zur methanol-synthese im mitteldruckbereich, Chemie Ingenieur Technik **57**, 482 (1985).

[42] G. Graaf, E. Stamhuis, and A. Beenackers, Kinetics of low-pressure methanol synthesis, Chemical Engineering Science **43**, 3185 (1988).

[43] P. Villa, P. Forzatti, G. Buzzi-Ferraris, G. Garone, and I. Pasquon, Synthesis of alcohols from carbon oxides and hydrogen. 1. kinetics of the low-pressure methanol synthesis, Industrial & engineering chemistry process design and development **24**, 12 (1985).

[44] O. Schermuly and G. Luft, Methanol-syntheses im treibstrahlreaktor, Ger Chem Eng **1**, 222 (1977).

[45] J. Monnier, G. Apai, and M. Hanrahan, Effect of CO_2 on the conversion of H_2CO to methanol over copper-chromia catalysts, J. Catal.;(United States) **88** (1984).

[46] M. Takagawa and M. Ohsugi, Study on reaction rates for methanol synthesis from carbon monoxide, carbon dioxide, and hydrogen, Journal of Catalysis **107**, 161 (1987).

[47] V. Leonov, M. Karavaev, E. Tsybina, and G. Petrishcheva, Kinetik der methanol-synthese an einem tieftemperatur-katalysator, Chemischer Informationsdienst **4**, no (1973).

[48] A. Y. Rozovskii, G. Lin, L. Liberov, E. Slivinskii, S. Loktev, Y. B. Kagan, and A. Bashkirov, Mechanism of methanol synthesis from carbon dioxide and hydrogen iii. determination of the rates of individual steps using carbon-14 monooxide, Kinet. Katal **18**, 691 (1977).

[49] A. Y. Rozovskii, Y. B. Kagan, G. Lin, E. Slivinskii, S. Loktev, L. Liberov, et al., Mechanism of methanol synthesis from carbon monoxide and hydrogen, Kinetika i Kataliz **16**, 810 (1975).

[50] J. Skrzypek, M. Lachowska, and H. Moroz, Kinetics of methanol synthesis over commercial copper/zinc oxide/alumina catalysts, Chemical engineering science **46**, 2809 (1991).

[51] Y. Borodko and G. Somorjai, Catalytic hydrogenation of carbon oxides–a 10-year perspective, Applied Catalysis A: General **186**, 355 (1999).

[52] T. Askgaard, J. Norskov, C. Ovesen, and P. Stoltze, A kinetic model of methanol synthesis, Journal of Catalysis **156**, 229 (1995).

[53] T. Kubota, I. Hayakawa, H. Mabuse, K. Mori, K. Ushikoshi, T. Watanabe, and M. Saito, Kinetic study of methanol synthesis from carbon dioxide and hydrogen, Applied organometallic chemistry **15**, 121 (2001).

[54] M. Šetinc and J. Levec, Dynamics of a mixed slurry reactor for the three-phase methanol synthesis, Chemical engineering science **56**, 6081 (2001).

[55] G. Chinchen, R. Logan, and M. Spencer, Water-gas shift reaction over an iron oxide/chromium oxide catalyst.: Ii: Stability of activity, Applied Catalysis **12**, 89 (1984).

[56] Z. Xu, Z. Qian, and H. Hattori, Mechanistic study of the hydrogenation of carbon dioxide to methanol over supported rhenium and copper–zinc catalysts, Bulletin of the Chemical Society of Japan **64**, 3432 (1991).

[57] J. S. Lee, K. H. Lee, S. Y. Lee, and Y. G. Kim, A comparative study of methanol synthesis from $CO_{2/}H_2$ and CO/H_2 over a $Cu/ZnO/Al_2O_3$ catalyst, Journal of Catalysis **144**, 414 (1993).

[58] I. Dybkjaer, Design of ammonia and methanol synthesis reactors, in Chemical Reactor Design and Technology (Springer, 1986) pp. 795–819.

[59] B. Denise, R. Sneeden, and C. Hamon, Hydrocondensation of carbon dioxide: Iv, Journal of Molecular Catalysis **17**, 359 (1982).

[60] K. Klier, V. Chatikavanij, R. Herman, and G. Simmons, Catalytic synthesis of methanol from COH_2: Iv. the effects of carbon dioxide, Journal of Catalysis **74**, 343 (1982).

[61] R. Bardet, J. Thivolle-Cazat, and Y. Trambouze, Hydrocondensation des oxydes de carbone, à la pression atmosphérique, sur des catalyseurs $Cu-ZnO-Al_2O_3$. influence de l'eau sur la formation du méthanol, Comptes-rendus des séances de l'Académie des sciences. Série 2, Mécanique-physique, chimie, sciences de l'univers, sciences de la terre **299**, 423 (1984).

[62] The role of CO_2 in methanol synthesis on [cu-zn, .

[63] G. Chinchen, C. Hay, H. Vandervell, and K. Waugh, The measurement of copper surface areas by reactive frontal chromatography, Journal of Catalysis **103**, 79 (1987).

[64] C. J. Schack, M. A. McNeil, and R. G. Rinker, Methanol synthesis from hydrogen, carbon monoxide, and carbon dioxide over a $CuO/ZnO/Al_2O_3$ catalyst: I. steady-state kinetics experiments, Applied catalysis **50**, 247 (1989).

[65] M. A. McNeil, C. J. Schack, and R. G. Rinker, Methanol synthesis from hydrogen, carbon monoxide and carbon dioxide over a $CuO/ZnO/Al_2O_3$ catalyst: Ii. development of a phenomenological rate expression, Applied catalysis **50**, 265 (1989).

[66] A. Y. Rozovskii and G. I. Lin, Fundamentals of methanol synthesis and decomposition, Topics in Catalysis **22**, 137 (2003).

[67] H.-W. Lim, M.-J. Park, S.-H. Kang, H.-J. Chae, J. W. Bae, and K.-W. Jun, Modeling of the kinetics for methanol synthesis using $Cu/ZnO/Al_2O_{3/}ZrO_2$ catalyst: influence of carbon dioxide during hydrogenation, Industrial & Engineering Chemistry Research **48**, 10448 (2009).

[68] L. Grabow and M. Mavrikakis, Mechanism of methanol synthesis on cu through CO_2 and CO hydrogenation, Acs Catalysis **1**, 365 (2011).

[69] N. Park, M.-J. Park, Y.-J. Lee, K.-S. Ha, and K.-W. Jun, Kinetic modeling of methanol synthesis over commercial catalysts based on three-site adsorption, Fuel Processing Technology **125**, 139 (2014).

[70] G. Graaf, H. Scholtens, E. Stamhuis, and A. Beenackers, Intra-particle diffusion limitations in low-pressure methanol synthesis, Chemical Engineering Science **45**, 773 (1990).

[71] W. L. Luyben, Design and control of a methanol reactor/column process, Industrial & Engineering Chemistry Research **49**, 6150 (2010).

[72] C. Ovesen, B. Clausen, J. Schiøtz, P. Stoltze, H. Topsøe, and J. K. Nørskov, Kinetic implications of dynamical changes in catalyst morphology during methanol synthesis over Cu/ZnO catalysts, Journal of Catalysis **168**, 133 (1997).

[73] A. Pinto and P. Rogerson, Heat transfer-impact of high fuel cost on plant design, Chemical Engineering Progress **73**, 95 (1977).

[74] J. LeBlanc and R. Schneider, Cape horn methanol: reliable performance in a remote location, in Proceedings of the 1991 World Methanol Conference, Vancouver, BC, Canada (1991).

[75] L. Engineering, Isothermal reactor, .

[76] I. Takase and K. Niwa, Mitsubishi (mgc/mhi) methanol process, Chemical economy and engineering review **17**, 24 (1985).

[77] E. Heydorn, B. Diamond, and R. Lilly, Commercial-scale demonstration of the liquid phase methanol (lpmeoh) process, Prepared for the US DOE, National Energy Technology Laboratory (2003).

[78] P. L. Spath and D. C. Dayton, Preliminary screening-technical and economic assessment of synthesis gas to fuels and chemicals with emphasis on the potential for biomass-derived syngas, Tech. Rep. (National Renewable Energy Lab Golden Co, 2003).

[79] E. Supp and R. Quinkler, The lurgi low-pressure methanol process, Handbook of Synfuels Technology. Edited by RA Meyers. New York: McGraw Hill , 2 (1984).

[80] J. Haid and U. Koss, Lurgi's mega-methanol technology opens the door for a new era in downstream applications, in Studies in Surface Science and Catalysis, Vol. 136 (Elsevier, 2001) pp. 399–404.

[81] S. Lee, Methanol synthesis technology (CRC Press, 1989).

[82] H. H. Kung, Deactivation of methanol synthesis catalysts-a review, Catalysis Today **11**, 443 (1992).

[83] F. Gallucci, L. Paturzo, and A. Basile, An experimental study of CO_2 hydrogenation into methanol involving a zeolite membrane reactor, Chemical Engineering and Processing: Process Intensification **43**, 1029 (2004).

[84] B. Sea and K.-H. Lee, Methanol synthesis from carbon dioxide and hydrogen using a ceramic memebrane reactor, Reaction Kinetics and Catalysis Letters **80**, 33 (2003).

[85] A. Basile, L. Di Paola, F. Hai, and V. Piemonte, Membrane reactors for energy applications and basic chemical production (Elsevier, 2015).

[86] R. Struis and S. Stucki, Verification of the membrane reactor concept for the methanol synthesis, Applied Catalysis A: General **216**, 117 (2001).

[87] L. G. van der Ham, H. van den Berg, A. Benneker, G. Simmelink, J. Timmer, and S. van Weerden, Hydrogenation of carbon dioxide for methanol production, CHEMICAL ENGINEERING **29** (2012).

[88] B. Tidona, C. Koppold, A. Bansode, A. Urakawa, and P. R. von Rohr, CO_2 hydrogenation to methanol at pressures up to 950 bar, The Journal of Supercritical Fluids **78**, 70 (2013).

[89] B. Haut, V. Halloin, and H. B. Amor, Development and analysis of a multifunctional reactor for equilibrium reactions: benzene hydrogenation and methanol synthesis, Chemical Engineering and Processing: Process Intensification **43**, 979 (2004).

[90] D. Perko, A. Pohar, and J. Levec, Hydrogenation of CO_2 and CO in a high temperature gradient field between catalyst surface and opposite inert cool plate, AIChE Journal **60**, 613 (2014).

[91] V. H. Atlas, Vdi-verlag gmbh, (1993).

[92] C. Graves, S. D. Ebbesen, M. Mogensen, and K. S. Lackner, Sustainable hydrocarbon fuels by recycling CO_2 and H_2O with renewable or nuclear energy, Renewable and Sustainable Energy Reviews **15**, 1 (2011).

[93] R. Lammerink, Mathematical characterization and simulation of natural convective flow in a condensing CO_2 to methanol reactor, Master Thesis (2015).

[94] A. M. Shulenberger, F. R. Jonsson, O. Ingolfsson, and K.-C. Tran, Process for producing liquid fuel from carbon dioxide and water, (2012), uS Patent 8,198,338.

[95] Blue fuel energy:low-carbon blue fuel gasoline, (2018).

[96] Sunfire-energy everywhere, .

[97] The engineering toolbox: Thermal conductivity of common materials and gases, .

[98] Cp lab safety: Viton chemical compatibility, .

[99] Eriks: Viton® temperature rating, .

[100] Riogen: Data sheet, .

[101] Permanent gases on a cox module using an agilent 490 micro gc, .

[102] Density and concentration calculator for mixtures of methanol and water, .

[103] C. Pears, Y. in Touloukian, R. Powell, C. Ho, and P. Klemens, Thermophysical and electronic properties information and analysis, TPRC Data Ser. **2**, 145 (1971).

[104] Modelling of natural circulation flow reactor for methanol synthesis from renewable sources, (2018).

[105] I.-C. Lo and H.-S. Wu, Methanol formation from carbon dioxide hydrogenation using cu/zno/al2o3 catalyst, Journal of the Taiwan Institute of Chemical Engineers (2018).

[106] J. Schumann, A. Tarasov, N. Thomas, R. Schlögl, and M. Behrens, Cu, zn-based catalysts for methanol synthesis: On the effect of calcination conditions and the part of residual carbonates, Applied Catalysis A: General **516**, 117 (2016).

[107] S. B. Dake and R. V. Chaudhari, Solubility of carbon monoxide in aqueous mixtures of methanol, acetic acid, ethanol and propionic acid, Journal of Chemical and Engineering Data **30**, 400 (1985).

[108] J. Xia, M. Jödecke, Á. Pérez-Salado Kamps, and G. Maurer, Solubility of CO_2 in (CH_3OH+ H_2O), Journal of Chemical & Engineering Data **49**, 1756 (2004).

[109] H. Yin, S. Jiang, Y. Zhang, and H. Ju, Thermodynamic analysis of thermal efficiency of htr-10 hydrogen production system, Journal of nuclear science and technology **43**, 1188 (2006).

[110] A. S. Dorcheh and M. Abbasi, Silica aerogel; synthesis, properties and characterization, Journal of materials processing technology **199**, 10 (2008).

[111] Engineering toolbox: Convective heat transfer, .

[112] The engineering toolbox: Methanol-thermophysical properties at varying temperature, ().

[113] Encyclopaedia britannica: Latent heat, ().

Appendices

A

Parameters for estimating equilibrium conversion of methanol

.

A one pass reactor model was developed in the open source software COCO for estimating the equilibrium methanol conversion (Figure A.1). The kinetics developed by Bussche and Froment were used [25]. The relevant parameters used in the simulation are summarized in Table A.1. While the catalyst density and mass flow rate of the feed are taken from the above mentioned literature, the feed mole fractions are chosen to have a SN of 2. All the parameters are kept the same as mentioned in [25], except the length which is increased so that equilibrium is reached in the reactor in a single pass.

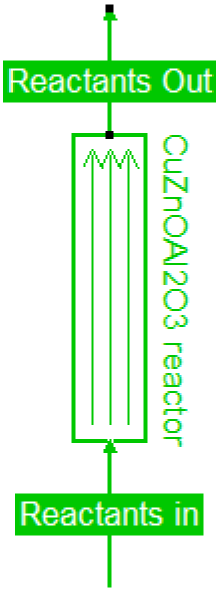

Figure A.1: Model developed in COCO for calculating equilibrium conversion to methanol in a single pass.

Table A.1: Parameters used for conversion of methanol in a single pass reactor.

Parameter	Value	Unit
Feed mole fraction		
H_2	0.82	-
CO_2	0.03	-
CO	0.04	-
Ar	0.11	-
Feed parameters		
Temperature	[200-300]	°C
Pressure	50	bar
Mass flow rate	2.80E-05	kg/s
Reactor		
Diameter	0.016	m
Length	7	m
Catalyst		
Porosity	0.5	-
Diameter	5.00E-04	m
Density	1775	kg/m^3

B

Reactor Dimensions

B.1. Reaction Zone

The dimensions of various components in the reaction zone are presented in Table B.1.

Table B.1: Dimensions of various components of the reaction zone.

Component	Dimensions	Comments
Aluminium block	Cross section: 45 mm * 45 mm Height: 204 mm	Thermocouples: 2
Channel dimension	Diameter: 18 mm Length: 184 mm	None
Flow channel	Diameter: 2 mm	Quantity: 20
O-ring 1	Outer diameter: 29 mm Inside diameter: 23 mm Thickness: 3 mm	Quantity: 1
O-ring 2	Outer diameter: 17 mm Inside diameter: 11 mm Thickness: 3 mm	Quantity: 2
Top plate	Width: 40 mm Length: 40 mm Thickness: 10 mm	None
Heater block	Cross section: 30 mm * 30 mm Length: 100 mm	Quantity: 2 Thermocouples: 2
Cartridge heaters	Power rating: 250 W (each) Diameter: 10 mm Length: 80 mm	Quantity: 2
PT 60 (paper)	Width: 10 mm Length: 30 mm Thickness: 0.5 mm	Quantity: 4

B.2. Heat Integration Blocks

The dimensions of the heat integration block are presented in Table B.2.

Table B.2: Dimensions of the various components of the heat integration block.

Component	Dimensions	Comments
Aluminium block	Width: 30 mm Thickness: 16 mm Height: 202 mm	Thermocouples: 2
Flow channel	Diameter: 2 mm	Quantity: 20
O-ring	Outer diameter: 17 mm Inside diameter: 11 mm Thickness: 3 mm	Quantity: 2
PT 60 (paper)	Width: 10 mm Length: 30 mm Thickness: 0.5 mm	Quantity: 4

B.3. Condenser Block

The dimensions of various components of the condenser block are presented in Table B.3.

Table B.3: Dimensions of the various components of the condenser block.

Component	Dimensions	Comments
Aluminium block	Cross section: 40 mm * 40 mm Height: 212 mm	Thermocouples: 1 To measure the surface temperature of the block Pressure gauge: 1 To measure the reactor pressure Purge valve: 1 For periodically purging the reactor of unwanted gas components (like CO)
Cylindrical channel	Diameter: 10 mm Length: 212 mm	None
Flow channel	Diameter: 2 mm	Quantity: 20
O-ring 1	Outer diameter: 29 mm Inside diameter: 23 mm Thickness: 3 mm	Quantity: 2
O-ring 2	Outer diameter: 17 mm Inside diameter: 11 mm Thickness: 3 mm	Quantity: 2
Top and bottom plate	Width: 40 mm Length: 40 mm Thickness: 10 mm	Bottom plate is connected to two open close valves for liquid sampling
PT 60 (paper)	Width: 10 mm Length: 30 mm Thickness: 0.5 mm	Quantity: 4

C

Industrial methanol production

Chen et al. [21] modelled the methanol production process of a quasi-isothermal Lurgi reactor in Aspen Plus™ and compared their simulation data with an industrial scale reactor with good agreement. The results of the calculation procedure for estimating the methanol production (in mmole $CH_3OH/g_{cat}/h$) are shown in Table C.1.

Table C.1: Calculation of methanol production using the results of Chen et al. [21].

Parameter	Value	Unit
Reactor		
Reactor tube diameter	0.04	m
Reactor length	7	m
Number of tubes	1620	-
Tube volume	8.9E-3	m^3
Catalyst		
Void fraction	0.285	-
Particle fraction	0.715	-
Density	1190	kg/m^3
Mass	10.47	kg_{cat}/tube
Methanol		
Methanol production	10526.4	kg/h
Methanol production per tube	6.5	kg/h/tube
Methanol production	0.621	$g/g_{cat}/h$
Methanol molar mass	32	g/mole
Methanol production	19.4	mmole $CH_3OH/g_{cat}/h$

D

Internal Fins

The internal fins used for an experimental study using N_2 as the fluid were made of aluminium sheets. A mould with corrugations on its surface was 3D printed along with a roller having ridges on its outer surface.

Ribs were created in an aluminium sheet of one micron thickness using the mould after which the sheet was folded to form fin like structures. The 3D mould is shown in Figure D.1a, while the fins themselves are presented in Figure D.1.

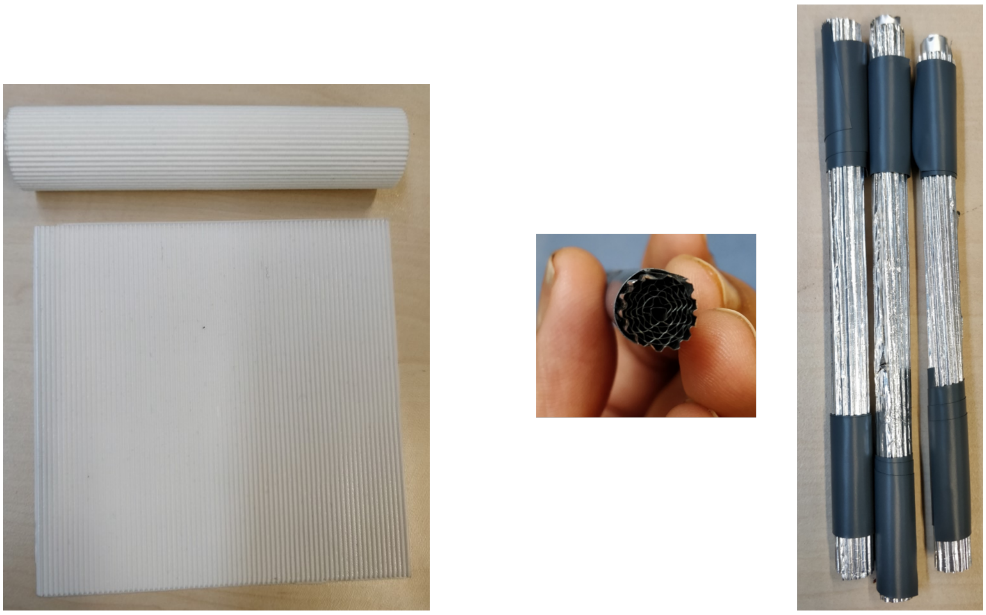

(a) 3D printed mould used for making the fins **(b)** Fins placed inside the condenser block

Figure D.1: Internal fins.

E

Efficiency Calculations

The calculations of the energy and overall efficiency of the system for the experiment using 5 mm pellets at 228 °C reaction temperature are presented in this chapter.

Mass of CH_3OH produced = 9.74E-3 kg/h.

Moles of CH_3OH produced = Mass of CH_3OH produced/Molar mass of CH_3OH = $\frac{9.74E-3}{0.032}$ = 3.04E-1 moles/h.

Assuming that methanol is only produced by hydrogenation of CO_2 (Equation 2.2), it follows that 3 moles of H_2 are consumed for every mole of CH_3OH produced. Therefore,

Moles of H_2 consumed = 9.13E-1 moles/h.

The heat released by the hydrogenation of CO_2 = 49.2 kJ/mole.

Heat released by H_2 consumption = Moles of H_2 consumed * Heat of CO_2 hydrogenation = 9.13E-1*49.2*1000/3600 = 4.2 W.

The heat input from the heaters to the reactor is calculated based on the amount of time the heater was switched on during the process.

Heat input from heaters = 64.8 W.

HHV of CH_3OH= 22.4 MJ/kg.

Heat content of CH_3OH produced = HHV of CH_3OH * Mass of CH_3OH produced = 60.6 W.

Heat content of H_2 fed into the reactor = HHV of H_2 * Mass of H_2 entering the reactor = 71.9 W.

The efficiencies of the reactor are calculated using Equations 4.2 and 4.3.

Energy efficiency = 43.0%.

Overall system efficiency = 44.3%.

The maximum theoretical efficiency is calculated as shown in Table E.1.

Table E.1: Maximum theoretical efficiency calculation for different reaction temperatures using 5 mm pellets.

Parameter	**Value**				**Unit**
	213 °C	220 °C	228 °C	235 °C	
Heat content of CH_3OH (HHV basis)	716800	716800	716800	716800	W
Heat content of H_2 (HHV basis)	850200	850200	850200	850200	W
Heat input (from heaters)	59.2	60.1	64.8	66.9	W
Maximum theoretical efficiency	84.3	84.3	84.3	84.3	%

Table E.2: Maximum theoretical efficiency calculation for different reaction temperatures using 5 mm pellets cut into two halves.

Parameter	**Value**				**Unit**
	210 °C	**220 °C**	**230 °C**	**240 °C**	
Heat content of CH_3OH (HHV basis)	716800	716800	716800	716800	W
Heat content of H_2 (HHV basis)	850200	850200	850200	850200	W
Heat input (from heaters)	68.8	71.5	78.5	82.8	W
Maximum theoretical efficiency	84.3	84.3	84.3	84.3	%

F

Heat Exchange Network Calculations

F.1. Heat loss through bolts

There are eight bolts in the system which hold the components of the reactor in place. These bolts are made of stainless steel, with one end placed inside the reaction zone and the other at the condenser. The heat loss through the bolts is calculated using Fourier's law of heat conduction (Table F.1).

$$Q_{\text{bolts}} = k_{\text{bolts}} \cdot A_{\text{bolts}} \cdot \Delta T_{\text{bolts}}$$

where Q_{bolts} is the heat loss through the bolts in W,

k_{bolts} is the thermal conductivity of the bolt material,

A_{bolts} is the cross sectional area of the bolts,

ΔT_{bolts} is the temperature difference across the bolts.

Table F.1: Heat loss through bolts.

Parameter	Value	Unit
Diameter	6.00E-03	m
Number of bolts	8	-
A_{bolts}	2.26E-04	m^2
k_{bolts}	30	W/m-K
ΔT_{bolts}	116	K
Length	9.45E-02	m
Q_{bolts}	**8.3**	**W**

F.2. Heat loss through PT 60

The PT 60 papers are placed between adjacent blocks (The position of these papers can be seen in Figure 3.5 and Figure 3.7). A part of the heat loss from the papers placed at the top and bottom in the gap between the reaction zone and the first heat integration block will be transferred to the subsequent papers due to axial heat flow. Therefore, heat loss through the paper is considered to be only the loss through the ones placed between the reaction and the first heat integration block.

Like for bolts, the heat loss in this case is also estimated using Fourier's Law:

$$Q_{\text{PT 60}} = k_{\text{PT 60}} \cdot A_{\text{PT 60}} \cdot \Delta T_{\text{PT 60}}$$

where $Q_{PT\ 60}$ is the heat loss through the PT 60 paper,

$k_{PT\ 60}$ is the thermal conductivity of PT 60 paper,

$A_{PT\ 60}$ is the cross sectional area of the paper, which is estimated using Autodesk Fusion.

$\Delta T_{PT\ 60}$ is the temperature difference across the paper.

Table F.2: Heat loss through PT 60.

Parameter	Value	Unit
Surface area	2.23E-04	m^2
ΔT_{top}	45.8	K
ΔT_{bottom}	41.3	K
$k_{PT\ 60}$	0.05	W/m-K
$Q_{PT\ 60,top}$	1.0	W
$Q_{PT\ 60,bottom}$	0.9	W
$Q_{PT\ 60}$	1.9	W

F.3. Heat loss through the insulation

The heat loss through the insulation is primarily due to convection. The temperature of the insulation surface was measured using an infrared temperature sensor while the ambient temperature was measured using a K-type thermocouple connected to the Arduino. Glass wool is the insulation material (sourced from?) and an insulation thickness of around 5 cm is used for the reactor (except the condenser which is uninsulated). The heat loss (presented in Table F.3) is calculated as:

$$Q_{ins} = h_c \cdot A_{ins} \cdot \Delta T_{ins}$$

where Q_{ins} is the heat loss through the insulation,

h_c is the heat transfer coefficient between the surface of the insulation and the ambient surroundings,

A_{ins} is the cross sectional area of the insulation,

ΔT_{ins} is the temperature difference between the outer surface of the insulation and the ambient.

Table F.3: Heat loss through the insulation.

Parameter	Value	Unit
Insulation dimensions	0.14 * 0.13 * 0.4	m
Insulation surface temperature	28	°C
Ambient temperature	22.8	°C
$h_{c,avg}$	30 [111]	W/m^2K
A_{ins}	2.01E-1	m^2
Q_{ins}	31.7	W

F.4. Heat loss through air gap

Heat can be lost through convection, conduction and radiation from the gap of 1 mm between adjacent blocks. Heat lost by conduction is calculated using Fourier's Law:

$$Q_{air\ gap,cond} = k_{air\ gap} \cdot A_{air\ gap} \cdot \Delta T_{air\ gap} / L_{air\ gap}$$

where $Q_{air\ gap,\ cond}$ is the heat loss through conduction,

$k_{\text{air gap}}$ is the thermal conductivity of the air,

$A_{\text{air gap}}$ is the cross sectional area of the air gap (found from Autodesk Fusion),

$L_{\text{air gap}}$ is the thickness of the air gap,

$\Delta T_{\text{air gap}}$ is the difference of the average temperatures of the reaction zone and the first heat integration block. Similar to heat loss through PT 60, the heat loss through the air gap is considered to be only the loss between the reaction and the first heat integration block.

Heat lost though radiation is found using the Stefan-Boltzman Law:

$$Q_{\text{air gap, rad}} = \epsilon \cdot A_{\text{air gap}} \cdot \sigma \cdot (T^4_{\text{reaction zone, avg}} - T^4_{\text{first Al block, avg}})$$

where $Q_{\text{air gap, rad}}$ is the heat lost through radiation,

ϵ is the air gap emissivity,

σ is the Stefan Boltzman constant,

$T_{\text{reaction zone, avg}}$ is the average temperature of the top and bottom of the reaction zone,

$T_{\text{first al block, avg}}$ is the average temperature of the top and bottom of the first heat integration block.

Heat loss through convective heat transfer is estimated using:

$$Q_{\text{air gap, conv}} = h_{\text{air gap}} \cdot A_{\text{air gap}} \cdot \Delta T_{\text{air gap}}$$

where $Q_{\text{air gap, conv}}$ is the heat lost through convection from the air gap,

$h_{\text{air gap}}$ is the convective heat transfer coefficient for still air. The heat lost from these three routes is given in Table F.4.

Table F.4: Heat loss through the air gap.

Parameter	Value	Unit
Conduction		
$L_{\text{air gap}}$	1E-3	m
$k_{\text{air gap}}$	2.4E-2	W/m-K
$A_{\text{air gap}}$	5.24E-3	m^2
$\Delta T_{\text{air gap}}$	43.6	K
$Q_{\text{air gap, cond}}$	5.5	W
Convection		
$h_{\text{air gap}}$	20	W/m^2-K
$Q_{\text{air gap, conv}}$	2.3	W
Radiation		
ϵ	0.09	-
σ	5.67E-08	W/m^2K^4
$Q_{\text{air gap, rad}}$	0.5	W
$Q_{\text{air gap}}$	8.3	W

F.5. Heat transferred to the condenser from COCO simulations

An analysis of the relevant streams from Figure 4.21 gives the results shown in Table F.5.

Table F.5: Flow rates and temperature values of some of the streams in the COCO model (Figure 4.21).

Stream	Temperature (°C)	Methanol flow (kg/s)	Water flow (kg/s)
Condenser In	138.8	5.31E-06	1.91E-06
Condenser Out	76	5.31E-06	1.91E-06
Liquid flash	76	2.70E-06	1.52E-06

The mixture cools down in the condenser, losing sensible as well as latent heat. The sensible heat loss is given as:

$$Q_{\text{sens}} = \dot{m}_{\text{condenser}} * C_{\text{p,condenser}} * \Delta\text{T,condenser} = 3.27E - 5 * 3784 * (138.8 - 76) = 7.8\,\text{W}$$

where,

Q_{sens} is the sensible heat loss in the condenser in W,

$\dot{m}_{\text{condenser}}$ is the sum of the mass flow rates of methanol and water in the condenser in kg/s,

$C_{\text{p,condenser}}$ is the specific heat of the mixture of gases in the condenser in J/kg-K,

ΔT,condenser in the temperature difference between the inlet and outlet streams of the condenser.

The latent heat loss is given as:

$$Q_{\text{lat, CH}_3\text{OH}} = \dot{m}_{\mathrm{CH_3OH}} \cdot \text{Latent heat of vaporization of methanol} = 2.7E - 6 \cdot 1085 \cdot 1E3 = 2.9\,\text{W}$$

$$Q_{\text{lat, H}_2\text{O}} = \dot{m}_{\mathrm{H_2O}} \cdot \text{Latent heat of vaporization of water} = 1.52E - 6 \cdot 2230 \cdot 1E3 = 3.4\,\text{W}$$

where,

$Q_{\text{lat, CH}_3\text{OH}}$ is the latent heat loss due to methanol condensation in W,

$Q_{\text{lat, H}_2\text{O}}$ is the latent heat loss due to water condensation in W,

$\dot{m}_{\mathrm{CH_3OH}}$ is the mass flow rate of methanol in kg/s,

$\dot{m}_{\mathrm{H_2O}}$ is the mass flow rate of water in kg/s,

Latent heat of vaporization of methanol is 1085 kJ/kg [112],

Latent heat of vaporization of water is 2230 kJ/kg [113].

The heat transferred to the condenser is summarized in Table F.6.

Table F.6: Mode of heat transfer in the condenser

Sensible heat	6.3	W
Latent heat	7.8	W
Total	14.1	W

G

Effect of condenser temperature and channel diameter variation on methanol yield

As mentioned in Section 5.2, reducing the condenser temperature can improve the methanol yield. This result is plotted in Figure G.1.

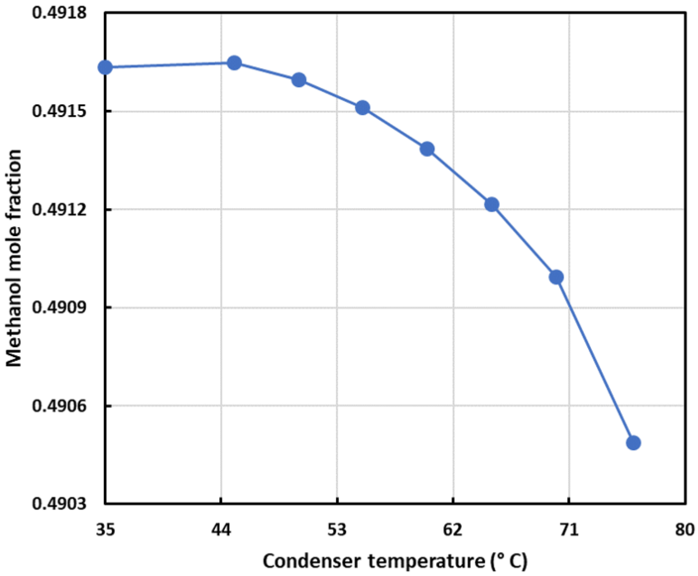

Figure G.1: Effect of changing condenser temperature on methanol mole fraction. Reducing the temperature ensures more liquid is condenser, leading to more methanol production.

H

Corrosion in aluminium blocks

Corossion in the flow channels of the blocks due to the presence of methanol is shown in Figure H.1.

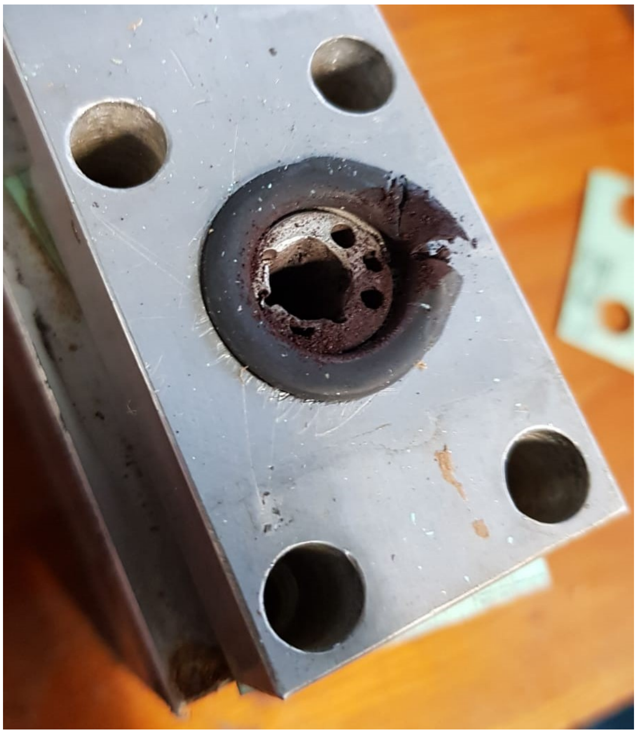

Figure H.1: Corrosion in the flow channels of the aluminium block.